General Disclaimer

One or more of the Following Statements may affect this Document

- This document has been reproduced from the best copy furnished by the organizational source. It is being released in the interest of making available as much information as possible.

- This document may contain data, which exceeds the sheet parameters. It was furnished in this condition by the organizational source and is the best copy available.

- This document may contain tone-on-tone or color graphs, charts and/or pictures, which have been reproduced in black and white.

- This document is paginated as submitted by the original source.

- Portions of this document are not fully legible due to the historical nature of some of the material. However, it is the best reproduction available from the original submission.

Produced by the NASA Center for Aerospace Information (CASI)

NASA Contractor Report 174807

Preliminary Evaluation of a Liquid Belt Radiator for Space Applications

(NASA-CR-174807) PRELIMINARY EVALUATION OF A LIQUID BELT RADIATOR FOR SPACE APPLICATIONS Final Report (Little (Arthur D.), Inc.) 180 p HC A09/MF A01 CSCL 10B

N85-15804

G3/20

Unclas
13115

W. Peter Teagan and Kevin Fitzgerald

Arthur D. Little, Inc.
Cambridge, Massachusetts

JAN 1985
RECEIVED

December 1984

Prepared for

NATIONAL AERONAUTICS AND SPACE ADMINISTRATION
Lewis Research Center
Under Contract NAS 3-22253

ABSTRACT

This report summarizes a program to assess the performance characteristics of a Liquid Belt Radiator (LBR) concept that has the potential for markedly improved characteristics such a.. lighter weight and more compact storage than currently used space radiators. In many cases, present construction techniques produce space radiators that represent 50 percent of the total weight of the power plant. Present radiator systems do not lend themselves particularly well to compact storage during space vehicle launch or ease of deployment once in space.

In the LBR concept described herein, a thin screen or mesh structure which support's menisci of a suitable material is drawn from a liquid bath which functions as a heat rejection sink for a spacecraft's thermal control or thermal power system. The ribbon is moved through space by means of a mechanical arrangement so that it functions as a lightweight radiator system. The liquid must have a very low vapor pressure ($<10^{-8}$) over the operating temperature range in order to keep evaporative losses within acceptable limits. Materials meeting this criteria include several diffusion pump oils, gallium, lithium, and tin. The selection of material will depend primarily on the temperature range of interest with the oils limited to about 350 K (171°F) and the metals being applicable to 2000 K (3140°F).

The LBR system can operate either in the sensible heat mode (the meniscus material remains in the liquid phase) of in the latent heat mode where the meniscus material changes phase during its transverse through space. The selection of operating mode depends on material selection, operating temperatures, and the requirements of the heat rejection systems.

Parametric analysis undertaken in this study shows that the LBR concept has the potential for reducing the mass of radiators by 70-90 percent when compared with conventional heat pipe technologies. This observation, however, is based on the LBR surface having a total emissivity in excess of 0.3 and preferably in excess of 0.6. Measurements made in this study indicated that the diffusion pump oils easily meet this criteria with emissivities greater than 0.8. Measurements made on gallium indicate that the material most likely has an emissivity in excess of

0.3 in the solid state when small amounts of impurities are on the surface. More accurate measurements, however, are required to clarify this issue.

The parametric studies and emissivity investigations were made to generate a radiator design for a Brayton cycle power system rejecting 75 kW of waste heat over the temperature range of 458 to 315 K (365-107°F) to an effective background heat sink temperature of 250 K (-10°F). The resulting point design consists of a moving belt in a cylindrical array which is deployed and maintains its configuration as a result of centripetal forces.

The point design includes a belt with an axial dimension of 3.4 m (11.0 ft) and a diameter of 13.7 m (45 ft). The dimensions of the LBR heat transfer bath are 0.38 m (1.25 ft) in the direction of belt travel and 3.4 m (11.0 ft) normal to the direction of belt travel. With a nominal belt thickness of .051 cm (.02 in) fully wetted with Santovac 6 diffusion pump oil, the overall weight of the radiator system is estimated to be 235 kg (517 pounds). This estimate includes all heat exchangers, rollers, drive motors, and spare fluid for one year of evaporative losses. The point design exhibits a characteristic mass of approximately 3.1 kilogram per kilowatt of power dissipation, a mass per unit prime radiating area of approximately 0.9 kilogram per square meter and a total package volume (assuming a rectangular storage canister) of approximately 2.50 m^3 (88 ft^2). This compares very favorably with conventional technologies which have weights on the order of 4 kg/m^2. Nearly one-half of the storage volume consists of a stuffing box used to stow the LBR during transport and during vehicle maneuvers. This point design and alternate means for stowing, deploying and supporting the belt radiator to withstand vehicle maneuvers need further study.

TABLE OF CONTENTS

TABLE OF CONTENTS (Continued)

TABLE OF CONTENTS (Concluded)

1.0 SUMMARY AND CONCLUSIONS

Current space radiators employ heat pipe technology or pumped single phase fluid systems. Future spacecraft will benefit from radiators that are lighter than those currently employed and are capable of being readily erected or deployed in orbit. This engineering study examines a new radiator concept called the Liquid Belt Radiator (LBR) that employs a thin moving belt of wetted fluid as the radiator.

The 17 month program described herein verified the potential for the LBR concept throughout a wide range of heat rejection temperatures of interest. Specific accomplishments of this program were:

- o A review of the properties of a wide range of materials for use in LBR concepts at different temperature levels.
- o The completion of wetting tests for over 25 different film/mesh material combinations.
- o An analytical determination of the criteria for menisci stability, liquid bath containment in a gravity-free environment, and the requirements for maintaining the liquid on the ribbon under inertia loads.
- o The parametric analysis of LBR system (including deployment systems) at three different heat rejection temperature levels of interest and estimate the total system sizes and weights for these designs for comparison with heat pipe radiator systems.
- o Completion of bench top experiments which verified the basic concept of the LBR by forming liquid belt radiators (2 inches wide and 13 inches long) using diffusion pump oil and a low melting point alloy.
- o Measurement of the emissivities of two low vapor pressure diffusion pump oils (Dow Corning 704 and Santovac 5) and gallium which are candidate materials for use in the LBR.
- o Preparation of a preliminary point design for an LBR system which could reject heat from a 37 kWe Brayton cycle engine which is under consideration as a power source by NASA. This system rejects 75 kW of thermal energy over the temperature range of 458.3-315 K (365.5-108°F). This design included consideration of the belt interface with the heat rejection

systems, means for deployment, and parasitic power losses associated with belt movement

Several of the more important results of the above effort are summarized below.

System Mass

With proper selection of working fluid, the mass of the LBR system will be between 30 and 50 percent that of a heat pipe radiator with the same heat rejection capacity. For the LBR, this assessment includes the mass of the liquid belt, heat exchanger bath, deployment system, make-up fluid, and ancillary equipment. The mass assumed for the heat pipe radiator was 4 kg/m^2.

The largest single factor influencing system mass is the emissivity of the radiating surfaces. If emissivities of 0.5 or greater can be achieved, the mass of the LBR system is consistently less than 40 percent that of a heat pipe system. At emissivities of 0.1, the mass of the LBR concept approaches the heat pipe radiator.

Material Emissivities

The emissivities of Santovac 5, DC-704, and gallium were measured during this program. Both oils exhibited emissivities in excess of 0.85 over the wave lengths of interest. The gallium tests demonstrated a low liquid state emissivity ($\approx$0.1). They did however indicated higher emissivities ($\approx$0.2-0.4) in the solid state which would prevail during a phase change operational mode. This conclusion must be made with reservation, however, since the surfaces were probably contaminated with oxides during these measurements.

The mesh on which the working fluid meniscus is formed tends to give the LBR a textured surface. Analysis indicates that such texturing can increase the apparent emissivity of the surface by a factor having an upper bound of 2 when using material with surface emissivities of 0.1 to 0.3. This suggests that belt emissivities may be increased to a range of practical interest for LBR's using liquid metals by proper belt design. Increasing the emissivity of the metal by

surface contamination (e.g., oxide layer) is another possibility which requires exploration.

Radiator Area

The area of the LBR can approach that of heat pipe radiators if the emissivity of the liquid film approaches 0.95. Measurements made during this program indicate that achieving such high emissivities will be possible when using low vapor pressure oils as the film material. However, liquid meatals do not exhibit such high surface emissivities. The surface area of LBR will, therefore, be larger than for heat pipe radiator systems for operation in the higher temperature ranges. Nevertheless the low unit area weight and method of deployment of the LBR will still often result in lower weight over a wide range of applications.

Material Options

The heat sink bath material in the LBR is directly exposed to space during the heat rejection process. As a result, materials with very low vapor pressures at the desired operating temperatures must be used so that:

- o Excessive material is not lost due to evaporation.
- o Belt material does not contaminate sensitive spacecraft surfaces.

Analysis indicates that vapor pressures below 10^{-8} torr are required to minimally satisfy the first of these conditions and that even lower vapor pressures are desirable. Selected materials which satisfy this minimum requirement are indicated in Table 1.1. For purposes of the parametric analysis, Santovac 6 was selected for low temperature heat rejection ($\sim$311 K, 100°F), lithium for intermediate temperature heat rejection (450 K, 350°F), and tin for high temperature heat rejection (550 K, 531°F).

Lithium and tin can be considered in both a sensible heat mode (where the film remains liquid throughout its transverse in space) and a change of phase mode

(where the film changes phase during its transverse in space). The oils are only applicable for operation in a sensible heat operating mode.

Meniscus Formation

Ideally, the liquid film material should easily wet the mesh material used as the substrate. Furthermore, to form ideally stable menisci, the spacing to diameter ratios of the mesh should fall within certain limits (Appendix B). For example, when using a 5 mil mesh wire, the spacing should be about 35 mils (for a diameter to spacing ratio of 0.13). Both experience and analysis during this program suggest, however, that neither complete wetting on or rigid adherence to lower limit stability requirements are necessary to form a liquid belt. These facts were experimentally determined by formation of menisci using diffusion pump oils on meshes with spaces which considerably exceeded the severest stability requirements and the formation of metal films on meshes where the material combinations do not wet.

The limits of stable mesh spacing for various wetting conditions have yet to be determined.

Bench Test Results

A bench test system capable of pulling mesh 2 inches in width and 13 inches long through a bath was assembled to verify the basic LBR concept. This experimental apparatus has been tested using a nylon screen with Santovac 5 diffusion pump oil and a low melting point eutectic metal (Cerralow @ 150°F). In both cases, a liquid belt approximately 15 mils thick was drawn from the bath.

The meniscus formed with diffusion pump oil was perfect as would be expected given the excellent wettability of diffusion pump oil on the mesh material. The menisci formed with the liquid metal were not everywhere complete as might be expected by the relatively poor wetting exhibited by the metal and the screen substrate. Figure 1.1 shows one such miniature belt radiator being drawn from a vat of molten gallium. These tests helped to relate laboratory wettability test results with actual performance in an LBR configuration.

Table 1.1

KEY PROPERTIES OF CANDIDATE LBR WORKING FLUIDS

Liquid	Vapor Pressure (Torr)	Molecular Weight	Density (kg/m^3)	C_p, Specific Heat (J/gm K)	C_p, Specific Heat (Btu/lbm°R)	h_{ls}, Latent Heat of Fusion (J/gm)	Melting Point K(°C)	Melting Point °R(°F)	Emissivity Solid	Emissivity Liquid	Surface Tension (g/s^2)	Viscosity $N-s/m^2$
DC 705	$4.4x10^{-8}$ @ 330°K	546	~1240	—	—	Not Applicable	Not Applicable		Not Applicable	0.8	20	0.19
Santovac 6	$7.2x10^{-9}$ @ 330°K	538	1240	1.55	0.37	Not Applicable	Not Applicable		Not Applicable	0.8	54.2	1.75
Gallium	$<10^{-30}$ @ MP	69.7	6100	0.34	0.008	82.1	303 (30)	546 (86)	.3	.1	720	$1.8x10^{-3}$
Indium	$<10^{-16}$ @ MP	114.8	7310	0.246	0.061	28.5	429 (156)	773 (313)	.3	.1	590	—
Lithium	$<10^{-10}$	6.94	530	3.47	0.83	663	453 (180)	815 (355)	.3	.1	394	$5.9x10^{-4}$

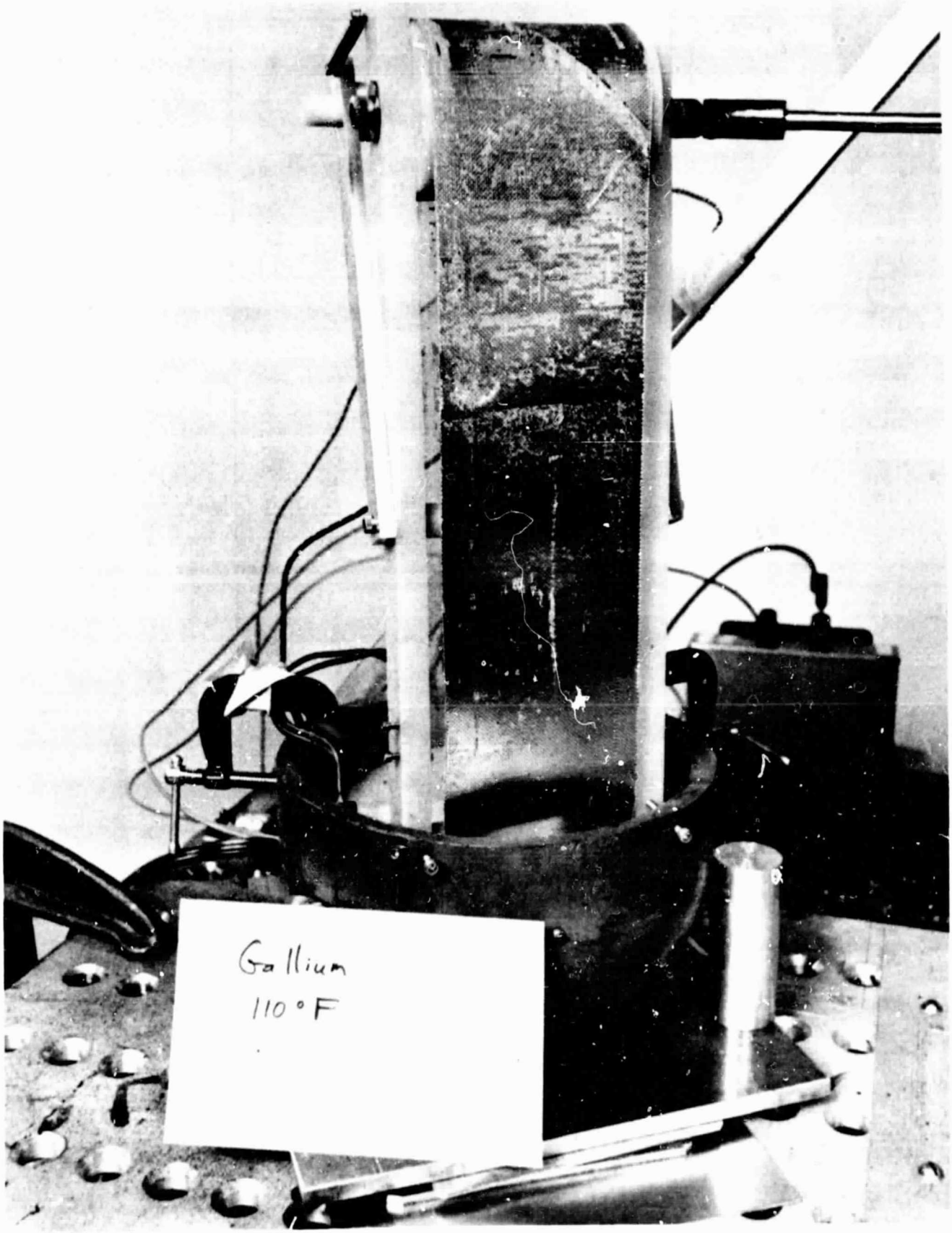

Figure 1.1 MENISCUS FORMATION ON THE LBR TEST RIG USING GALLIUM

ORIGINAL PAGE IS
OF POOR QUALITY

Point Design Results

The potential of the LBR concept was assessed by applying it to a specific operational requirement defined by NASA. As indicated on Table 1.2, the specified requirement was a space radiator for a 37.5 kWe Brayton cycle power unit where the heat rejection is over a temperature range of 458-315 K (365-108°F). The quantity of heat to be dissipated was 75 kW. This application is of great interest due to the fact that the heat rejection is over a rather wide temperature range as compared to the rejection associated with a Rankine cycle power plant or the cooling of electronic equipment. Several modes of LBR operation were considered for this mission, including:

- Heat rejection in the latent heat mode using gallium as the belt fluid and a constant belt temperature of 303 K (86°F).
- Heat rejection in the sensible heat mode using gallium as the belt fluid operating over a temperature range of 310-450 K (98.6-351°F).
- Heat rejection in the sensible heat mode using Santovac 6 as the belt fluid operating over the temperature range of 300-330 K (135-81°F). The upper temperature in this case was determined by the need to limit evaporative material losses which increase exponentially with temperature.

The latter option was selected for the point design since it led to the lowest mass LBR system meeting specified requirements.

The resultant point design is indicated pictorally in Figure 1.2 with corresponding specifications in Table 1.3. It consists of a screen mesh belt which is 3.5 m wide and 43 m long having an area approximately 145 m^2. The belt is 0.051 cm thick and moves with a velocity of 0.8 m/sec. The overall system mass is 235 kg of which 92 kg (39 percent) is associated with the belt and associated fluid menisci and the remainder with the heat exchanger bath and ancillary equipment. This mass compares very favorably with conventional heat pipe designs, assuming 4 kg/m^2.

Figure 1.3 is an artist's rendition of the system as it might be applied to such a mission.

Table 1.2

Mission Requirements of LBR Point Design

Parameter	Value
Average Power Dissipation	75 kW_t
Brayton Cycle Temperature Range	458.3 to 315 K
Effective Heat Sink Temperature	250 K
Launch	Max. 4.6-m (15-ft.) dia. x 18.3m (60-ft.) Cargo Bay
Deployment Sequence	Fully Automatic
Orbit Parameters	o 502-km (311-mile) Circular Orbit (T = 94.6 min/orbit) o 28.5° Inclination to Earth's Equatorial Plane o Air Density (high solar activity) < 1.2×10^{12} kg/m^3 o LBR Drag Coefficient: 2.5
Mission Life	One Year (Assumed)

ORIGINAL PAGE IS
OF POOR QUALITY

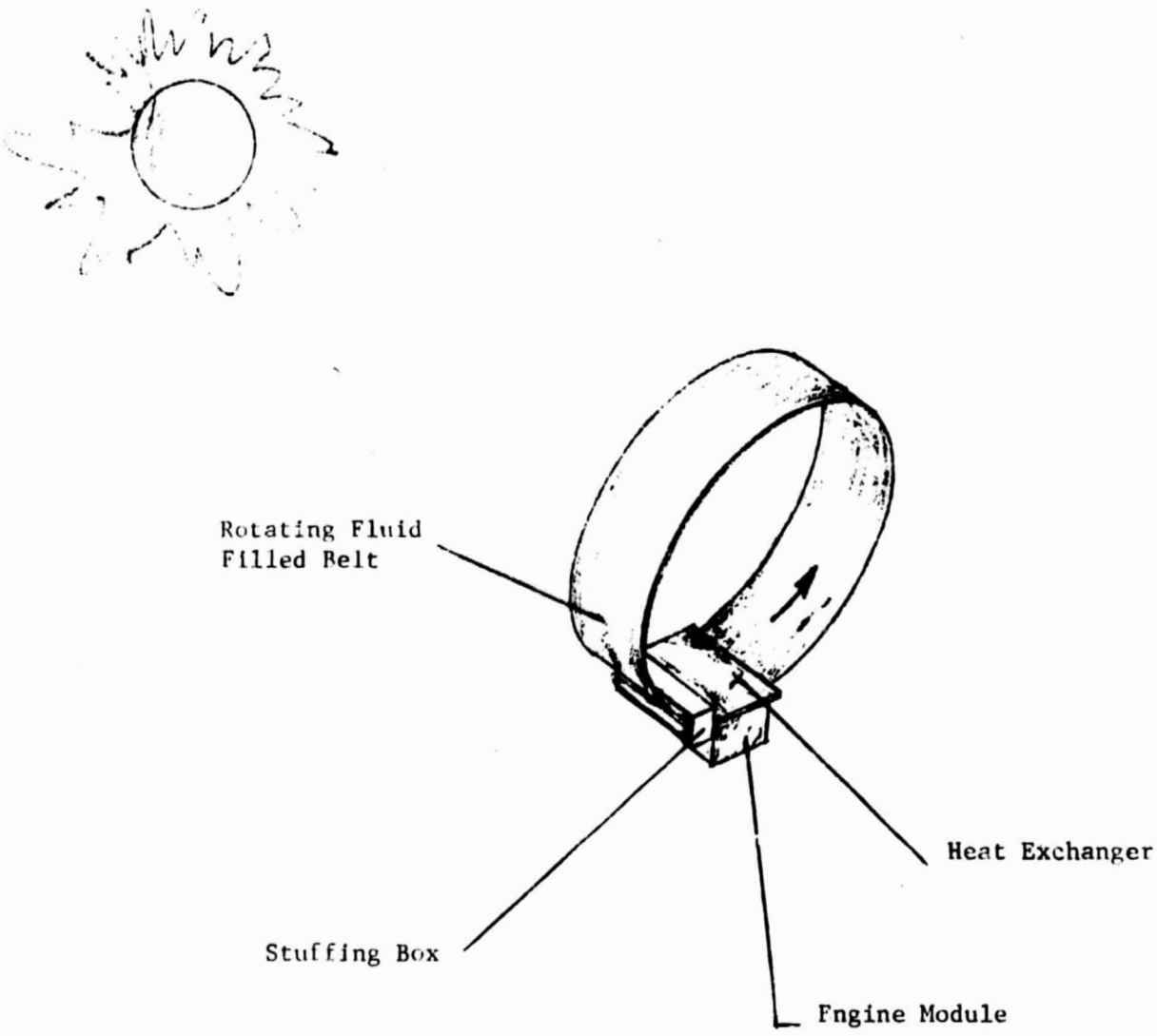

Figure 1.2 POINT DESIGN

Table 1.3

POINT DESIGN PHYSICAL PARAMETERS

Working Fluid	:	Santovac 6
Mode of Operation	:	Sensible
Heat Rejection Rate	:	75 kWth
Exit Temperature	:	330 K (135°F)
Inlet Temperature	:	300 K (81°F)
Belt Width[1]	:	3.4 m (11 ft)
Belt Thickness	:	5.1×10^{-4} m (1.7×10^{-3} ft)
Belt Circumference	:	43.0 m (141 ft)
Belt Diameter	:	13.7 m (45 ft)
Belt Area[2]	:	290 m^2 (3110 ft^2)
Belt Weight	:	92 kg (202 lbm)
Belt Speed	:	0.8 m/s (2.5 fps)
Yearly Material Loss	:	14.4 kg (31.716 m)
% of Belt Weight	:	14.1 percent
Heat Exchanger Length[3]	:	0.38 m (1.25 ft)
Heat Exchanger Single Sided Gap, Distance	:	5.8×10^{-3} m (0.0190 ft)
Parasitic Power[4]	:	<1.00 kW (∿1.3 hp)
Orbital Drag[5]	:	0.0012 N (0.0002 lbf)

NOTES

(1) Selected so that storage aboard NASA STS is possible.
(2) Refers to inner and outer surface area.
(3) Refers to the length in the direction of belt travel assuming an overall heat transfer cooefficient of 570 w/m^2 K and a LMTD of 53 K.
(4) Assumes a gap distance of ∿225 mils from the surface of the belt to heat exchanger plates. Also additional drag forces effectively double the fluid friction effects.
(5) Based on a 270 nautical mile circular orbit and a maximum atmospheric density of 5×10^{-12} Kg/m^3.

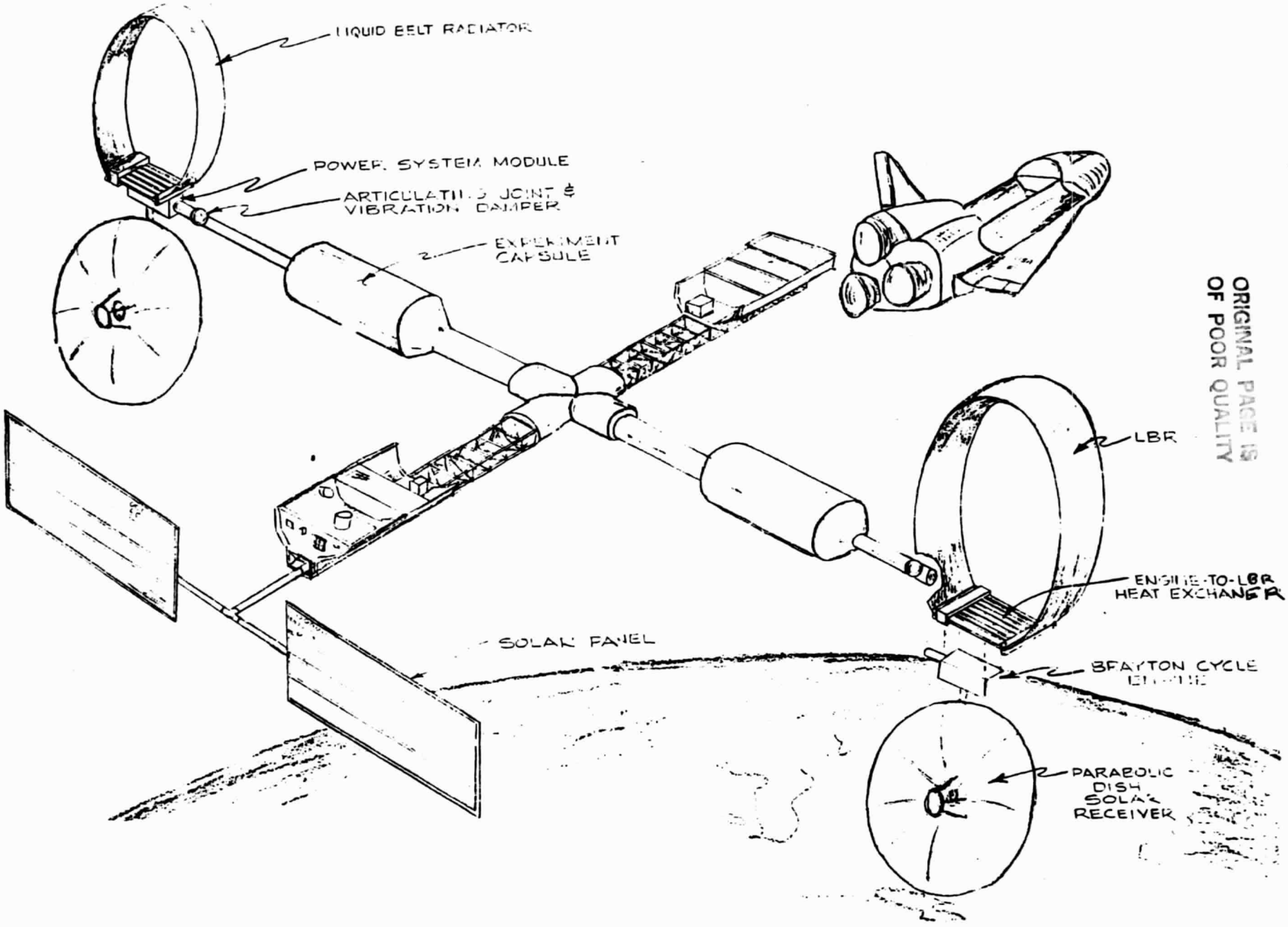

ORIGINAL PAGE IS OF POOR QUALITY

Figure 1.3 ARTIST'S SCHEMATIC OF THE CYLINDRICAL LBR POINT DESIGN

Figure 1.4 shows the LBR in the stowed position for the assumed mission. The interface heat exchanger is seen to consist of parallel flat plates which are heated by a fluid loop in contact with the Brayton cycle power plant. The heat to be rejected is transferred to the bath material and then to the moving belt which moves through the gap. In the stowed position the belt/heat exchanger combination (not including rollers and drive system) takes up an estimated volume of $0.74\ m^3$.

An important issue with any radiator concept is the level of parasitic power required for its operation. In the LBR system, this power arises from the viscous drag forces on the belt as it moves through the heat exchanger bath. For the point design the resultant parasitic power was estimated to be 0.75 kW, which is about 1 percent of the energy being dissipated.

ORIGINAL PAGE IS
OF POOR QUALITY

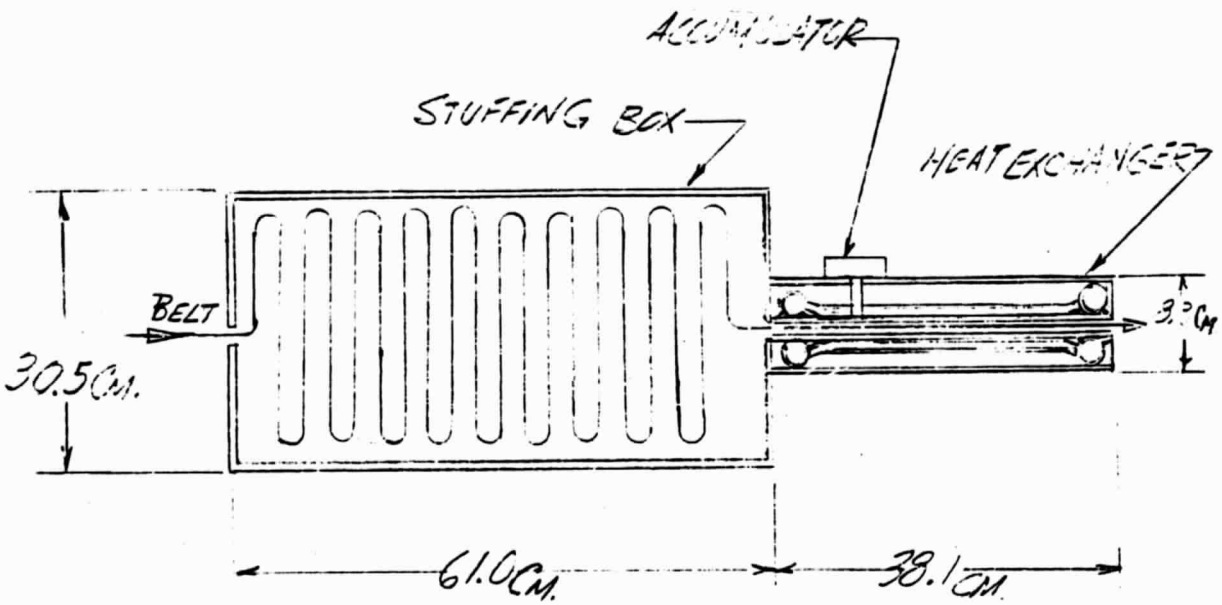

Figure 1.4 STOWED LBR CONFIGURATION

2.0 INTRODUCTION

2.1 Background and Introduction of the Liquid Belt Radiator Concept

The heat rejection needs of spacecraft are projected to increase significantly over the coming decades as both civilian and military missions operate at increased power levels. In space vehicles which must reject large amounts of heat, the size and weight of the space radiator impact the design of other vehicle structures and overall represent a major design consideration. As an element of a closed-cycle power system, it represents about one-half the weight of a weight-minimized design. As an element of a thermal utility for maintaining manned working spaces or instruments within their tolerable operating temperatures, the weight of the space radiator is typically 60 percent or more of the total weight.

Besides being a major contributor to system weight, large space radiators necessarily have large extended surfaces for heat rejection. The characteristics of conventional heat pipe radiators normally introduce such design complications as deployment and repair or servicing requirements. The design employed should be adaptable for operation at different temperature levels, and if desired should additionally serve to control temperature at different power levels. Finally, the space radiator should be invulnerable to micrometeorite impact damage.

Currently, most advanced design concepts for large space radiators meeting these requirements utilize a lightweight extended surface of honeycomb construction upon which parallel rows of heat pipes are bonded for purposes of heat distribution and isothermalization of the extended surface. One end of the heat pipes are connected to a common heat exchanger which serves as a thermal busbar. Commonly, a heat transfer fluid which carries the heat load to the radiator is circulated through this heat exchanger, but alternately another master heat pipe may serve this function. The weight per unit of projected area of radiators having this construction typically range from 3 to 5 kg/m^2 (0.6 to 1 lb/ft^2).

Best designs and methods for storage and erection are yet to be finalized and proven as practical solutions. Problems associated with assembling and maintaining leak-tight and thermally conducting joints are not trivial.

The Liquid Belt Radiator (LBR) system described in this report is one of several advanced radiator concepts being investigated as an alternative for the heat pipe radiator systems. As indicated in Figure 2.1 the LBR system is a thin film (0.13-0.51 cm [5-20 mils] thick) of liquid in the form of menisci which adhere to or wet a solid mesh substrate. This fluid filled belt, which functions as a heat sink within the spacecraft, is drawn through space so that it can radiate thermal energy. The belt may remain as a liquid, working in the sensible heat mode, or it may change phase as it traverses through space. For the analyses presented herein design choices are based on the desire for the minimum LBR weight to accomplish a specified mission, this often being governed by the range of heat rejection temperatures required. The belt weight must be traded off against parasitic power dissipation associated with friction in the fluid and seals.

As has been discussed, the LBR utilizes a thin layer of heat rejection material (in the form of meniscii) attached to lightweight mesh having proper mesh dimensions to ensure stable meniscus formation and adequate mesh strength. The concept shows promise of resulting in very lightweight, easily deployable, reliable radiators, not subject to catastrophic damage from micrometeorites. Material combinations are available which will allow utilization of the concept over operating temperature ranges from 300 K (81°F) to relatively elevated temperatures of 561 K (550°F) consistent with the heat rejection temperatures of some advanced thermal power systems. An LBR radiator system is projected to have a mass of less than half that of heat pipe systems. It should be noted, however, that if the weight and deployability advantages of the LBR can be demonstrated in practice, such a radiator would tend to change the optimum operating temperature of thermal power systems in the direction of lower heat rejection temperatures and correspondingly higher power system efficiencies. Ongoing studies of a similar concept by other investigators indicate similar promise to the LBR (Knapp, 1983).

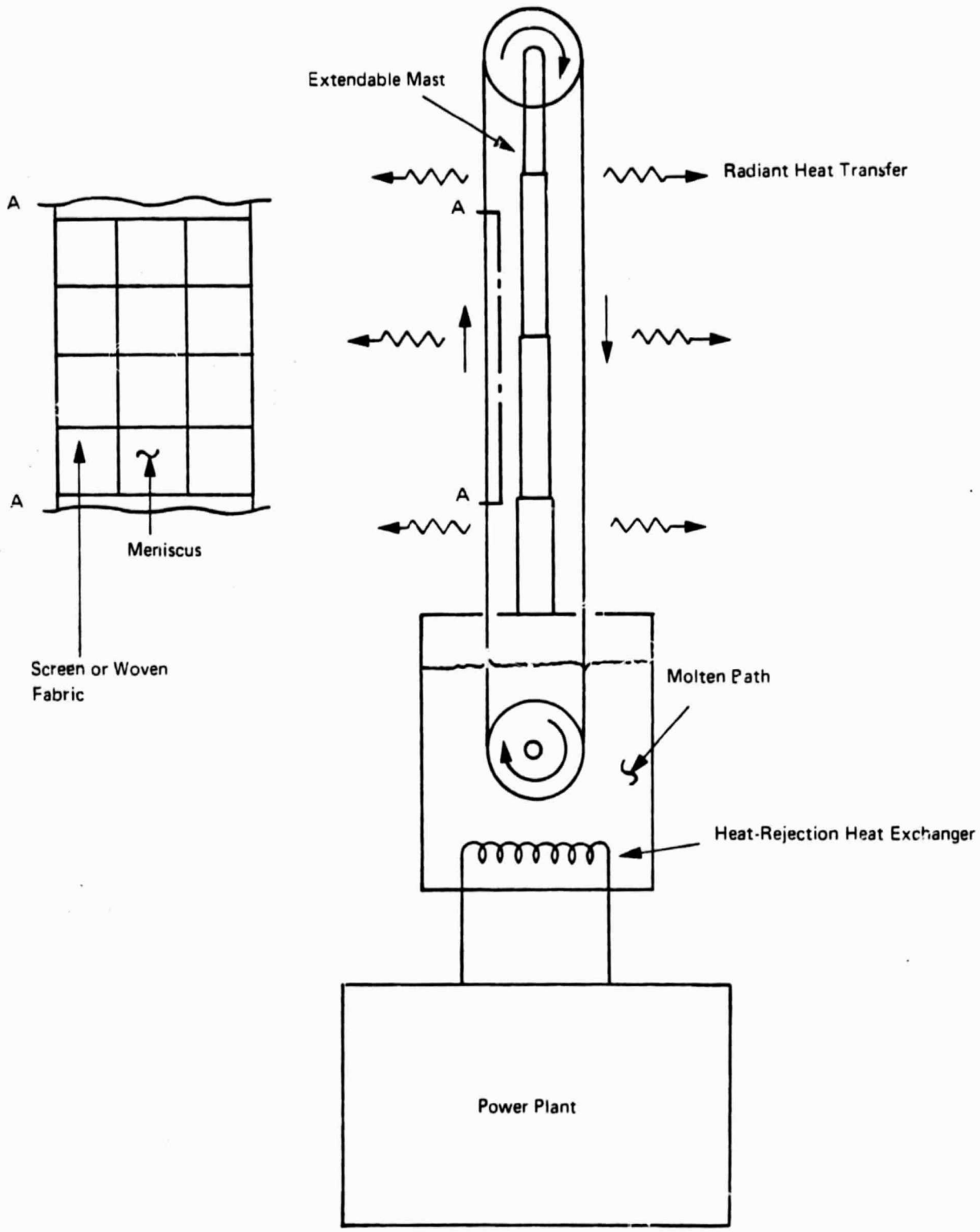

Figure 2.1 LIQUID BELT RADIATOR (LMBR) SYSTEM CONCEPT

The LBR consist of the following primary structures:

- o A bath of a low vapor pressure liquid (oils, liquid metals, molten salt) which acts as the heat rejection sink for a power-generating system, or a spacecraft equipment cooling system.
- o Screen mesh belt of lightweight material.

During operation, the belt would be drawn through the molten bath. A thin (5-20 mils) liquid web of the bath material would be formed within the boundaries defined by the filaments of the belt (similar to the soapy water meniscus formed in bubble-blowing). As the belt is drawn through space, the liquid menisci would radiate to the environment and thereby dissipate energy. The cooled material would then be returned to the bath for reheating, and new menisci formed from the heated material.

By suitable combinations of belt speed, material properties, and operating temperature levels, two basic modes of LBR operation are possible: a non-phase change and a phase change mode. These are described in more detail below:

- o Non-Phase Change Mode. The menisci are made to remain in liquid form throughout the process. In this mode, the heat dissipation takes place in the form of a sensible heat loss (and corresponding temperature reduction) in the liquid material during its traverse through space.
- o Phase Change Mode. The menisci are made to gradually solidify during radiant heat rejection. In this mode, the heat rejection to space results in a change of phase of the material forming the menisci, and this change can take place over a very narrow temperature range.

Both operational modes offer advantages and disadvantages. For example, the advantage of phase change operation is that the belt velocity can be relatively low, since large amounts of heat can be rejected by small mass flow rates of the working fluid. However, in this case, the belt matrix may contain webs of solidified material which must conform without failure to the structural

configuration of the moving belt. This problem is eased in the case in which no phase change occurs, but at the penalty of requiring greater belt speeds.

Overall the LBR concept appears to offer promise as a large, lightweight radiator system. It is conjectured that material combinations (i.e., working fluid and screen belts) will be determined which will allow utilization of the concept from ambient temperatures (100°F) all the way up to relatively elevated temperatures (550°F) consistent with the heat rejection temperature of some advanced thermal power systems. Furthermore, if the weight and deployability advantages of the LBR can be demonstrated in practice, such a radiator would tend to change the optimum operating temperature of thermal power systems in the direction of lower heat rejection temperatures and correspondingly higher power system efficiencies.

2.2 Project Description

This report discusses results from a 17 month program with a level of effort of about 12 man-months. The objective of the program was to provide preliminary analytical and experimental verification of the LBR concept and to identify major issues which need to be addressed in order to effectively pursue the concept for practical space applications. These objectives were addressed during two program phases with the following tasks.

PHASE 1: Working Fluid Characterization and Parametric Studies

Task 1.1: Review of Technical Data

A data and literature search was conducted to identify available state-of-the-art information for this concept. This activity focused on physical properties of candidate heat transfer film materials, characteristics of belt mesh (screen) materials and the experience to date on the physical processes (wetting, etc.) associated with meniscus formation in space environment.

Task 1.2: Analytical Evaluation

Analytical studies were conducted to examine the performance characteristics of this concept for a range of candidate heat transfer fluids, operating temperature levels and deployment configurations.

Performance characteristics of phase-change and non-phase-change options were compared to aid in defining the most favorable system configurations, pulling speeds, and working fluid (bath) materials. Special attention was given to the effect of pulling speed on meniscus thickness and overall radiator weight. This effort examined the effect of screen materials, mesh spacing, and filament diameters on system weight and on the stability of the menisci formed. The output of this task provided a preliminary identification of the working fluid materials, screen configuration, deployment options and the parameters for systems operating at selected temperatures and was used as input for the conceptual designs of Task 1.4.

Task 1.3: Bench Top Tests

A series of bench top tests were undertaken in support of the analytical efforts of Task 1.2. These tests included:

- Determining the wetting properties of over 25 mesh/fluid film combinations which might be appropriate for low temperature operation.
- Assemblying a small scale (2" wide - 6" long) motor driven LBR which was operated with diffusion pump oils and low melting point eutectic metals.

Task 1.4: Conceptual Designs

Preliminary conceptual designs for systems using the parameters identified in Task 1.2 were prepared for the three heat rejection temperatures of 311 K, 450 K, and 505 K (100°F, 350°F, and 450°F) and heat rejection rates from 25 kW to 100 kW. These conceptual designs were used to examine alternative LBR design

options and to allow preliminary comparisons of the weight, size, and reliability of LBR radiator systems with conventional systems.

Phase II: Emissivity Measurements and Preliminary Point Design

The results of Phase I indicated the need to generate additional information on the emissivities of candidate materials and to characterize the LBR in more detail via a point design for a specific mission. This was undertaken in the following tasks.

Task 2.1: Emissivity Measurements

The performance of the LBR concept and several other advanced radiator systems being considered by NASA depends critically on the emissivity of the materials being utilized. Unfortunately there is very little published data on the emissivity of these materials--particularly under the operating conditions of space radiators. In order to be able to better assess the potential of the LBR concept, emissivity measurements were made on 3 of the candidate materials.

- Santovac-5
- DC-704
- Gallium

Measurements on the diffusion pump oils were made using an infrared emittance optics arrangement attached to a spectrometer system. Measurements on gallium were made using both a reflectance measurement system and an infrared thermal imaging system.

Task 2.2: Emissivity Enhancement

Analytical studies were undertaken to assess the potential for increasing the effective emissivity of the belt by providing it with a high degree of geometric texture. This could, in turn, influence the selection of belt mesh configuration.

Task 2.3: System Analysis and Design

Using emissivity estimates based, in part, on the results of Task 2.1 and 2.2, a conceptual design of a complete LBR system based on a NASA defined mission was prepared. This design depicts the LBR in both the stowed and deployed position and provided estimates for:

- Total system weight.
- Parasitic power requirements.
- Stored position volumes.

3.0 SYSTEM REQUIREMENTS

This section provides a brief description of the overall system requirements for the liquid belt radiator (LBR) and identifies the various considerations evaluated in reaching the point design described in Chapter 5.0.

3.1 Overall System Requirements

The utility of the Liquid Belt Radiator Concept depends on a number of requirements. Any system design must incorporate or address the following general issues:

- o Ability to satisfy thermal load requirements and respond to any changes in load.
- o The need for a lightweight easily deployable and stowable structure.
- o The requirements for structural integrity and dynamic stability during perturbations and maneuvers.
- o The selection of a working fluid/belt combination which ensures the formation and stability of individual menisci structure during transit through space.
- o The selection of a working fluid that is optically and thermodynamically suitable for use in a space environment.

3.2 Working Fluid Requirements

Because of the importance of working fluid selection, a more detailed account of bath material requirements is presented. For all operating temperatures of the LBR, the bath material must have the following properties.

- o A low vapor pressure in the liquid state, so that the amounts of material lost to space by evaporation and the concomitant problems of contamination that this loss may impose, will be tolerable.
- o Sufficiently high surface tension and wettability to form and maintain stable menisci between the filaments of the screen material.

- A liquid state or melting point in a range of temperatures corresponding to the heat sink of the system serviced by LBR.

Within these constraints, the selection of the working fluid will depend on additional factors such as cost, surface emissivity, density, heat of fusion and/or specific heat, viscosity, and chemical compatibility with the belt matrix material. Table 3.1 shows a partial list of materials which are likely candidates for the application.

The oils listed in Table 3.1 are used primarily in high vacuum diffusion pumps and have very low pressures for organic compounds. All these oils easily wet candidate belt materials (including plastics) facilitating their potential use in the LBR concept. While their emissivities are generally unknown two oils, Santovac 5 and DC-704, were experimentally shown to have normal emissivities in the range 0.9 to 0.95 at thicknesses greater than 0.06 cm (25 mils). The diffusion pump oils are viewed as excellent candidates for use in LBR systems of heat rejection temperatures in the vicinity of 310 K (100°F). These properties lead to selection of the oil Santovac 6 (Monsanto Corp.) for use in the point design.

In addition to the oils, metals with low melting points have a mix of properties which make them prime candidates for application to the radiator concept. Their characteristically low emissivity constitutes the major deficiency which must be overbalanced by their other desirable properties. In a pure state, uncontaminated liquid-metal surfaces typically have emissivity values less than 0.1. Uncontaminated solid surfaces would have higher emissivities, but nevertheless are also quite low. Methods for purposely contaminating the belt surface (for instance, with an oxide film) to raise its emissivity may well prove practical and should be pursued in future phases of work.

Liquid metals are highly reactive; therefore, their compatibility with other materials would have to be considered in the selection process. Gallium could be a particularly interesting material for rejecting heat in a phase change mode of operation at the relatively low temperature levels ($\sim$90°F) required for equipment cooling and the efficient operation of thermal (isotope and solar)

Table 3.1

KEY PROPERTIES OF CANDIDATE LBR WORKING FLUIDS

Liquid	Vapor Pressure (Torr)	Molecular Weight	Density (kg/m^3)	C_p, Specific Heat (J/gm K)	C_p, Specific Heat (Btu/lbm°R)	h_{ls}, Latent Heat of Fusion (J/gm)	Melting Point K(°C)	Melting Point °R(°F)	Emissivity Solid	Emissivity Liquid	Surface Tension (g/s^2)	Viscosity $N-s/m^2$
DC 705	$4.4x10^{-8}$ @ 330°K	546	~ 1240	—	—	Not Applicable	Not Applicable		Not Applicable	0.8	20	0.19
Santovac 6	$7.2x10^{-9}$ @ 330°K	538	1240	1.55	0.37	Not Applicable	Not Applicable		Not Applicable	0.8	54.2	1.75
Gallium	$<10^{-30}$ @ MP	69.7	6100	0.34	0.008	82.1	303 (30)	546 (86)	.3	.1	720	$1.8x10^{-3}$
Indium	$<10^{-16}$ @ MP	114.8	7310	0.246	0.06i	28.5	429 (156)	773 (313)	.3	.1	590	—
Lithium	$<10^{-10}$	6.94	530	3.47	0.83	663	453 (180)	815 (355)	.3	.1	394	$5.9x10^{-4}$

power plants. Liquid tin or lithium may be appropriate for higher temperature heat rejection systems associated with space nuclear (or isotope) space power systems. Lithium operating in a phase of change mode appears to be particularly interesting due to its very low density with respect to gallium (0.53 g/cc vs. 6.10 g/cc) and its high heat of fusion (663 J/g). The advantages of using lithium in such a phase change mode are displayed in the parametric analysis of Section 4.0.

3.3 Mechanical Configurations

Various mechanical configurations were considered in reaching the point design concept. The overall concerns of low weight, ease of deployment, and potential for extended periods of highly reliable operation were of paramount importance.

3.3.1 Belt Configurations

The LBR concept employs a belt mesh to transport the working fluid from the bath into space. This design is unlike existing moving belt radiator concepts (i.e., solid belt radiators) in that the heated fluid is directly exposed to the space environment and acts as the prime source of radiative energy transfer.

The mesh structure is akin to common screen materials used in filtration and ventilation applications. Candidate belt materials include:

- Metals (aluminum, tantalum, etc.)
- Low vapor pressure plastics (nylon, etc.)
- Reinforced composite materials (carbon, silicon carbide, etc.)

The selection of a particular material will depend on operating temperature levels, compatibility with the working fluid, and its reliability and degradation characteristics in the space environment.

An important criterion for the belt is that the working fluid adhere to the screen structure. The ability for the fluid to wet the solid is crucial to the formation of stable menisci. Initial studies, detailed in Appendices B and C

relate a derived absolute meniscus stability criterion to material stress limits. In general, the belt mesh material must have sufficient strength to withstand vehicle maneuvers or forces associated with belt motion.

3.3.2 Bath Configurations

The fluid bath must be configured to ensure adequate heat transfer from the reject heat loop of the power cycle to the LBR working fluid and provide sufficient capacity to make up for working fluid losses. Although heat transfer area is of prime importance, the weight of the bath heat exchanger structure(s) must also be kept as low as possible. Both concerns will necessitate the design of a compact light-weight heat exchanger.

In addition to the area and weight considerations, the design of reliable and efficient bath sealing techniques is of major concern. The seal technology developed will be derived from existing sliding seal designs, and must be sufficient to minimize the loss of working fluid as the belt transits through the bath. The overall bath design, including exit seals, must be consistent with acceptable parasitic power losses resulting from the viscous forces on the belt as it is "dragged" through the bath material. The criterion used in the studies was that these parasitic power requirements be less than 1-2 percent of the thermal heat being dissipated.

Natural evaporative losses due to vapor pressure considerations must also be compensated for. This will require the storage of make-up material aboard the spacecraft in the event that the material losses become significant. This extra on-board fluid requirement and its effects on the total mass of the radiator system will depend upon the mission length and vapor pressure of the working fluid at its operating temperature.

4.0 DESIGN CONSIDERATIONS

4.1 Parametric Studies

The success of the belt radiator concept depends upon the ability of the design to satisfy NASA's thermal energy rejection requirements while demonstrating a comparative mass advantage with respect to existing radiator systems (i.e., heat pipe radiator systems). In this section, a parametric evaluation of the equations governing the operational characteristics of a prototypical LBR based on a simple parallel plate configuration are developed. This study examines the effect of optical properties, belt velocities, belt geometrics, operating temperatures, operating mode (sensible heat versus change of phase) and fluid properties on radiator performance.

Particular attention is given to estimating the weight of LBR configurations and determining under what conditions these weights compare favorably to those of heat pipe radiator systems.

These analyses are then applied to three specific cases of interest to NASA covering a temperature range of 311 K-644 K (100-700°F).

4.1.1 Thermal Analysis

The primary task of any radiator system is to provide a means for rejecting heat produced by various spacecraft operations. In space, the only mode of energy transport is radiation. The amount of energy transferred from the belt via radiation depends on the total radiating area, surface optical properties, view factors, and the radiating and background temperature.

A first order heat transfer analysis of the LBR was completed using standard radiative heat transfer relations and certain basic assumptions. The actual energy transfer was assumed to be between only the LBR and space. All effects of the sun and exchange with other portions of the spacecraft or nearby planetary objects were ignored. In addition, these parametric studies assumed space to be at 0 K.

Figure 4.1 depicts the LBR structure used in these parametric analyses and the radiating surfaces of interest. This simple design was considered representative of LBR structures. The two parallel sections comprised the primary radiating surfaces while the top portion was ignored. Analysis has shown this section to be small compared with the two rectangular belt surface areas.

From the same figure, it may be seen that with the outer rectangular surfaces have a view factor to space of unity. The heat exchange to space from the inside belt surfaces must consider the mutual radiant heat exchange between these surfaces. The amount of energy the inside surfaces actually transfer to space may be expressed in terms of the view factor, F. The view factor, F_{ij}, is defined as the fraction of energy emitted from a surface i that is incident upon a surface j. It may also be considered as a geometric parameter referring to how well one surface "sees" or views another.

Since the primary goal is heat rejection, it is desired to maximize the amount of energy transferred to space by an inside surface. For a particular inside surface, the following expression may be written:

$$1 = F_{1TOT} = F_{12} + F_{1\text{-space}} \qquad (4\text{-}1)$$

where F_{12} refers to the energy transfer between inside surfaces 1 and 2 and $F_{1\text{-space}}$ between surface 1 and space. Geometrically it may be seen that F_{12} approaches unity for wide, closely spaced parallel surfaces and goes to zero for well separated ones. Obviously, the latter configuration, where energy transfer to space is maximized, is the best design approach.

From a practical standpoint, however, the optimization of internal view factor must be done with regard to realizable LBR configurations. Figure 4.2 provides a relation for the internal view factor associated with long narrow rectangular plates as a function of the ratio α, α is defined as:

$$\alpha = \frac{\text{Smaller Rectangular Side}}{\text{Separation Distance}}$$

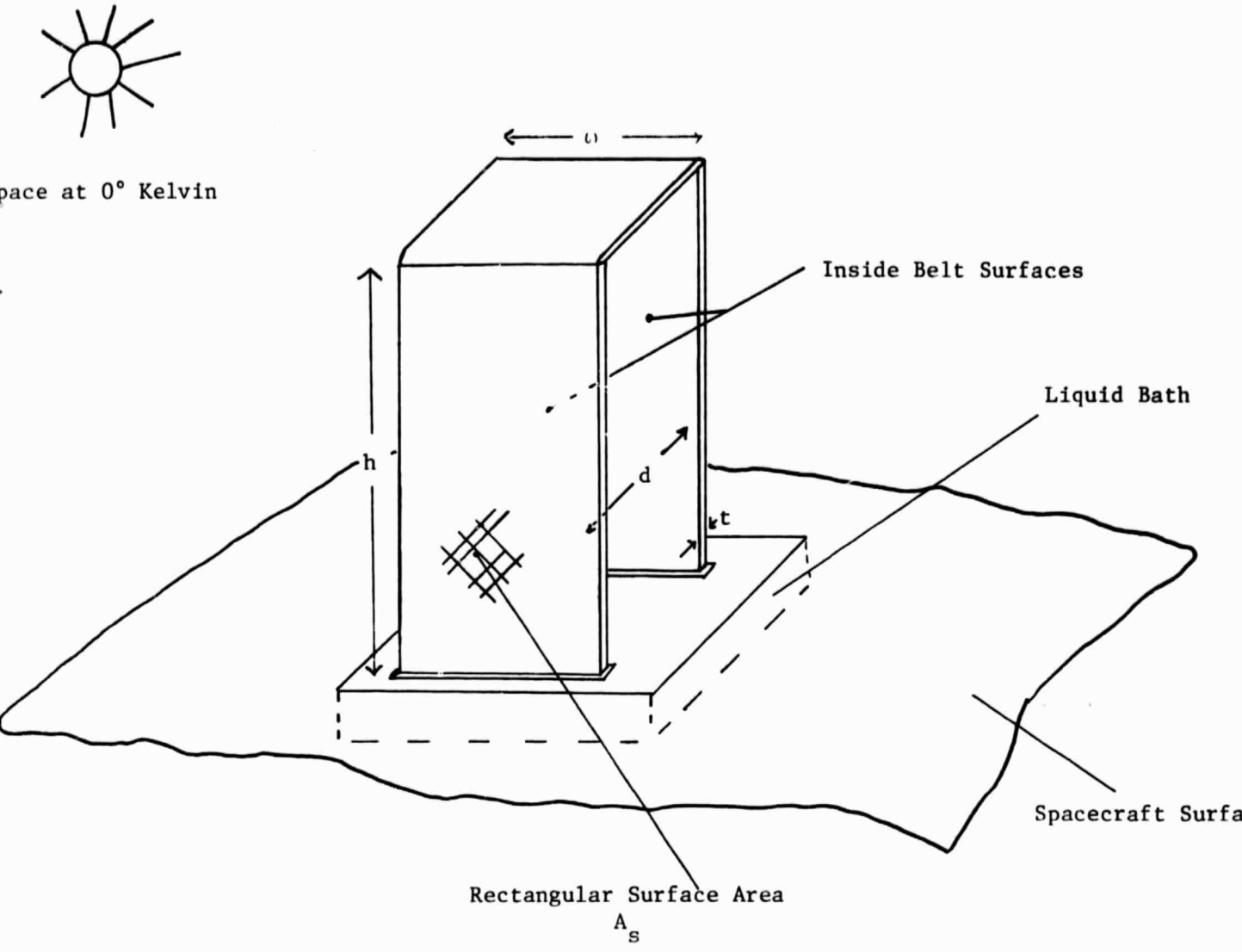

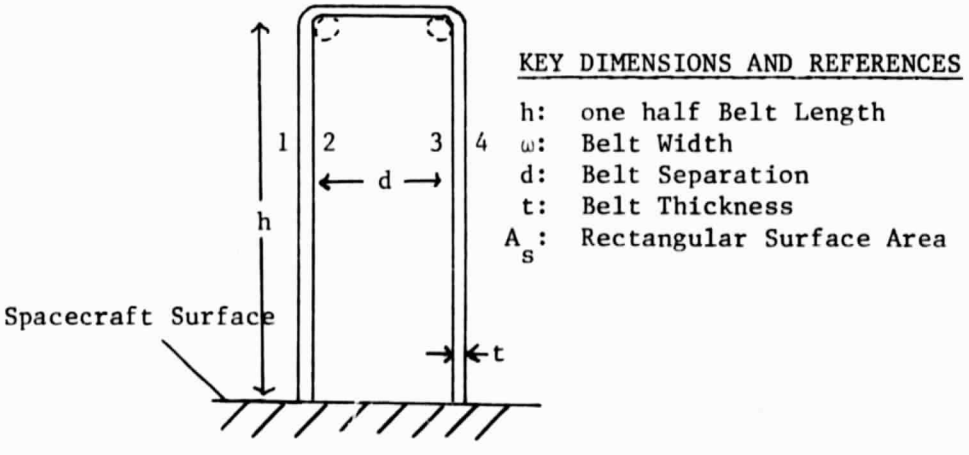

Figure 4.1 PARAMETRIC LIQUID BELT RADIATOR MODEL WITH DEFINED RADIATING SURFACES

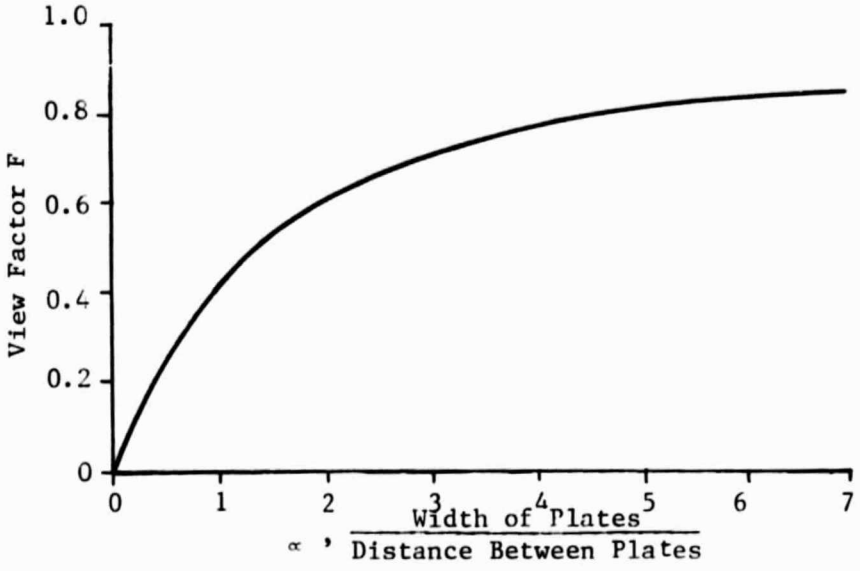

Figure 4.2 VIEW FACTOR F BETWEEN DIRECTLY OPPOSED PARALLEL PLATES, PARAMETRIC MODEL ANALYSES (Rohsenow & Choi, pg 342, 1961)

and may be thought of as the governing design parameter. For example, if α is unity the internal view factor assumes a value of 0.4.

4.1.1.1 Heat Transfer Analysis and Radiative Area Equation Developments

In Appendix D the derivation of the area required to satisfy a given thermal load is presented. This analysis is based on the structure shown in Figure 4.1 and assumes that all belt surfaces have a constant average radiating temperature T_{rad}.

The area required to reject a specified amount of thermal energy, Q_{load} may be expressed in terms of the single sided rectangular surface area A_s, defined in Figure 4.1. A_s may be expressed as:

$$A_s = hw$$

where:

h is the height of the LBR

w is the width of the LBR

From Appendix D, the required area A_s may be written as:

$$A_s = \frac{Q_{Load}}{2(2-F_{23})\ \epsilon_{BR} T_{rad}^4} \qquad (4\text{-}2)$$

where:

T_{rad} = the average radiating temperature associated with the belt surfaces.

F_{23} = the view factor associated with internal belt surfaces 2,3.

ϵ_{BR} = the total hemispherical emissivity (assumed constant for all surfaces).

A_s = the single sided rectangular area.

From Equation 4-2, it may be seen that for a fixed radiating temperature and heat rejection rate (i.e., T_{rad} and Q_{load}) the projected rectangular surface

area A_s varies inversely with the emissivity of the LBR surface and directly with internal view factor F_{23}.

It should be noted that the total effective area required for a specific energy rejection is constant for a given emissivity, Q_{load}, and radiating temperature. In the case of the LBR, an "effective" total radiating area or prime area may be written as:

$$A_{TOT} = 2 A_s (2 - F_{23}) \qquad (4\text{-}3)$$

Thus the effect of the internal view factor is to vary the amount of the actual rectangular surface area, A_s, required.

From the foregoing equations, certain useful relationships can be deduced. Figure 4.3 depicts the rectangular area, A_s versus emissivity relationship associated with conjectured future low and high temperature NASA mission requirements. Extreme values of the internal view factor F_{23} are parameters ($F_{23} = 0$ and $F_{23} = 1$), while emissivity and rectangular area per kilowatt are the respective abcissa and ordinate.

From the curves in Figure 4.3, certain general results are apparent:

- High values of emissivity are required in order to reduce the dimensions of the rectangular area A_s.
- Extreme values of the view factor F_{23} result in required surface rectangular areas (A_s) which differ by a factor of 2. Along with higher emissivity, view factor values less than one but practical from a mechanical design standpoint should be sought.
- Higher values of heat rejection temperature greatly reduce the area required for radiative energy transfer.

4.1.1.2 Modes of Operation

The LBR system can function at two basic operating conditions; the sensible heat rejection mode and the latent heat rejection mode. Each of these is discussed below.

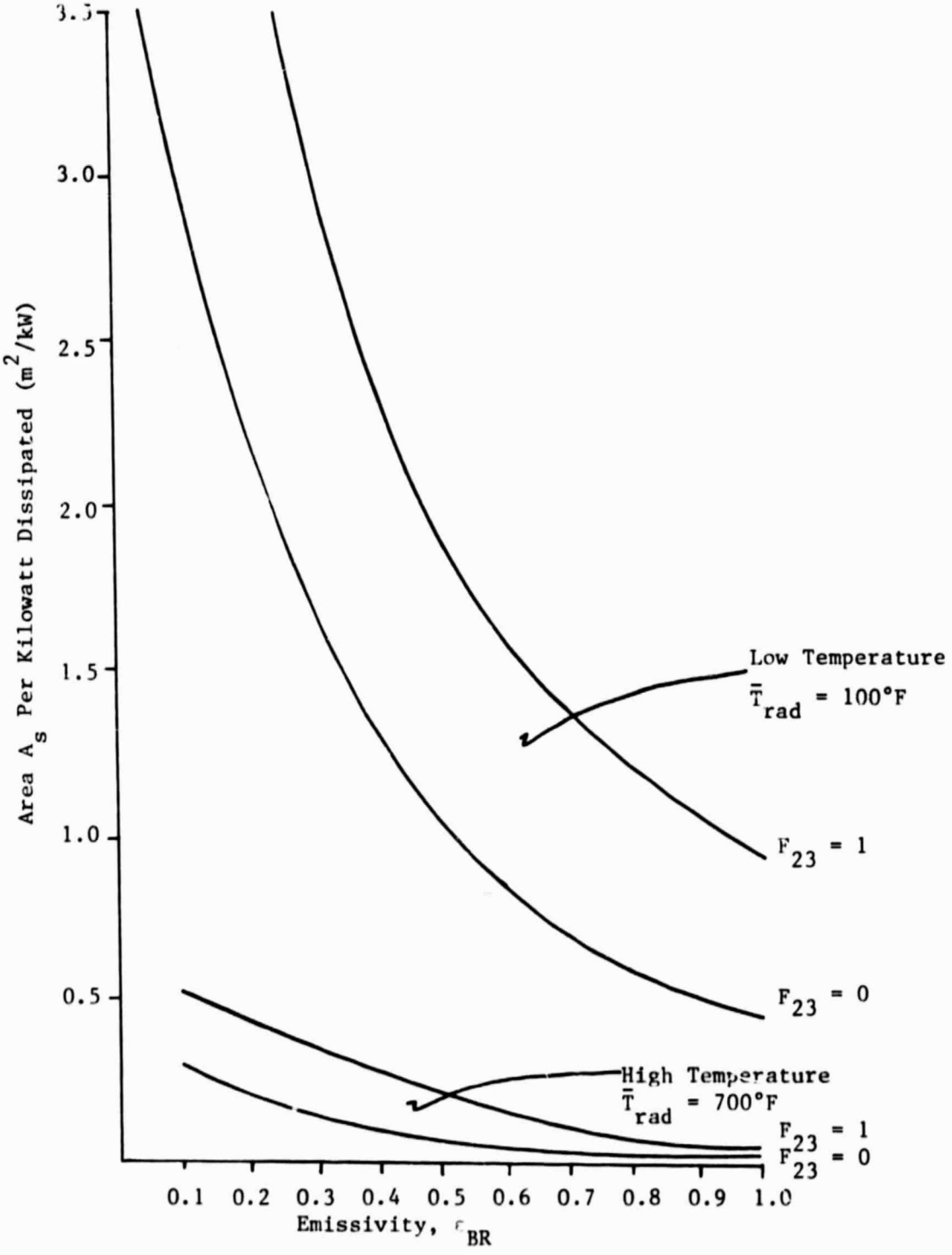

Figure 4.3 EFFECT OF BELT EMISSIVITY ON RADIATOR AREA REQUIREMENTS

The sensible heat mode refers to a condition in which the fluid menisci forming the LBR do not change phase during transport through space. In this mode of operation the radiative heat transfer results in a reduction of the temperature of the LBR between its exit from and entry into the bath. The magnitude of this reduction, in general, will be set by the heat rejection requirements of the spacecraft and depends on a number of parameters including belt thickness and speed. The combined effect of these parameters may be examined through a first law formulation where:

$$Q = (\rho V_b t w) C_p (T_e - T_i) \qquad (4\text{-}4)$$

and:

ρ_{fl}: Density of the working fluid
V_b : Velocity of the belt
t : Thickness of the belt
w : Width of the belt
C_p : Working fluid specific heat
T_e : Working fluid bath exit temperature
T_i : Working fluid bath inlet temperature

In order to reduce LBR mass, it is desirable to minimize the belt thickness, t. So doing however will tend to increase the belt speed, V, since a fixed amount of heat must be rejected along the belt length. The selection of belt thickness and V_b will require trade-offs between radiator weight, structural safety margins, reliability and life.

For the purposes of parametric studies the temperature drop, (T_e-T_i) was kept small in order to avoid the unnecessary (at this level of analysis) complications due to large variations in heat flux along the belt. Using Equation 4-4, the variation of belt velocity with belt thickness and temperature drop was examined. The results obtained are based on a 25 kW thermal load and the use of a diffusion pump working fluid (sp. gr. = 1.05). Figure 4.4 shows the diffusion pump oil working fluid over a 1-50 mil range of belt thicknesses.

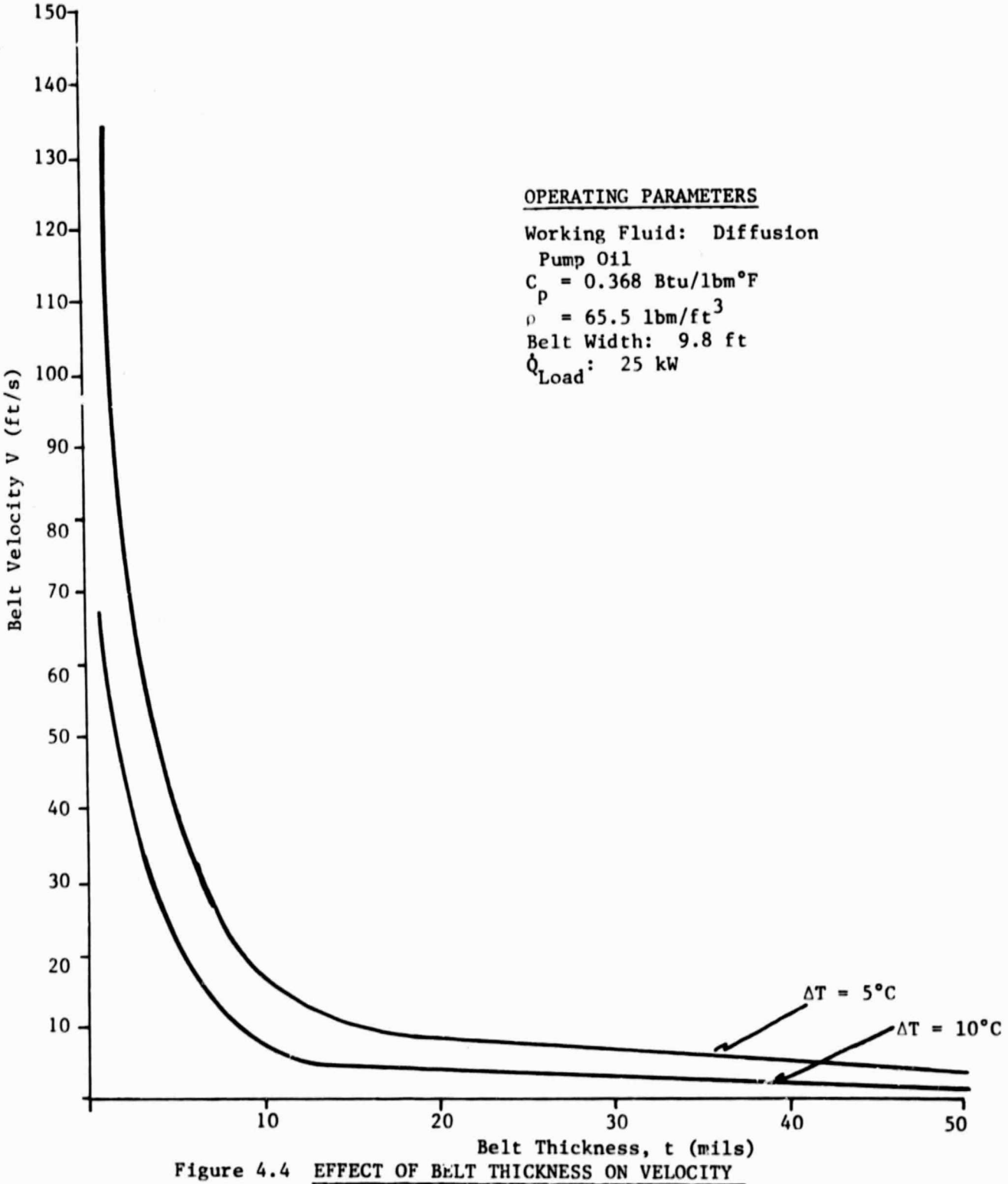

Figure 4.4 EFFECT OF BELT THICKNESS ON VELOCITY

As indicated from the figure, belt thicknesses below 5 mils require speeds in excess of 13 ft/sec for ΔT equal to 10°C, and 27 ft/sec for ΔT equals 5°C. The analysis of Appendix E indicates that belt speeds exceeding this level could cause meniscus stability problems. Therefore for these temperature differences, a diffusion pump working fluid will have a 5 mil belt thickness as the lower bound constraint.

The latent heat mode refers to a change of phase of the working fluid, from a liquid to a solid during its traverse through space. In this mode the ribbon remains at a constant temperature equal to the fusion temperature. The First Law equation governing this mode of operation is given by:

$$Q = (\rho_{fl} V_b w t) h_{\ell s} \qquad (4\text{-}5)$$

where:

- Q = thermal load
- V_b = belt velocity
- $h_{\ell s}$ = heat of fusion
- w = width of belt
- t = thickness of belt
- ρ_{fl} = density of fluid

This equation is the same as for the sensible heat mode except that the heat of fusion, $h_{\ell s}$, replaces the sensible heat term, $C_p (T_e - T_i)$. For lithium the heat of fusion is 19 times the sensible heat associated with a 10°C reduction in temperature. Consequently, the belt velocity required to dissipate a fixed amount of energy in this latent heat mode of operation (i.e., two-phase lithium) is approximately 5 percent of the sensible heat mode speed using the same thickness of material. Smaller parasitic power loads and increased system reliability are the expected advantages of such slower speed phase change operation.

4.1.2 Mass Analysis

As has been stated, in order to be competitive with existing radiator designs, the LBR must offer a distinct mass advantage while simultaneously satisfying the thermal rejection capacities cited by NASA. In this section a first order mass comparison between the belt radiator described in Section 4.1.1.2 and the currently used heat pipe radiator is developed.

4.1.2.1 Mass Ratio ϕ

In order to compare the masses of the LBR and existing systems, the Mass Ratio ϕ was defined. This ratio is expressed by:

$$\phi = \frac{\text{Mass of the Belt Radiator System}}{\text{Mass of the Heat Pipe Radiator}}$$

The details of the derivation of ϕ are given in Appendix F. Both the numerator and denominator of this expression were formulated using certain basic assumptions. For the mass of the LBR:

- The entire space exposed volume of the belt was considered to contain only fluid. Thus the effects of screen material mass were ignored. This assumption is largely justified when the density of the working fluid approximates that of the screen mesh material, as in the case of diffusion pump oils and plastic belt structures.
- The structural mass of the LBR (i.e., deployment system bath heat exchangers, motors, etc.) exclusive of make-up or replacement fluid, was considered by including the mass scaling factor X. The structural mass was defined as being X times the mass of the fluid carried into orbit.

For the mass of the heat pipe radiator:

- A specific mass (i.e., mass per unit prime area) of 4 kg/m^2 was chosen for the baseline heat pipe radiator system. This value corresponds to the range of values cited by NASA.

- The area of the heat pipe radiator (necessary to determine its mass) refers to its prime radiating area.

Using these assumptions (and referring to Appendix F) the Mass Ratio may be expressed as:

$$\phi = \frac{1.1\ \rho_{f1} t\ [1 + X]\ \varepsilon_{HP}}{2\ (2 - F_{23})\ \varepsilon_{BR}} \qquad (4\text{-}6)$$

where:

ρ_{f1} = working fluid density
t = belt thickness
X = mass scaling factor associated with structural elements of the LBR
F_{23} = inside belt surface view factor
ε_{HP} = emissivity of the heat pipe radiator
ε_{BR} = emissivity of the LBR

with all units in the SI system

Since the emissivity of the heat pipe radiator is assumed constant (in the range of 0.75 to 1.0) an order of magnitude examination of the variables in equation 4-6 reveals that the variation of the emissivity of the LBR has the greater significance. In general, the relation for ϕ shows the mass ratio ϕ to be dependent upon:

- The material used as the bath fluid.
- The mass scaling factor X.
- The belt thickness.
- The emissivity of the bath material.
- The view factor associated with inside belt surfaces.

Section 4.1.3 will consider in greater detail the consequences of this equation for low and high temperature themal requirements.

4.1.3 Applications of Rectangular Area and the Mass Ratio ϕ Equations

The equations developed to estimate LBR area requirements and Mass Ratios were applied to a range of mission requirements of interest to NASA. These requirements include:

- Low Temperature heat rejection (311 K, 100°F) corresponding to the need to reject heat dissipated in spacecraft electronic components.
- Medium Temperature heat rejection (422 K, 300°F) corresponding to heat rejection from a range of moderate temperature thermal power systems.
- High Temperature heat rejection (644 K, 700°F) corresponding to heat rejection from advanced, high temperature, thermal power systems.

4.1.3.1. Low Temperature Heat Rejection

In this application, the thermal loading was fixed at 25 kW and the bath or heat sink temperature set at 311 K (100°F). The LBR design utilizes a sensible heat transfer mode employing a low vapor pressure diffusion pump oil. For the temperature ranges of interest, the vapor pressure of such materials is of the order of 10^{-8} torr, resulting in negligible evaporation losses to space.

A ΔT (i.e., the difference between the exit and inlet bath temperatures) of 10°C was chosen. Assuming the belt to exit at the bath temperature (in this case the specified heat sink temperature of 311 K) an average radiating temperature of 306 K was determined. Using Equation 4-2, the rectangular Area A_s was plotted as a function of the emissivity, with internal view factor F_{23} as the parameter. From Figure 4.5 it may be easily seen that this relation is hyperbolic, and very dependent on the emissivity. For example, it may be seen from the figure that an emissivity of 0.6 yields a rectangular area A_s of approximately 21 m^2 as the internal view factor approaches zero.

Figure 4.6 portrays the Mass Ratio ϕ, emissivity variation with F_{23} as the parameter. Using Santovac 5 (a product of the Monsanto Corp.) as the working fluid, ϕ may be evaluated. In this case the mass scaling factor X was assumed to be two and the heat pipe radiator emissivity 0.85. From Figure 4.6, it can

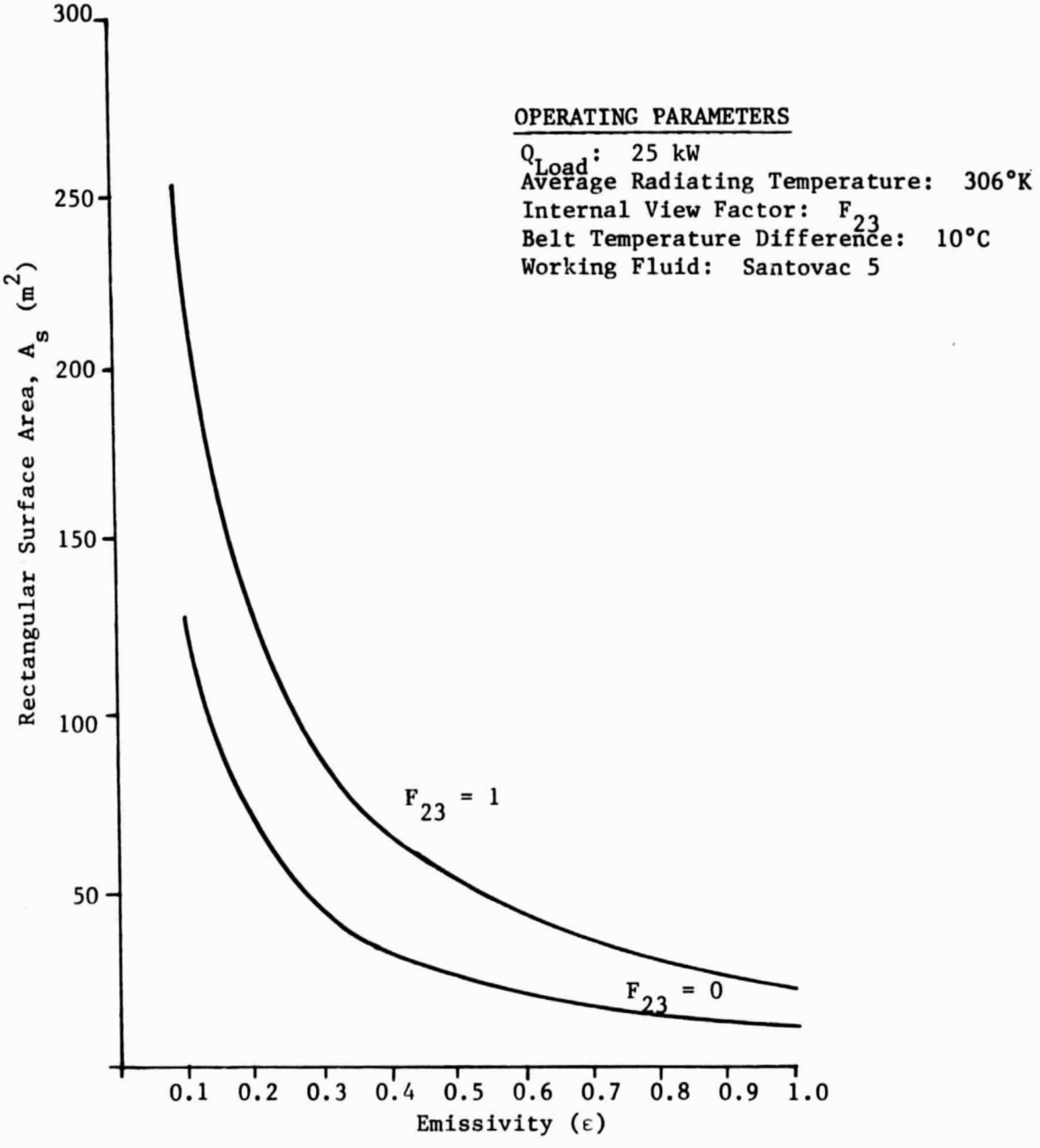

Figure 4.5 RECTANGULAR SURFACE AREA A_s VERSUS EMISSIVITY FOR LOW TEMPERATURE HEAT REJECTION WITH SANTOVAC 5

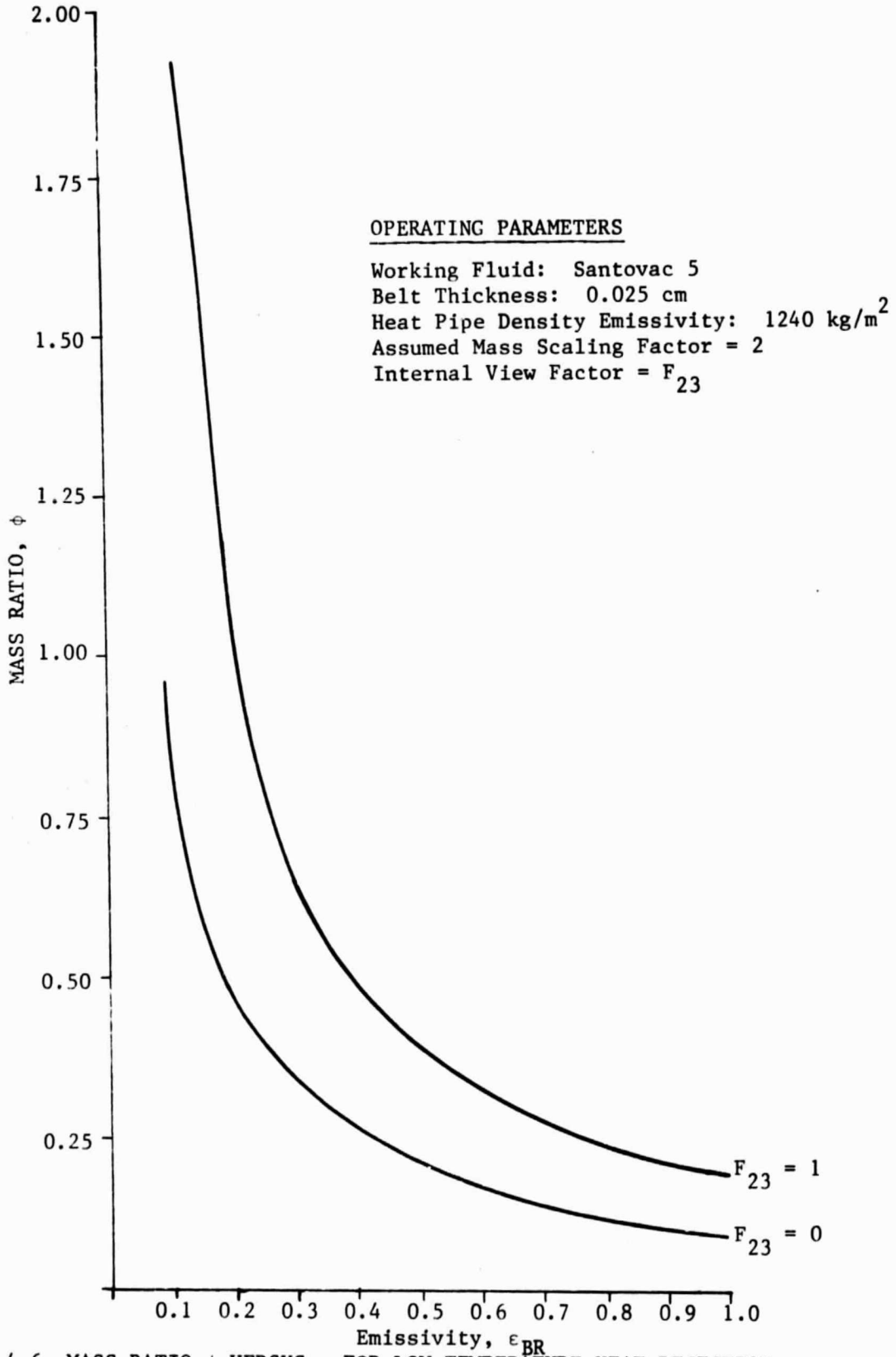

Figure 4.6 MASS RATIO ϕ VERSUS ε FOR LOW TEMPERATURE HEAT REJECTION

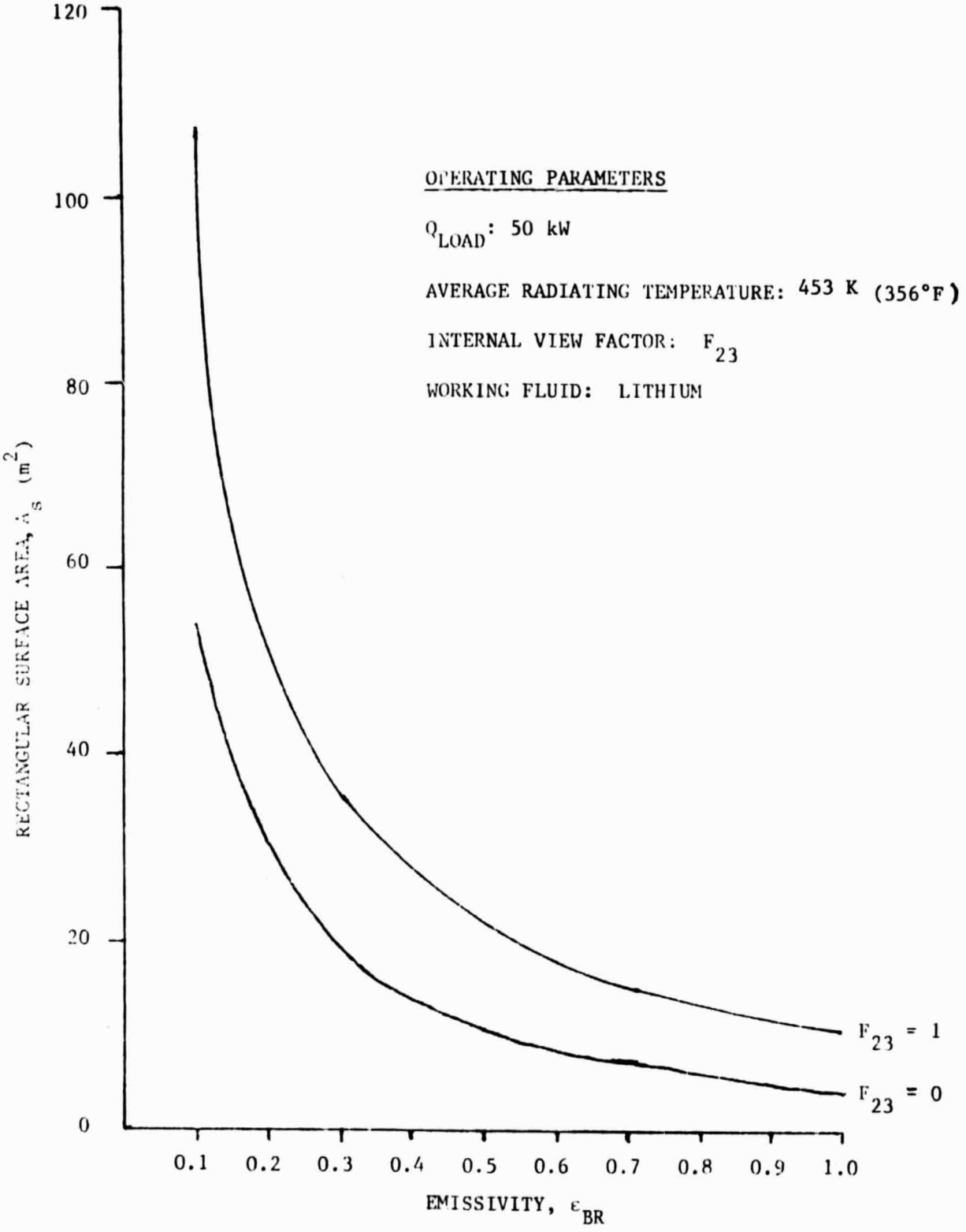

Figure 4.7 RECTANGULAR SURFACE AREA, A_s vs WORKING FLUID EMISSIVITY, ε_{BR} FOR INTERMEDIATE TEMPERATURE HEAT REJECTION

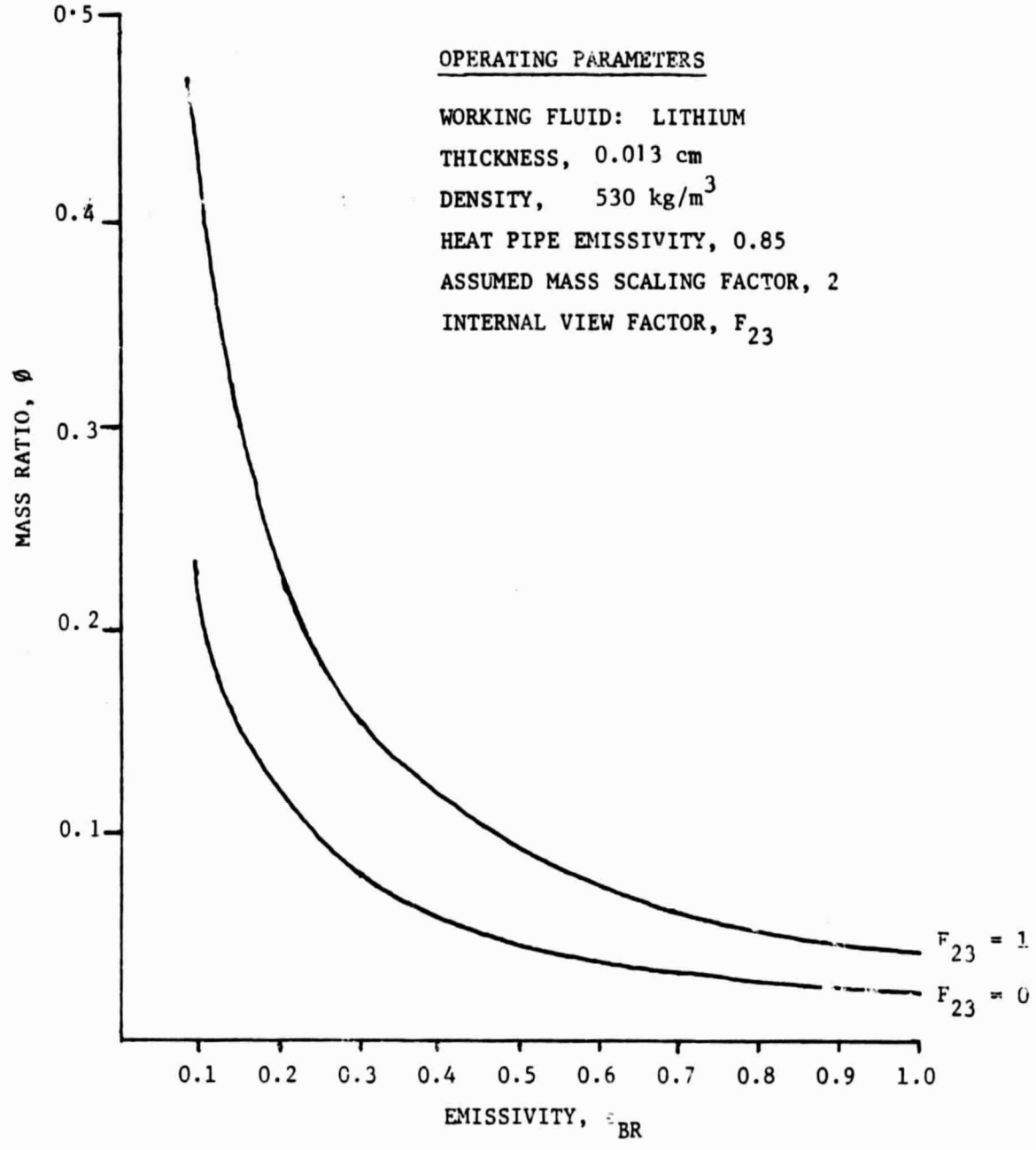

Figure 4.8 MASS RATIO Ø, vs WORKING FLUID EMISSIVITY, ε_{BR} FOR INTERMEDIATE TEMPERATURE HEAT REJECTION

be seen that as the internal view factor approaches 0 and the emissivity becomes greater than 0.5, distinct mass advantages accrue to the LBR. For example, as the view factor goes to zero an emissivity of 0.7 results in the mass of the LBR being only 14 percent of a heat pipe radiator in the same application.

4.1.3.2 Intermediate Level Heat Rejection

In this case, the latent heat mode of operation was employed using two-phase lithium as the coolant material. The thermal rejection rate was set at 50 kW with the radiating temperature set at the melting point of lithium. As discussed in Section 4.1.1 the latent heat mode of operation assumes that the working fluid's thermodynamic state varies from a saturated liquid at the bath outlet to a saturated solid at the inlet.

Since the melting point of lithium is 453 K, an average radiating temperature of 453 K was used. Figure 4.7 displays the rectangular area A_s versus emissivity ε_{BR}, using the internal view factor F_{23} as parameter. Because of the higher radiating temperature, the areas required for energy transfer are significantly lower than those of the low temperature sensible heat mode case. For example, with an emissivity of 0.1 and F_{23} approaching zero, the rectangular area required for radiative heat transfer is approximately 66 square meters (710 ft^2).

The variation of the ratio ϕ with emissivity is shown in Figure 4.8. In this case we have assumed a belt thickness of five mils, a structural mass scaling factor X of two, and the emissivity of the heat pipe to be 0.85. Because of the low density of lithium, the LBR offers distinct advantages with respect to the heat pipe radiator. For view factors approaching zero, emissivities of the order of 0.2 still result in an LBR with a mass of only 12 percent of that of a heat pipe radiator in the same application.

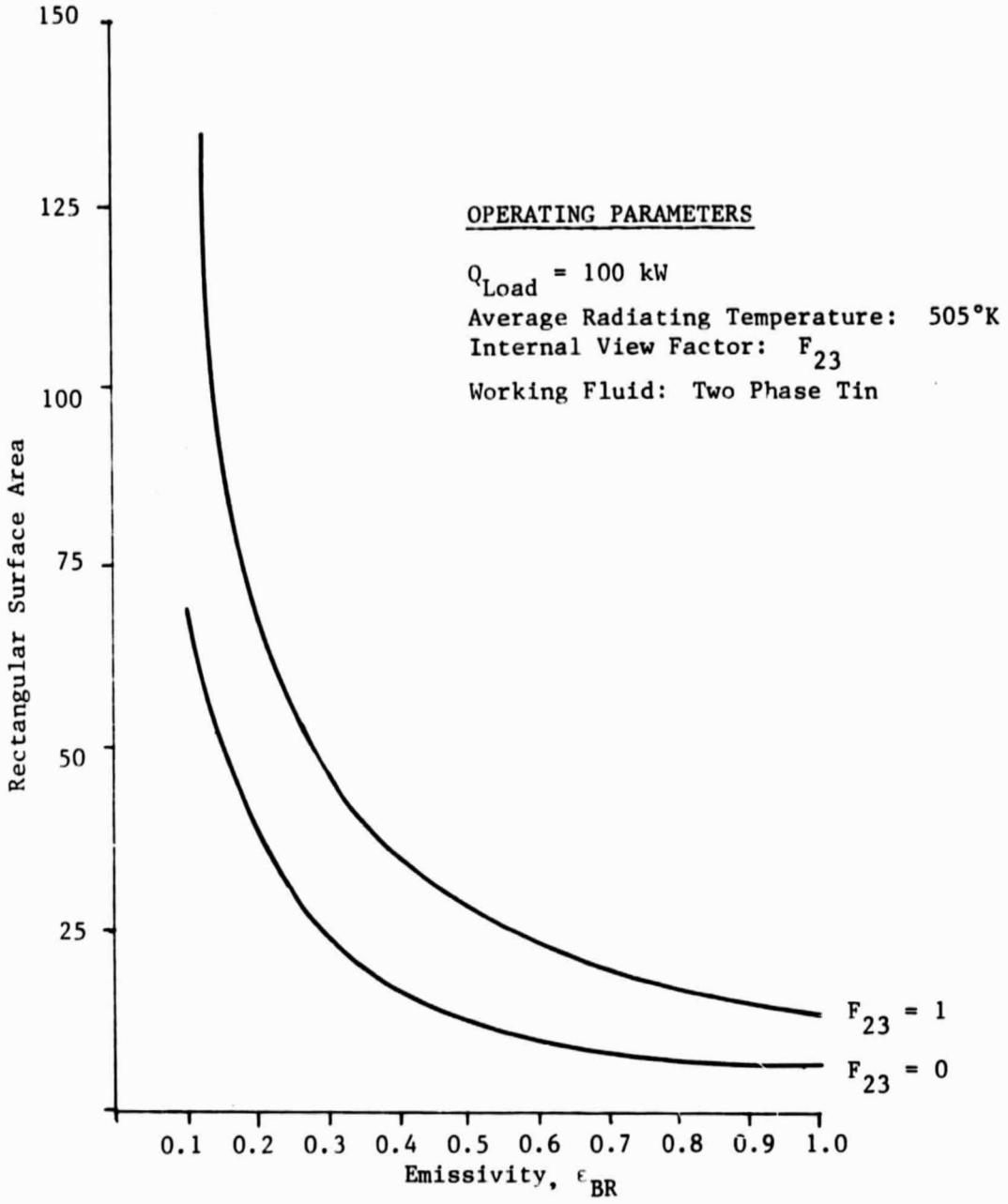

Figure 4.9 RECTANGULAR SURFACE AREA A_s VERSUS EMISSIVITY FOR HIGH TEMPERATURE HEAT REJECTION

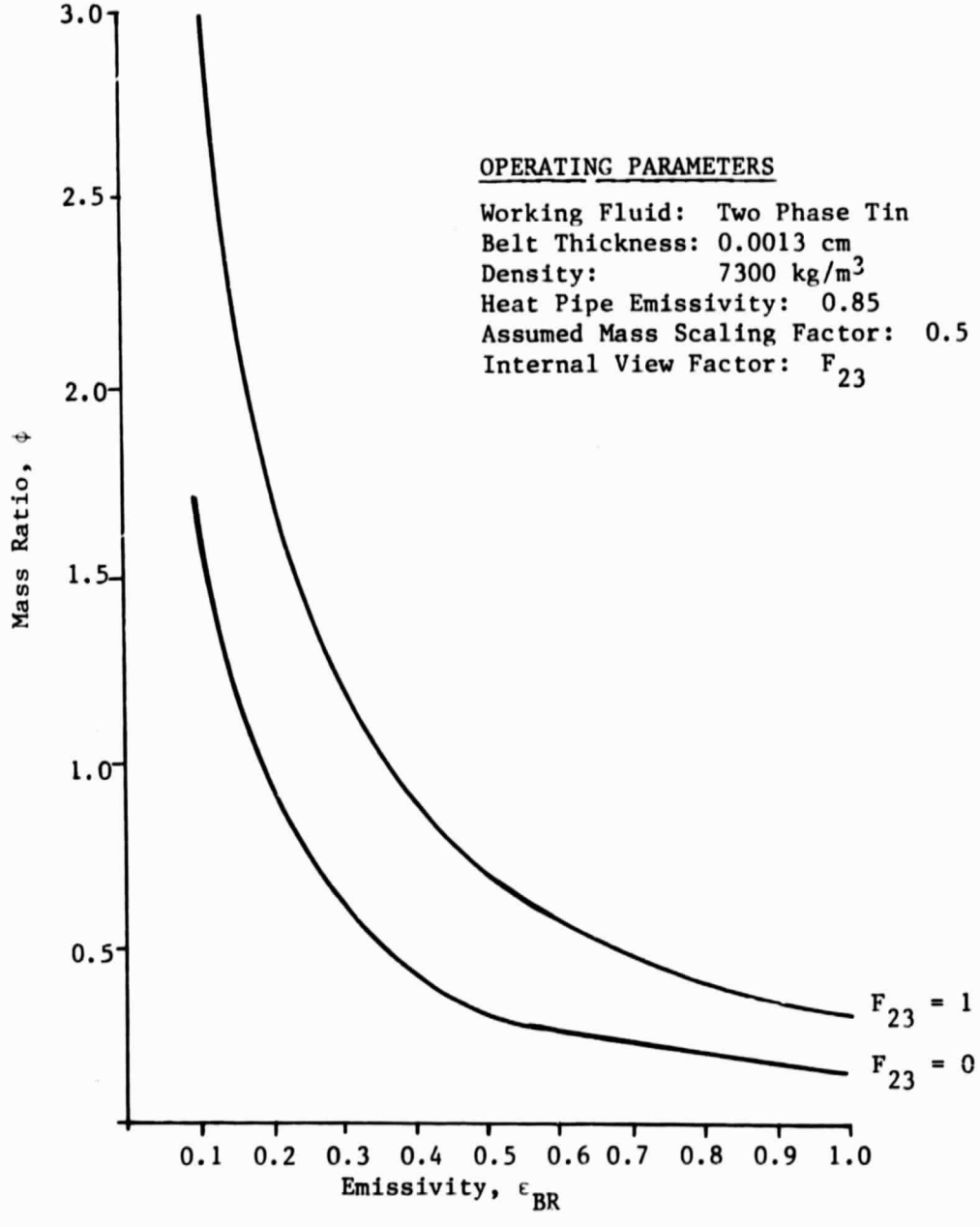

Figure 4.10 MASS RATIO ϕ VERSUS EMISSIVITY ε FOR HIGH TEMPERATURE HEAT REJECTION

4.1.3.3 High Temperature Heat Rejection

The rejection of 100 kW of thermal power is presented in this section. A latent heat mode of operation using tin as the bath fluid has been employed.

The high density of tin (ρ = 7300 kg/m^3) poses some difficulty in achieving a comparable mass advantage with respect to heat pipe radiators. Figures 4.9 and 4.10 portray the rectangular area A_s and mass ratio ϕ versus emissivity and internal view factor. From Figure 4.10 it may be seen that for the application to be advantageous not only must the structural mass be small but the emissivity of the bath material must be sufficiently large as well. For example if X is 0.5, and the view factor F_{23} is unity, the emissivity of the tin must be greater than 0.3 for the LBR to offer an advantage when compared with a heat pipe radiator.

4.1.4 Parametric Study Conclusions

The parametric studies described in the previous sections were conducted to determine the importance of a number of properties on the performance of the LBR. These investigations were carried out using the simple parallel plate LBR design discussed in Section 4.1.1. Certain general conclusions may be drawn from these studies:

- It is critically important to develop a design that utilizes high emissivity working fluids or makes provisions for emissivity enhancement via texturing or surface contamination.
- The weight of the deployment structure (X in the parametric studies) must be minimized in order for an LBR design to be feasible. Innovative concepts, which do not require large structures for deployment or stability are required.
- A design which effectively maximizes the exposure of all belt surfaces to space is necessary. As documented in the parametric study, the required single-sided surface area can be greatly reduced by the proper geometrical arrangement of belt surfaces (i.e., maximizing the amount that a surface "sees" of space).

The technique of emissivity enhancement by means of surface texturing is discussed in greater detail in Appendix G. The contamination of a surface to increase surface emissivity is a concept that requires additional study. The most important concern in contamination enhancement is that the dopeant remain molecularly bound to the working fluid and unperturbed by thermal cycling and the environment of space.

The importance of the LBR deployment structure has been stated. In Section 4.? alternative concepts are explored and the scheme chosen for use in the point design described.

4.2 Storage and Deployment Concepts

During the course of the LBR development program, two deployment/storage schemes were considered. These were:

- A telescoping T-type boom with four rollers.
- A centrifugally actuated flexible cylindrical belt.

Salient features of each design are presented in Table 4.1. Figures 4.11 and 4.12 schematically portray these concepts.

4.2.1 Telescoping Boom (T-Boom) Deployment System

The T-boom deployment design (Figure 4.11) was the first deployment concept developed and originated from the parallel plate design used in the parametric studies of Section 4.1. The knowledge that similar telescoping technology is currently being developed by a number of manufacturers for use in space applications gave credibility to this concept.

The T-boom structure consisted of two telescopic booms made from aluminum or magnesium which deployed the screen mesh structure across four rotating rollers. The rollers were mounted with sprockets at each end so that the screen could be advanced through space and the bath. Two of these rollers were located inside

Table 4.1

LBR BELT DEPLOYMENT SCHEMES

	Name	Description	Advantages	Disadvantages
(1)	Extended Roller Actuation	o Stowed roller extends out by actuators o Motion multiplied by mechanism	o May be able to remain deployed during maneuvers o High probability of proper deployment o Reversible for stowage during maneuvers*	o Weight o Complexity
(2)	Centripetal Actuation	o Centripetal force of belt motion provides deployment	o Very simple and potentially reliable o Lightweight o Reversible for stowage during maneuvers	o Uncertain dynamics o Shape will deform during maneuvering

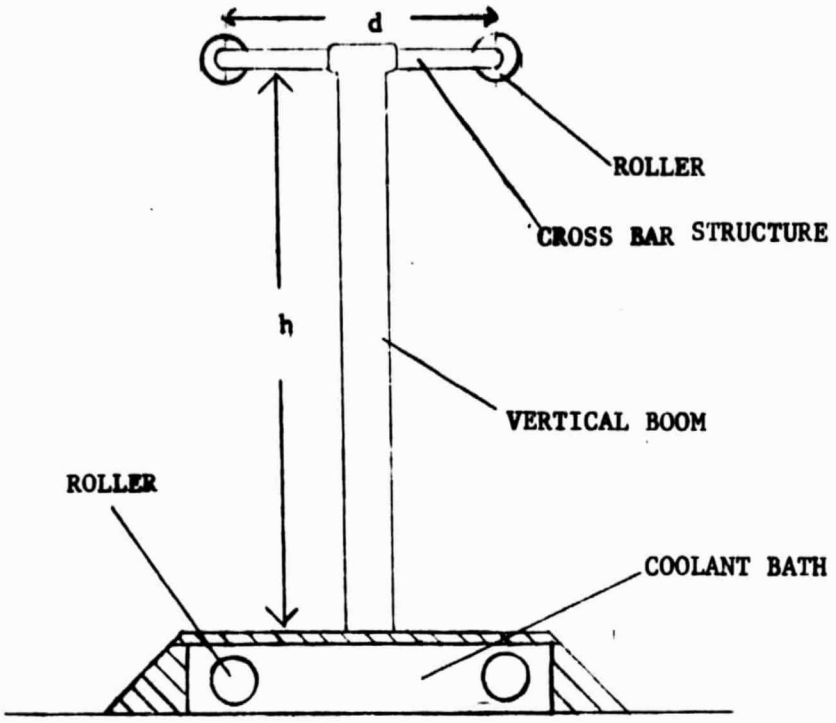

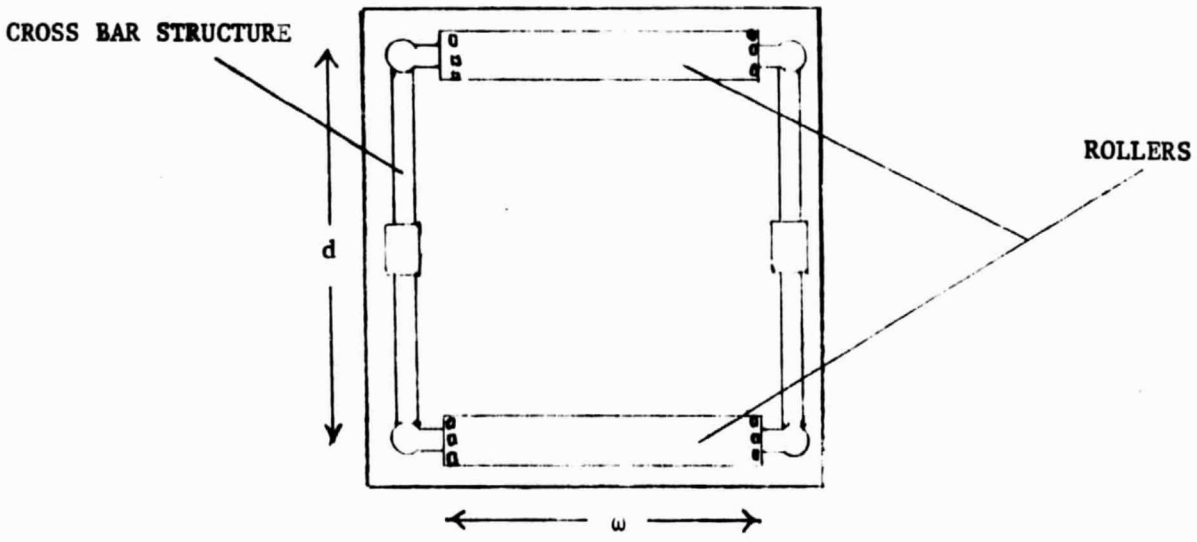

Figure 4.11 T-BOOM LBR DEPLOYMENT STRUCTURE

the bath containment vessel, while the others were exposed to the space environment.

The dimensions of the telescopic boom deployment system were fixed by the total area required to dissipate a particular thermal load. The telescoping character was thought to allow for a compact stowed configuration.

Table 4.2 indicates preliminary estimates of the weights of such boom structures for a low temperature heat rejection case and compares them with that of the radiator structure itself (liquid material). As indicated, the boom structures considered could be from 1/2 to 10 times the weight of the belt itself. The boom structures considered were by no means optimum. Nevertheless the analysis indicated that they would add significantly to overall system weight. Also, the roller arrangements indicated added to system complexity and possibly increase the reliability problems over long-term operation.

4.2.2 Cylindrical Hoop LBR Design

Due to the inadequacies of the telescoping boom deployment system, an alternative design was considered. A structure showing great promise is a free standing cylindrical belt radiator, resembling a large flexible hoop. This design is characterized by centripetal actuation and the absence of external belt supports. In theory the radial forces associated with rotational motion in the steady state would lead to the formation of a stable cylindrical shape. The size of this LBR design (i.e., the cylinder width and diameter) would be fixed by the radiative heat transfer requirements associated with a particular mission.

The steady state cylindrical LBR design is projected to have a number of salient advantages. These include:

- A simple, gradually curved shape which averages centripetal forces over all belt segments.
- The absence of structural supports as a result of centripetal actuation, tending to minimize system weight.

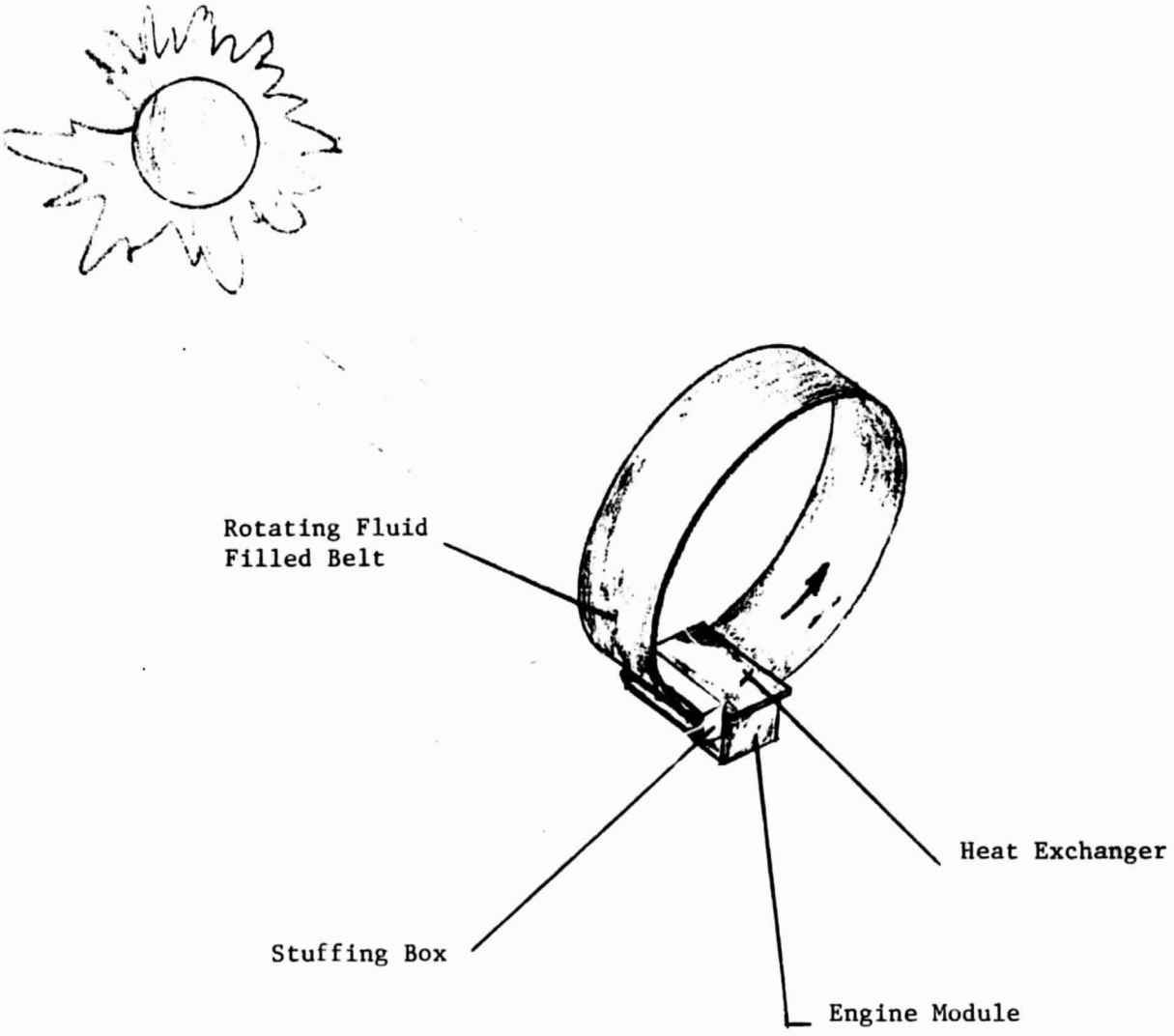

Figure 4.12 CONCEPTUAL DRAWING OF CYLINDRICAL HOOP LBR SYSTEM

Table 4.2

MASS SUMMARY: LOW TEMPERATURE T-BOOM LBR SYSTEM

A) Deployment System

	Length (ft)	Diamter (inches)	Thickness (inches)	Mass: Aluminum (lbm)	Mass: Magnesium (lbm)
Telescopic Boom	21.5	6	0.025	23.3	15.0
Cross Bar Struts	9.8	3	0.025	5.3	3.4
Roller Elements	9.8	12	0.015	26.7	17.2

Total Mass:

Aluminum - 55.3 lbm

Magnesium - 35.7 lbm

B) Radiator Mass (ie: $M_{mat'l}$) - 25.8 lbm

C) Mass Scaling Factor, X

with Aluminum $\equiv \frac{55.3}{25.8} \equiv 2.14$

with Magnesium $\equiv \frac{35.7}{25.8} \equiv 1.38$

- The utilization of more of the total available area for radiative heat transfer (thus potentially reducing both system size and weight).

This last point is a result of the shape of LBR and arises due to the excellent view factor of the inside cylinder surface to space. The development of the geometrical view factor for a cylindrical structure is presented in Appendix H, with the results displayed in Figure 4.13. Referring to this figure, it can be seen that a cylindrical design with a diameter to width ratio of four will have approximately 90 percent of its total surface area (inner and outer belt surfaces) participating in the radiative energy transfer process. This value corresponds to an internal surface view factor approaching zero. From the parametric studies of Section 4.1.1 this implies a full utilization of all radiating surfaces, and the reduction of both the size and weight of the LBR.

Preliminary conceptualizations of the cylindrical LBR design include three major equipment components:

- Four rollers with associated belt drives, motors, and supports which advance the belt through space.
- A "stuffing box" used to store the belt during maneuvers, launch, or non-use.
- A compact interfact heat exchanger which transfers reject heat from a power cycle to the working fluid of the LBR.

Figure 4.14 is a schematic of these structures assuming the belt is fully deployed in its cylindrical steady state form.

Future efforts will be directed at enhancing overall cylindrical LBR system thermal and weight performance. Additional areas requiring design work necessary to further develop these preliminary equipment concepts are discussed below.

ORIGINAL PAGE IS
OF POOR QUALITY

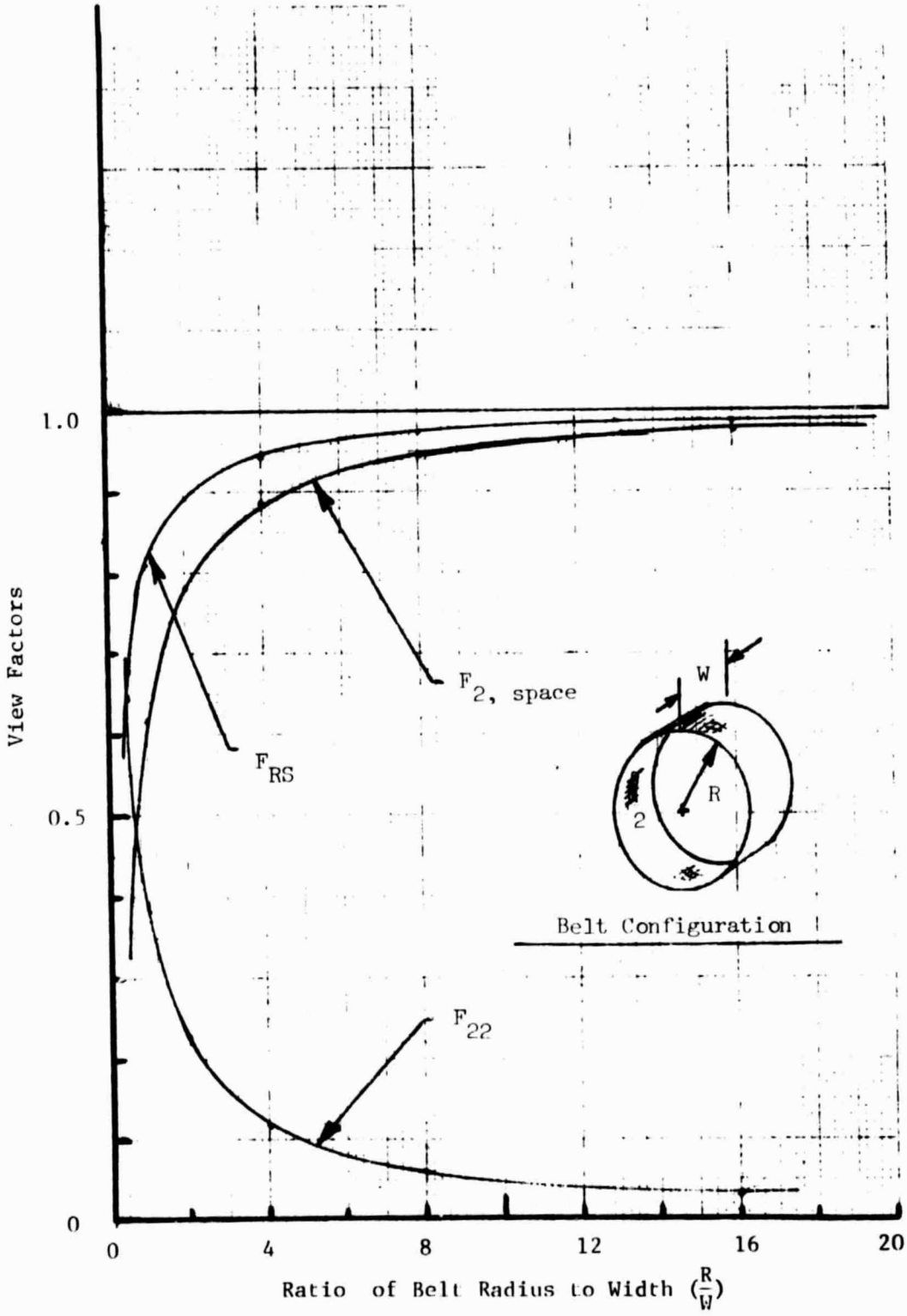

Figure 4.13 VIEW FACTORS FOR CYLINDRICAL LBR CONFIGURATION

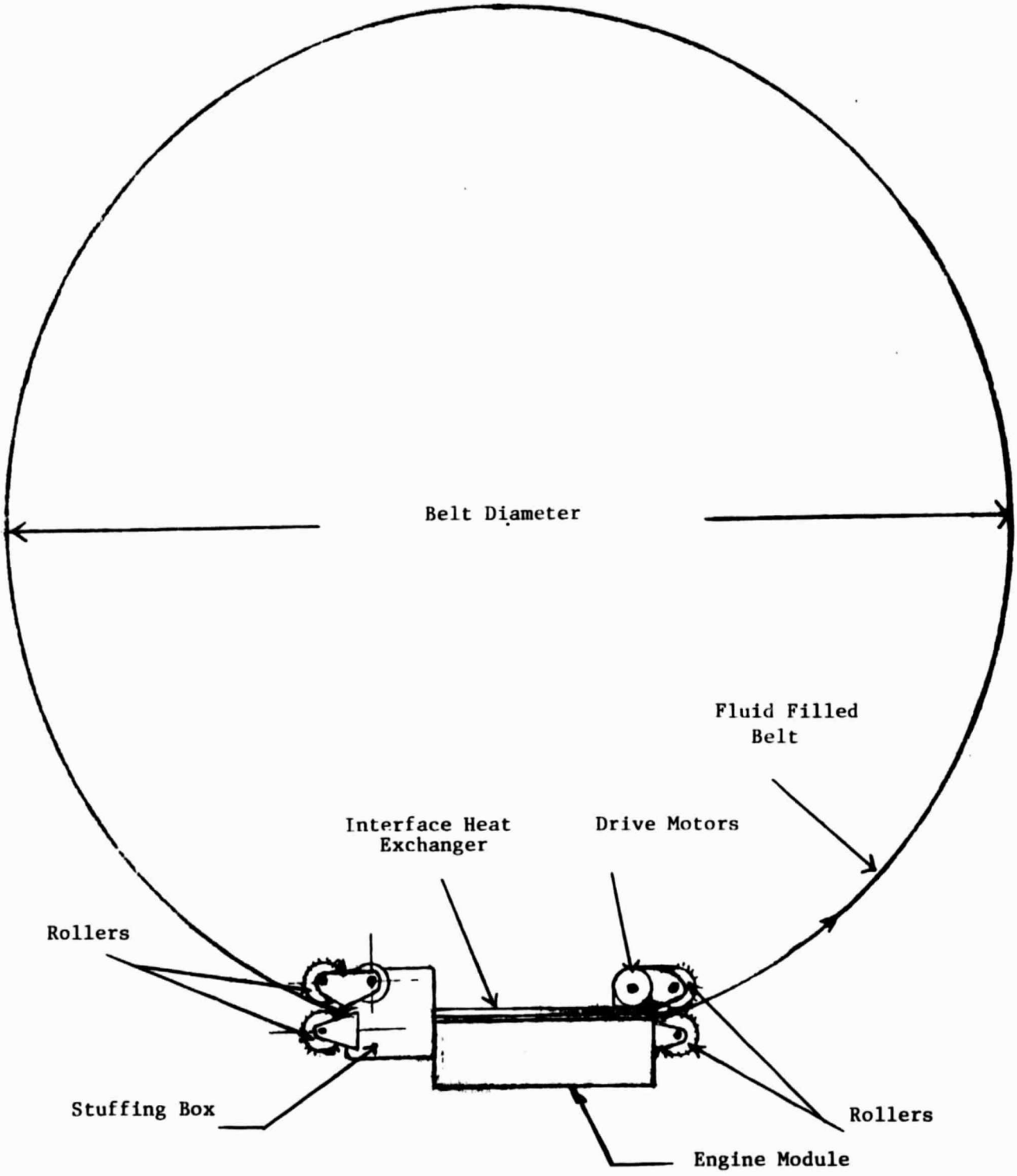

Figure 4.14 PRELIMINARY REQUIREMENTS AND LOCATION OF CYLINDRICAL LBR EQUIPMENT.

4.2.2.1 Transition to the Steady State

An important issue associated with the cylindrical LBR is the transition from a stowed to a fully deployed hoop-like configuration. This process is a very complex dynamic phenomenon involving the interaction of bending stresses and radial accelerations in a zero gravity environment. Intuitively, it appears that like a cowboy's lasso rope, the moving belt will assume a cylindrical shape over time. The proof of this, however, is believed quite difficult, especially if the belt assumes an arbitrary shape when initially removed from the stuffing box. Rigorous analysis would require use of the minimum energy principle and other advanced formulations of dynamic analysis. The goal of such analysis would be to demonstrate that the net force acting on the belt is expansive and that the cylindrical shape is indeed the configuration associated with stable equilibrium. This analysis is beyond the scope of this program and must be addressed in additional studies. For purposes of this study it is assumed that the LBR will in time assume a stable cylindrical shape as a result of motion induced forces.

4.2.2.2 Stowage and Deployment of the Cylindrical LBR

Various methods of deployment and stowage for the cylindrical LBR design have been examined. The scope of the present program has precluded any rigorous design analysis. Consequently the concepts presented here are still only in the feasibility stage and will require additional study. Only when these detailed design evaluations are completed can the true merit of any particular deployment or stowage strategy be realized.

Two methods of cylindrical LBR deployment are described in the next paragraphs. The Stinger Boom Deployment operational sequence would be as follows:

Step 1: A very lightweight extendable boom would stretch the dry mesh into an elongated shape before the roller system imparts motion to the belt.

Step 2: The rollers are actuated to impose linear motion on the belt. The lightweight extendable boom progressively collapses when the belt has a circular or nearly circular shape. At this time it is hypothesized that the belt shape is determined by centrifugal forces alone, with the extendable boom serving no structural purpose.

Step 3: Once the belt is in its equilibrium condition, bath material can be introduced into the primary heat rejection volume containing the moving belt and interface heat exchangers. The system would then be operational.

The Roller Advance Deployment operational sequence may be described as follows:

Step 1: After orbital insertion drive motors on the outgoing end of the LBR will move the belt out of the stuffing box and into space. The operation will continue until all of the stowed belt is pulled from the stuffing box. At this point, a motor will activate the incoming rollers. The belt existing from the stuffing box will carry working fluid into space.

Step 2: Due to the zero gravity field, the belt will initially float loosely in space. As the incoming rollers move the belt into the heat exchanger, the belt will experience centripetal forces and in time establish a cylindrical configuration.

Both concepts need further design and development work in order to determine their utility as cylindrical LBR deployment schemes. It is also recognized that other methods of deployment are possible and worthy of study. For the purposes of this program, the roller advance concept was chosen to deploy the LBR.

In order to store the LBR before operation, the majority of the belt structure (including working fluid) is to be folded up on itself and stored within the stuffing box (Figure 4.15). The remainder of the belt is to be looped tightly about the top rollers (not seen in Figure).

ORIGINAL PAGE IS
OF POOR QUALITY

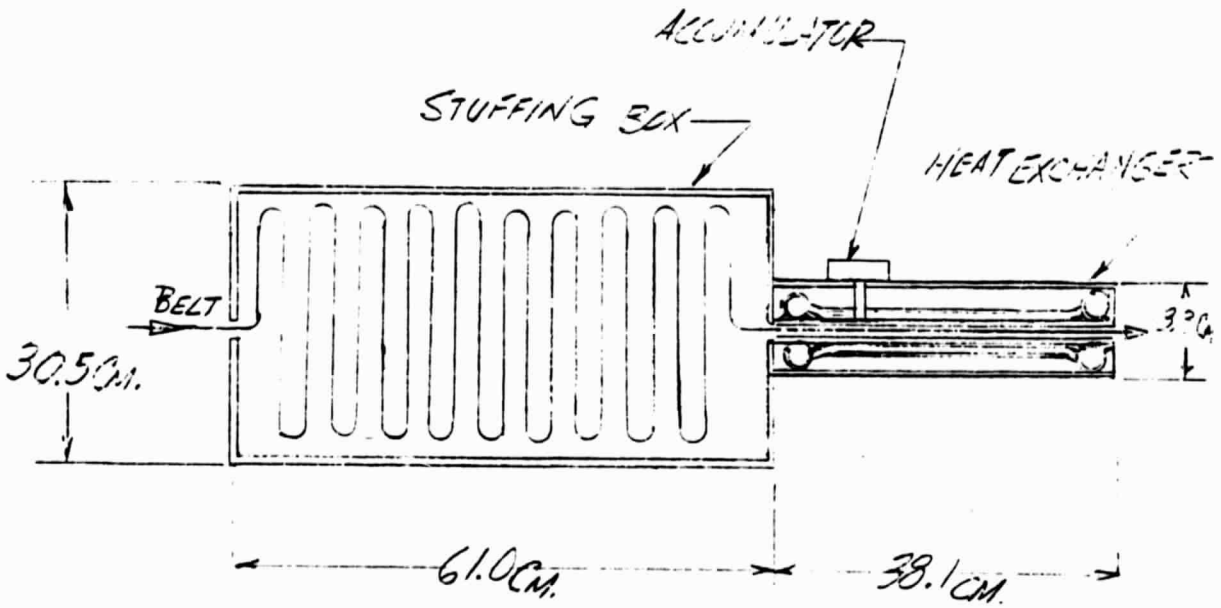

Figure 4.15 STOWED CYCLINDRICAL LBR

One assembly concept is to situate the top half of the LBR (rollers, belt, etc.) within a jettisonable or servo-operated container. This motor controlled container would provide an element of protection if the belt is redrawn into its stowed position. This stowage design could however increase system weight and complexity and its merit must be carefully examined in further development studies.

4.2.2.3 Dynamic Consideration

In addition to the transition dynamics discussed in Section 4.2.2.1, the cylindrical LBR could potentially face a number of other dynamics problems. While offering the advantage of reduced system weight, the absence of structural supports would result in a flexible structure susceptible to a variety of disturbances. Possible dynamic disturbances include:

- Vehicle or power cycle vibrations.
- Spacecraft maneuvers.
- Effects of the solar wind.
- Corilois effects.

While these conditions require more thorough investigation, preliminary analyses suggest that the LBR be returned to the stowed position in the event of vehicle maneuvers or potential disturbances. Mechanical damper or spring-like systems may also be applied to effectively reduce dynamic oscillations or instabilities.

4.3 Design Conclusions

Despite the uncertainties associated with the cylindrical LBR design, this concept offers many potential advantages including low weight and ease of storage. It is believed that the development of the cylindrical LBR will offer a lightweight, thermally effective space radiator capable of being utilized in a variety of applications. For this reason, the cylindrical LBR design was employed in the point design studies presented in Section 5.0.

5.0 POINT DESIGN STUDY

5.1 Mission Description

In this section, the cylindrical LBR concept is applied to a specific mission requirement defined by NASA LeRc. The system considered is a 37.5 kW (electric) Brayton cycle power plant.

The design parameters provided by NASA which most influence LBR size and material selection are:

- o The requirement to reject 75 kW of thermal energy.
- o A power cycle (closed cycle Brayton) which rejects heat over the temperature range from 458 K (365.5°F) to 315 K (108°F).
- o A background space temperature of 250 K (-9.4°F).

Of the above, the fact that the power cycle rejects heat over a wide temperature range represents the largest deviation from the parametric analysis of Section 4.1. With materials identified to date these requirements present three possibilities for configuring the engine heat rejection/LBR system (Figure 5.1).

5.1.1 Option 1 - Latent Heat With Gallium

The heat from the power cycle could all be rejected to a heat sink comprised of molten gallium at a temperature of approximately 310 K (98.6°F). The molten gallium would then be drawn through space and undergo a phase change (at 302.8 K) during the process of dissipating the thermal energy. This option has the advantage of utilizing the large amounts of energy associated with the change of phase. However, it has the disadvantage of rejecting all the heat at the relatively low radiator temperature of 303 K (86°F, the fusion temperature of Gallium) despite the fact that the engine rejects its heat over a temperature range up to approximately 460 K (369°F). This results in relatively large radiator areas as compared to the other options.

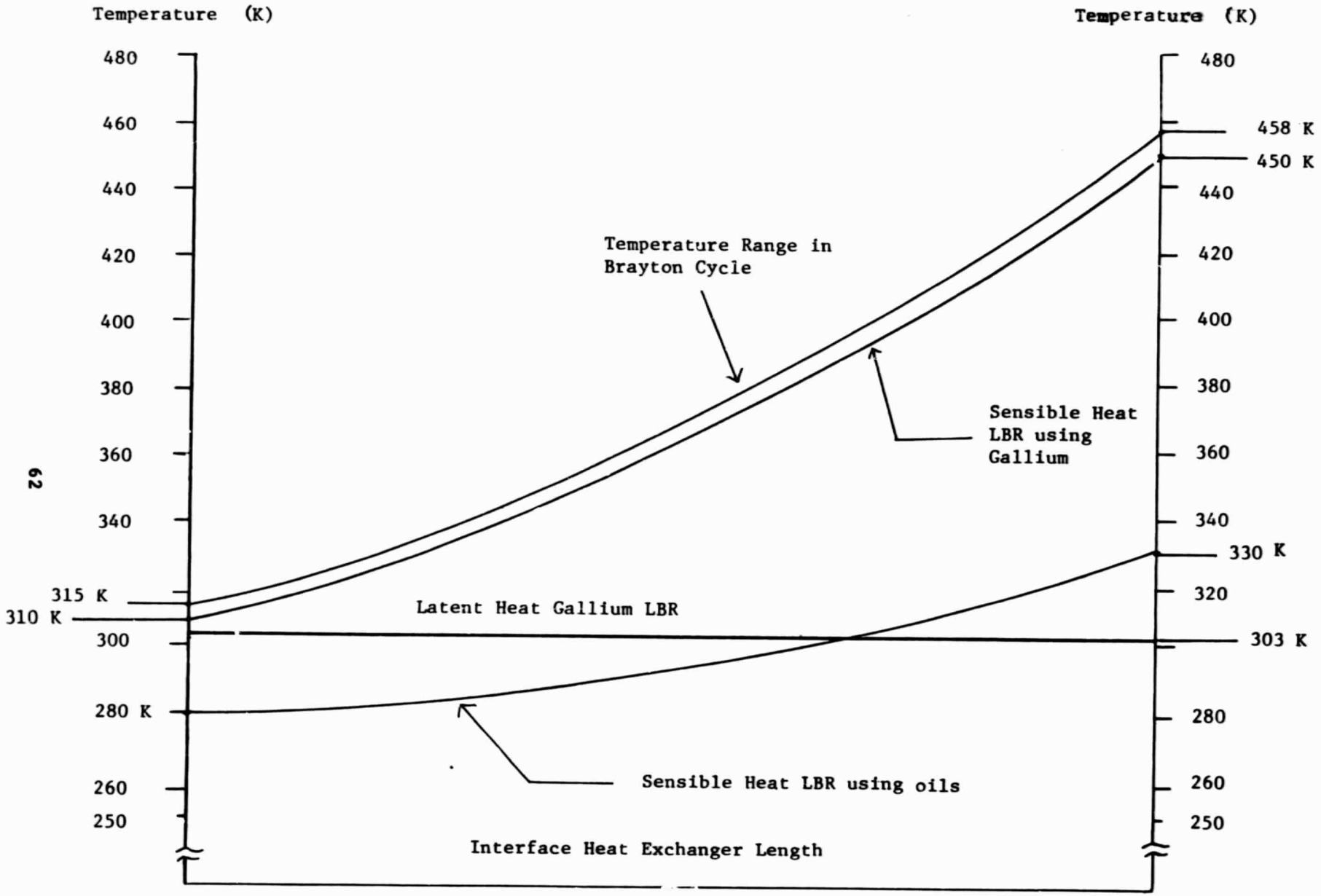

Figure 5.1 HEAT REJECTION OPTIONS FOR POINT DESIGN STUDY (NOT TO SCALE)

5.1.2 Option 2 - Sensible Heat With Gallium

The power cycle/LBR interface can be designed such that the gallium is heated in its liquid state to a temperature approaching the maximum heat rejection temperature of the engine (460 K, 369°F). During the transverse through space, the liquid gallium will cool down to a temperature somewhat below the minimum engine heat rejection temperature before reentering the interface heat exchanger. This option has the advantages of:

- Extracting over 100 K of sensible heat from the liquid gallium resulting in a per unit weight heat rejection comparable to the constant temperature change of phase option (Option 1).
- Producing a much higher average heat rejection temperature thereby reducing LBR area requirements as compared to Option 1 (assuming similar emissivities).

5.1.3 Option 3 - Sensible Heat With Oils

The power cycle/LBR interface can be designed such that a low vapor pressure oil is heated to the highest temperature consistent with acceptable vapor pressure. For oils identified to date this implies heating from about 280 K (45°F) to about 330 K (135°F). This results in about 50 K (90°F) worth of sensible heat extraction from the oil during its transverse through space.

5.2 Cylindrical Belt Design Equations

The basic design equations for the cylindrical LBR system are given below:

$$Q_R = W(\rho\ \delta\ V\ C_p)\ [T_{RMax} - T_{RMin}] \qquad (5\text{-}2)$$

$$\Psi \equiv \frac{F_{RS}\sigma\varepsilon b(T_{RMAS})^3(\Delta T_{RAD})}{p\ w\ V\ Cp} \qquad (5\text{-}3)$$

$$b = + \frac{T_s}{T_{MAX}} + \left(\frac{T_s}{T_{MAX}}\right)^2 + \left(\frac{T_s}{T_{MAX}}\right)^3 \qquad (5\text{-}4)$$

$$T(x) = T_{RMax} - (T_{RMax} - T_s)\,[1 - e^{-\psi \ell}]$$

The derivation of these relationships and their impact on:

- o Interface heat exchanger sizing
- o Parasitic power loss
- o Evaporative mass loss
- o Orbital aerodynamic drag

are presented in Appendix I. Appendix A gives the nomenclature used.

Figure 5.2 outlines the calculation procedure for fluids which exhibit significant weight loss due to high vapor pressure (i.e., diffusion pump oils). If evaporative loss is not a concern (due to low fluid vapor pressures), the range of operating belt temperatures can be specified in accordance with the heat rejection temperatures of the Brayton cycle.

5.3 Preliminary Results

Using the equations developed in Appendix I, the three heat rejection options discussed in Section 5.1 were evaluated.

Table 5.1 indicates the design parameters used in these preliminary evaluations. A critical parameter influencing these results is the assumed emissivity of the LBR materials. For this analysis these emissivities were assumed as:

Liquid Gallium	-	0.1
Solid/Phase Change Gallium	-	0.3
Oil	-	0.8

The oil emissivity is consistent with measurements taken on several oils made as part of this program. The gallium emissivities may still be somewhat optimistic but may be achievable by some combination of surface texturing and/or doping.

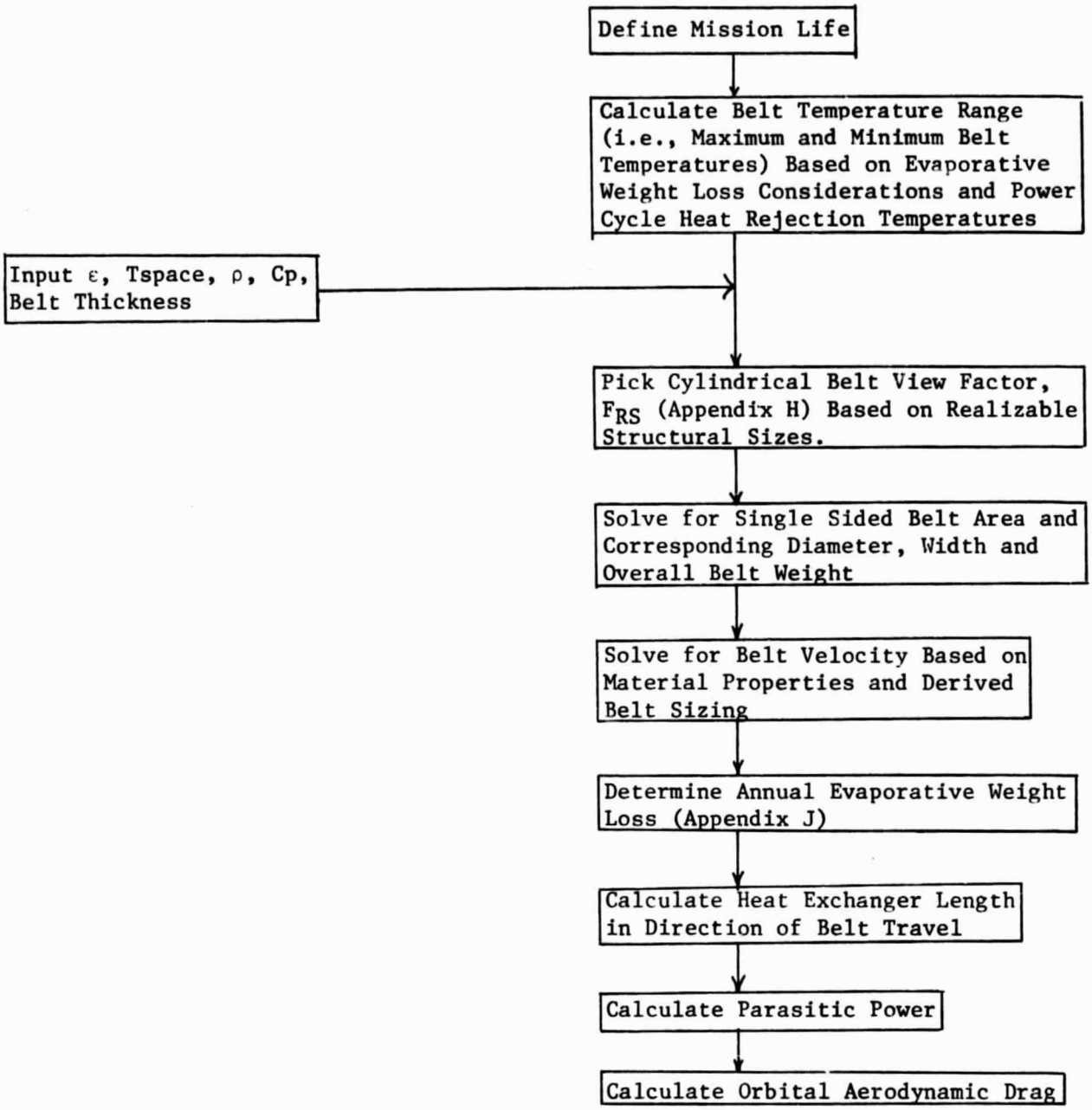

Figure 5.2 LBR CALCULATION PROCEDURE FOR FLUIDS WHERE WEIGHT LOSS IS A CONCERN

Table 5.1

CHARACTERISTICS OF LBR DESIGN OPTIONS

	AREA (m^2)[1]	DIAMETER (m)	WIDTH (m)	PULLING SPEED (m/sec)	MASS (kg)[2]
Latent Gallium OPTION 1	506	36	4.5	∿0.3	392
Sensible Gallium OPTION 2	∿330	29	3.6	∿0.6	256
Diffusion Pump Oil OPTION 3	172	21	2.6	∿0.6	108
Conventional Technology[3]	146	NA	NA	NA	1168

(1) Single sided surface area assuming an approximate 0.95 view factor from the radiator to space.
(2) The fluid alone assuming a 0.05 cm thickness for Option 3 and approximately 0.01 cm thickness for Options 1 and 2.
(3) Assuming a radiating temperature of 310 K, an emissivity of 0.85, a unity view factor to space and a specific mass of 4 kg/m^2 of prime area. The "Area" here corresponds to the single sided heat pipe area.

As indicated in Table 5.1, the option which leads to the lowest mass system is that using a diffusion pump oil in a sensible heat mode. This is due to the relatively high emissivity of the oils as compared to the gallium. The merits of the gallium options depend importantly on the assumed emissivities. For the most likely values of these parameters (i.e., a pure metal in the liquid state having an emmisivity of 0.1 and in the solid state of 0.3), the gallium options are considerably more massive (2 to 3 times) than the oil system. However, if the emissivity of the gallium can be increased to more attractive levels (0.3 for the liquid, 0.5 for the solid) by adding impurities (stable oxides, etc.) as suggested by the emissivity measurements, the gallium-based systems approach the mass of the oil system. The potential for achieving such increases in emissivity remains, however, to be demonstrated. Consequently, the system using oils was selected for the point design study since the thermal and optical characteristics of these materials have been well documented.

For purposes of the point design therefore, the LBR system depicted schematically in Figure 5.3 was selected. This system uses a counterflow heat exchanger between the Brayton cycle engine heat rejection system and the LBR. This allows the belt to operate over a wide temperature range, the upper limit of which is determined by the rate of evaporative loss. As indicated in Section 5.1, the upper temperature of belt operation for Santovac 6 was assumed to be 330 K (135°F). At this upper temperature, the material loss from the belt is only approximately 15 kg per year. The weight loss of this material for a number of operating temperatures is presented in Table 5.2.

It should be noted that the above conclusion is not necessarily a universal truth; i.e., oils will not always be preferable to gallium in such applications. Factors which could modify such a conclusion include the following:

- Gallium has a much lower vapor pressure than any of the oils identified to date. In some applications, the contamination or necessary make-up mass associated with oil evaporation may be unacceptable and the use of gallium will be required.
- Some applications may require that the heat all be dissipated at the lower end of the temperature range so that oil would operate over a very narrow

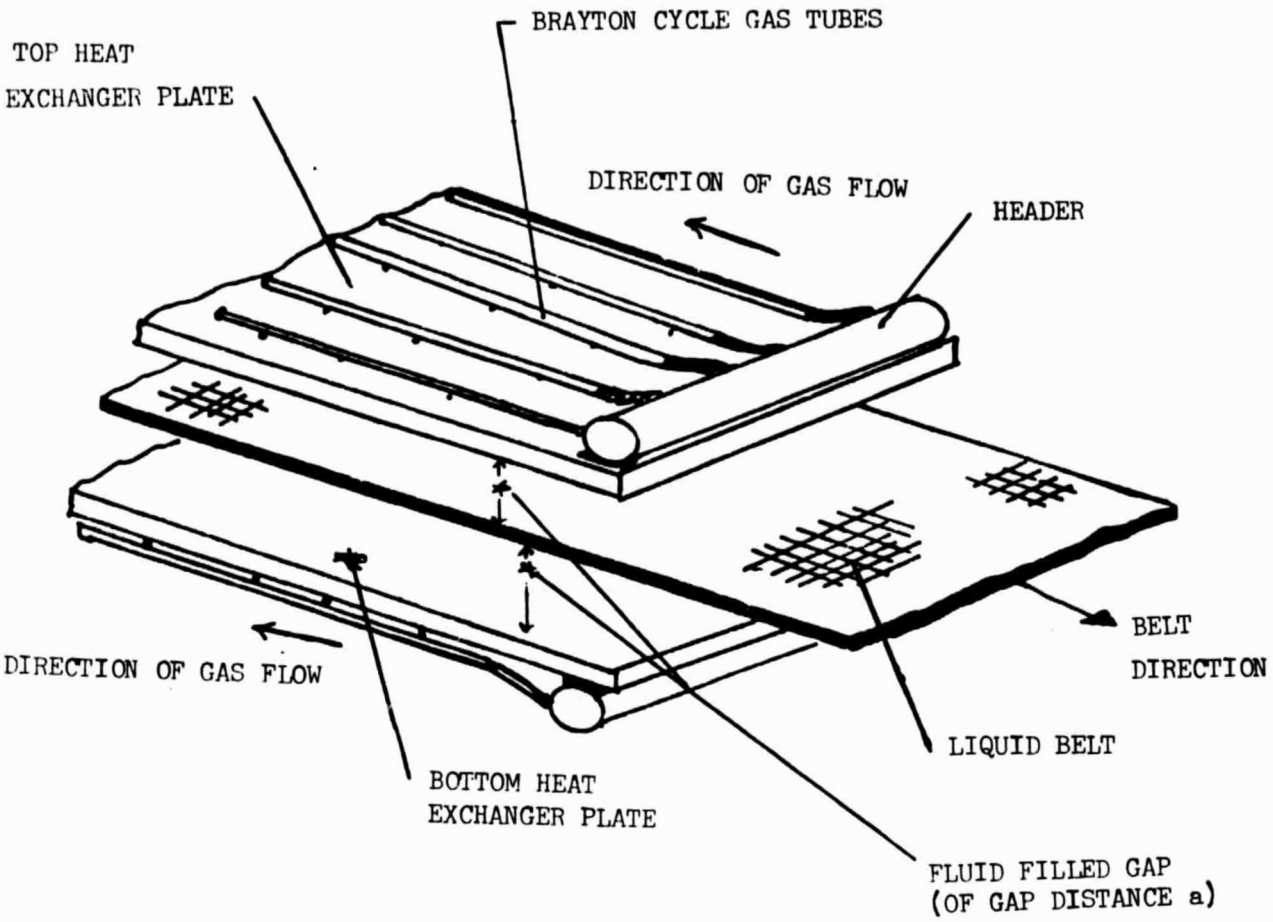

Figure 5.3 POINT DESIGN CONFIGURATION

Table 5.2

WEIGHT LOSS FOR SANTOVAC 6 AS A FUNCTION OF PEAK BELT TEMPERATURE[1]

Exit Temperatures (K)	Mass Loss Per Year (kg/yr)	Percent of Point Design[2]
340	31.8	220%
345	46.6	324%
350	70.5	490%
360	154.3	1071%
380	629.9	4374%
400	3927	27270%

Notes

(1) Based on the Evaporative Loss Relations derived in Appendix J and the radiative area equations derived in Appendix I.

(2) Point design material loss determined to be 14.4 kg/yr.

temperature range (10°F rather than 90°F) of this example. In such applications the use of gallium in a phase change made could well be the most attractive choice.

5.4 Cylindrical Liquid Belt Radiator Point Design

5.4.1 Design Overview

Using the preliminary results of the oil heat rejection option discussed in Sections 5.1.3 and 5.3, a detailed point design of the 75 kW cylindrical LBR was completed. This evaluation was based on the following assumptions:

- Working Fluid: Santovac 6
- Working Fluid Hemispherical Emissivity: 0.8
- Cylindrical Belt View Factor: 0.9
  (Based on a diameter to width ratio of 4)
- Bath Exit Temperature: 330 K (135°F)
- Bath Inlet Temperature: 300 K (81°F)
- Belt Thickness: 0.051 cm (0.02 in)
  (To insure optical thickness)

Table 5.3 summarizes the point design physical dimensions and operating specifications. The total surface area of the cylindrical belt (including inner and outer surfaces) is 290 m^2 (3110 ft^2). This corresponds to a shape having a diameter of 13.7 m (45 ft) and a width of 3.4 m (11 ft). The speed of the belt was determined to be 0.8 m/s (2.5 fps), resulting in an inward centripetal acceleration of 0.09 m/s. The weight of the fluid belt (assuming the volume of the belt structure to contain all fluid) was 92 kg (202 lbm). The annual evaporative loss is derived from the interval loss summation method discussed in Appendix J. For the point design, the yearly material loss was 15 kg or 16 percent of the total fluid belt weight.

Table 5.3

POINT DESIGN PHYSICAL DIMENSIONS AND OPERATING SPECIFICATIONS

Working Fluid	:	Santovac 6
Mode of Operation	:	Sensible
Heat Rejection Rate	:	75 kWt
Exit Temperature	:	330 K (135°F)
Inlet Temperature	:	300 K (81°F)
Belt Width[1]	:	3.4 m (11 ft)
Belt Thickness	:	5.1×10^{-4} m (1.7×10^{-3} ft)
Belt Circumference	:	43.0 m (141 ft)
Belt Diameter	:	13.7 m (45 ft)
Belt Area[2]	:	290 m^2 (3110 ft^2)
Belt Weight	:	92 kg (202 lbm)
Belt Speed	:	0.8 m/s (2.5 fps)
Yearly Material Loss	:	14.4 kg (31.716 m)
% of Belt Weight	:	14.1 percent
Heat Exchanger Length[3]	:	0.38 m (1.25 ft)
Heat Exchanger Single Sided Gap, Distance	:	5.8×10^{-3} m (0.0190 ft)
Parasitic Power[4]	:	<1.00 kW (∿1.3 hp)
Orbital Aerodynamic Drag[5]	:	0.0012 N (0.00027 lbf)

NOTES

(1) Selected so that storage aboard NASA STS is possible.
(2) Refers to inner and outer surface area.
(3) Refers to the length in the direction of belt travel assuming an overall heat transfer cooefficient of 570 w/m^2 K and a LMTD of 53 K.
(4) Assumes a gap distance of ∿225 mils from the surface of the belt to heat exchanger plates. Also additional drag forces effectively double the fluid friction effects.
(5) Based on a 270 nautical mile circular orbit.

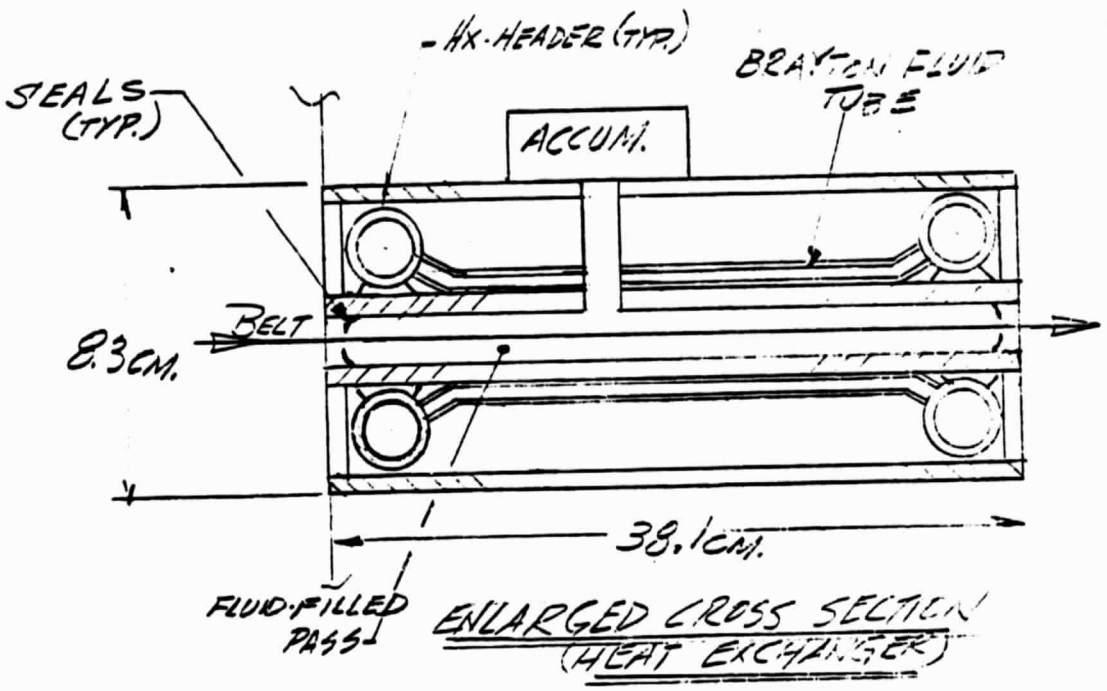

Figure 5.4 INTERFACE HEAT EXCHANGER DESIGN

As explained in Appendix I, the sizing of the interface counterflow heat exchanger is based on the reasonable assumption that an overall heat transfer coefficient of approximately 570 W/m^2- K (100 Btu/ft^2-hr-°F) could be readily attained.

The interface heat exchanger design consists of two parallel plates separated by a 0.58 cm (0.23 in) gap. This gap is filled with Santovac 6 and contained by advanced linear sealing technology. Heat from the Brayton cycle heat rejection system is transferred to this thin film of oil via tubes brazed to the back of the parallel plates. As the belt moves up the centerline of the gap it acquires energy through combined mass and heat transfer mechanisms. The interface heat exchanger is shown in Figure 5.4.

For this analysis, it was assumed that only heat transfer existed. Using the log mean temperature difference approach (LMTD = 53 K, 95°F) an area of 2.5 m^2 was determined necessary to transfer the 75 kW of Brayton cycle reject heat. This corresponded to a length of 0.38 m (1.25 ft) in the direction of belt travel and a width of 3.4 m, as set by the radiative area derivations.

For the specified heat exchanger gap distance, the parasitic power is predicted to be approximately 1 kW. It is believed that parasitic power losses can be kept within acceptable bounds by proper selection of design parameters and internal heat exchanger geometry.

The orbital drag force acting on the belt as a result of the molecular impact may be estimated from the formulations developed in Appendix I. For a 270 n.m. circular orbit, the drag force per unit normal area is calculated to be 2.53×10^{-5} N/m^2. For the point design using Santovac, the drag force does not exceed 0.0012 N, and therefore has little impact on system dynamics.

5.4.1.1 Micrometeorite Damage

The belt of the LBR is expected to be tolerant to damage from meteorite impact due to the dispersed nature of the radiating surface. However, if the belt is torn badly by a collision, it may not be able to freely enter and move through

the heat exchanger area without becoming fouled. Therefore, care must be exercised in the design and testing of the belt material to assure that if it tears or is punctured, it will still be able to function. A thin, flexible nylon mesh is expected to exhibit the proper behavior as long as the belt temperature remains well below this materials melting temperature (485 K, 414°F).

If meteorites impact the heat exchanger area, the heat transfer performance of the LBR is not expected to be affected immediately. However, over the long-term, fluid may be lost as a consequence of impact and this loss must be replenished from storage.

5.4.2 Point Design Configuration Mass Budgets

Table 5.4 is a summary of the mass budget estimates for a complete cylindrical liquid belt radiator system operating at the point design conditions. A conceptual design of this application is shown in Figure 5.5. It may be recalled that the dimensions of this system were given in Table 5.3.

Each of the key elements in the conceptual design (i.e., motors, heat exchangers, rollers, etc.) are taken into account (Figure 5.5). Generally, the components of the mechanical design are assumed to be fabricated of 0.127 cm (0.050 in) thick plates of aluminum. For calculation purposes only, the heat exchanger pipes, rollers, and roller flanges are also assumed to be of aluminum.

To operate the roller drive system, two Hoover Corporation 1.5 hp, DC, electric motors (model 2370) were selected. It was assumed that the exit rollers would be the motor drive master rollers and the entrance rollers the clutch-actuated slaves. As shown in Figure 5.3, the top and bottom rollers would be linked by belts or flexible chain couplings. The weight of these motors was specified by manufacturers literature to be 6 kg (13.5 lbm). To make the weight budget as complete as possible, an electronic control system is included as well as an as yet unspecified pair of extenders and dampers that may be needed to assist in the deployment of the LBR. If dynamic oscillations develop within the belt,

ORIGINAL PAGE IS
OF POOR QUALITY

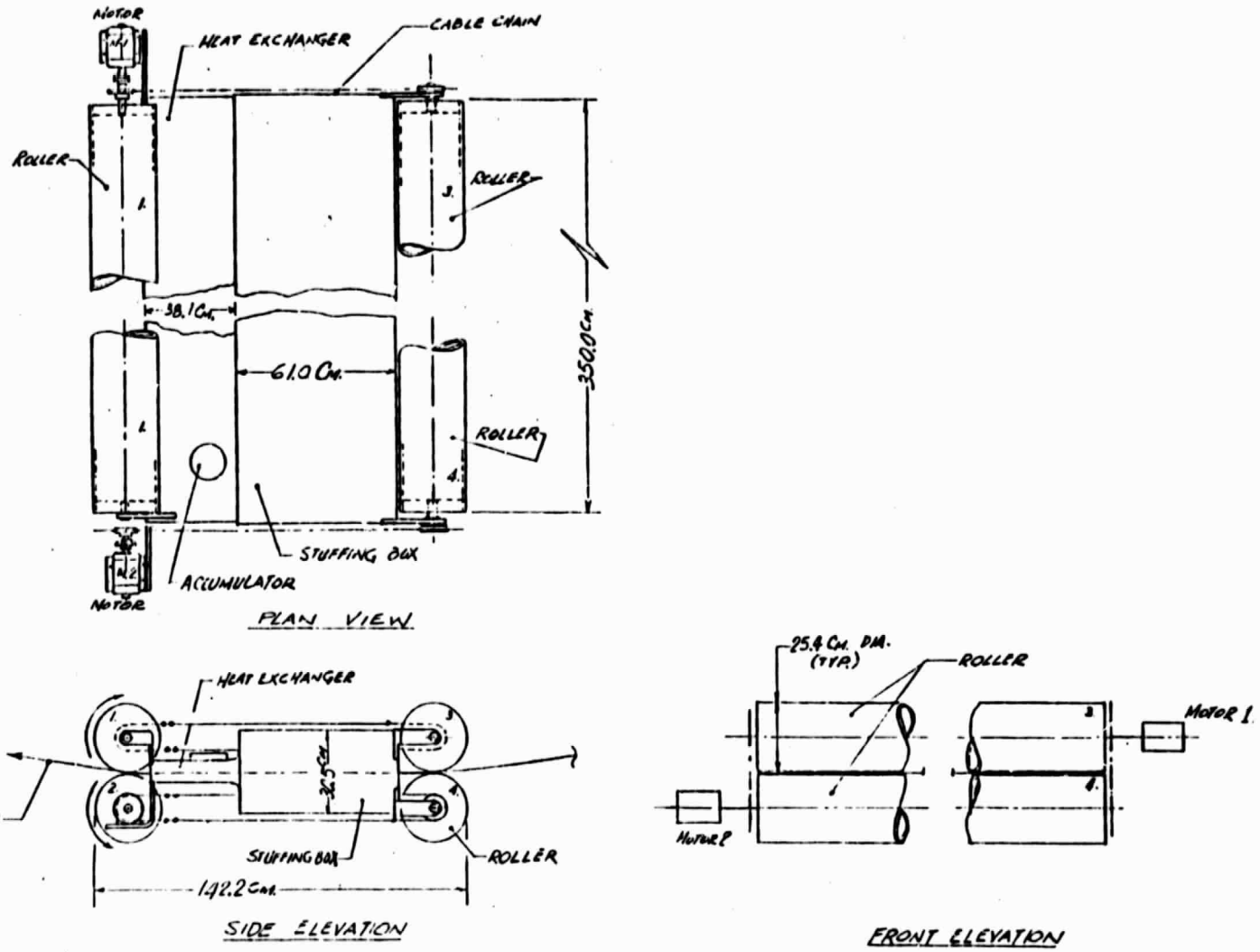

Figure 5.5 POINT DESIGN CONFIGURATION

Table 5.4

ESTIMATED WEIGHT BUDGETS FOR POINT DESIGN USING SANTOVAC 6 OVER 300-330K TEMPERATURE RANGE

Component	Dimensions	Material	Mass for Santovac 6 Design (kg)
1. Belt/Fluid Combination	- Santovac (.051 cm thick)		92.0
2. Spare Santovac fluid for 1-yr (@ 33°K)	0.3 x 0.3 x 3.4m accumulator	Santovac 6	∿ 14.5
3. Stuffing box (including accumulator)	0.3 x 0.6 x 3.4m Rectangular Structure with 0.127 cm thick walls	Aluminum	21.0
4. Heat exchanger covers (2)	0.051 cm thick	Aluminum	3.5
5. Heat Exchanger Plates (2)	0.127 cm thick	Aluminum	8.9
6. Heat exchanger			
- Pipes (142)	1 cm dia. (0.076 cm wall)	Aluminum	3.5
- Headers (4)	4 cm dia. (0.236 cm wall)	Aluminum	10.9
7. Rollers (4)	0.25 dia. (0.127 cm thick)	Aluminum	36.6
- Support Flanges	0.127 cm thick	Aluminum	2.7
8. Drive Motors (2)	1.5 hp		
Belts, et al	0.75		12.0
9. Miscellaneous pipes	—	Aluminum	4.0
10. Control System	—	—	3.0
11. Extenders & Dampers	Not Available	Aluminum	20.0
		TOTAL	232.6

this system element may also be very useful in providing the necessary energy dissipation to control the most deleterious modes of oscillation.

Table 5.5 presents the point design in terms of quantities used often in space power system analysis. One important parameter is the specific mass, or the ratio of the system mass to prime radiating surface area. The point design has a specific mass of 0.9 kg/m^2, which compares favorably to the 4 kg/m^2 value associated with current heat pipe radiator technology (<25 percent).

5.4.3 System Trade-Off Studies

In order to determine the effect of various properties on a cylindrical LBR, different system designs were performed. These designs consider the variation of:

- Parasitic power
- Fluid belt weight
- Evaporative mass loss

with maximum exit temperature. While the first two parameters decrease with with temperature, the evaporative loss increases rapidly with temperature. The selection of a particular design point and resultant structural configuration will be governed by the desire to optimize any one or perhaps all of these parameters. The point design developed in this program was established to avoid excess material loss and consequently resulted in a maximum belt temperature of 330 K.

Figure 5.6 depicts the variations of these important parameters for different design conditions.

Table 5.5

CYLINDRICAL LBR POINT DESIGN SUMMARY

Electric Power Generated	:	37.5 kWe
Thermal Load	:	75 kW
Required Single Sided Belt Area	:	145 m^2 (1555 ft^2)
Total System Mass (1)	:	235 Kg (517/bm)
Total System Volume	:	2.5 m^3 (89 cu ft)

Mass Per Unit Power Dissipated	:	313 Kg/kW
Power Dissipated Per Unit Area (3)	:	0.52/kW-Kg
Electric Power Generator Per Unit Area	:	0.26 kWe/Kg
Specific Mass (3)	:	0.85 kg/m^2 (0.17 lbm/ft^2)

NOTES

(1) Includes all Ancillary Equipment.

(2) Area Refers to Single Sided Area.

(3) Specific Mass is Defined as the Mass Per Unit Prime Radiating Area.

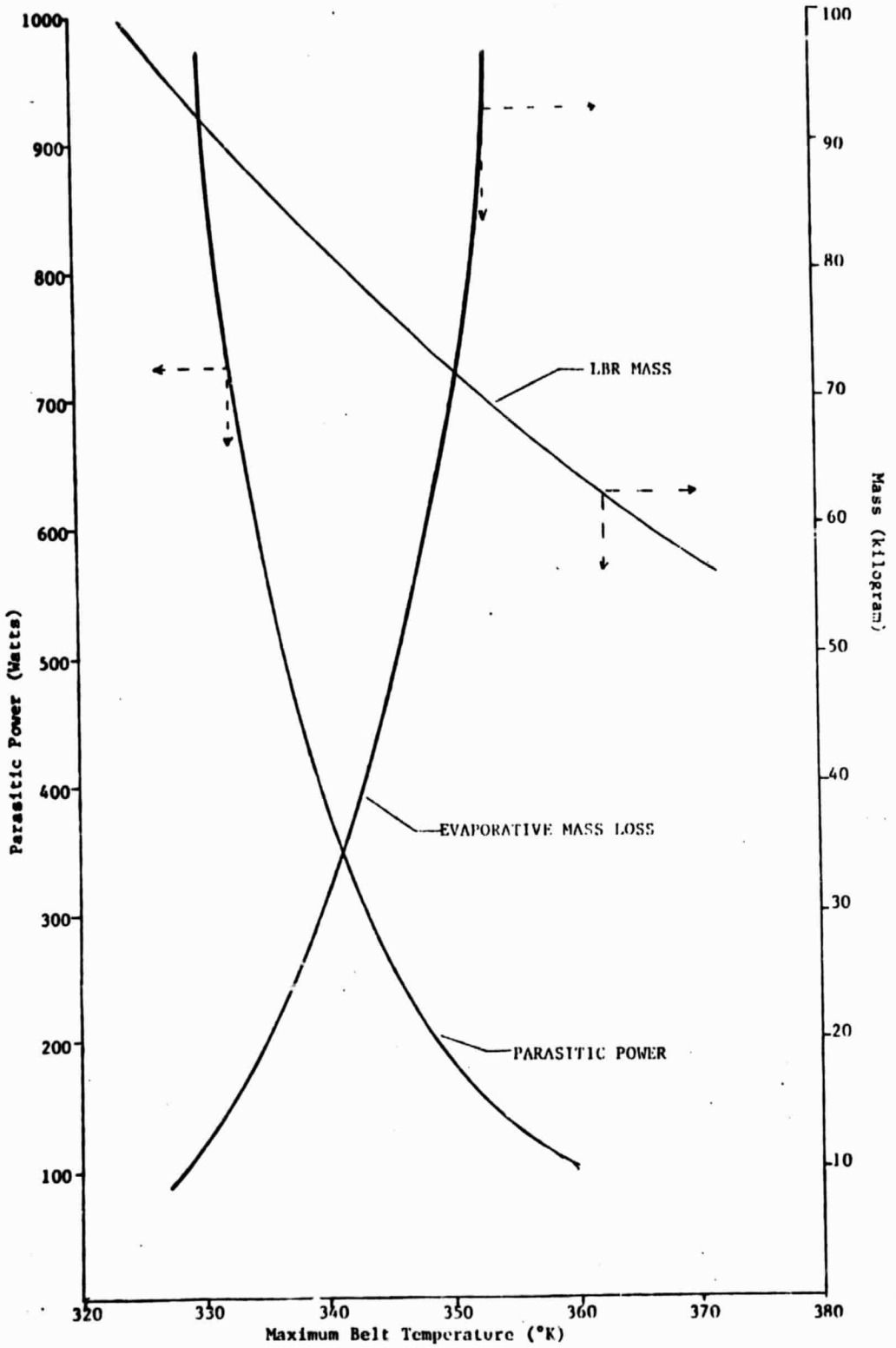

Figure 5.6 LBR MASS, PARASITIC POWER AND EVAPORATIVE LOSS STUDY FOR SANTOVAC 6 (SINGLE SIDED HEAT EXCHANGER GAP ASSUMED TO BE 0.58 cm)

6.0 EXPERIMENTAL STUDIES

6.1 Introduction

The viability of the LBR concept depends upon two important properties:

- o The formation and stability of working fluid menisci on a screen belt structure.
- o The selection of a high emissivity ($\varepsilon \geq 0.3$) working fluid with both low density and low vapor pressure ($\sim 10^{-8}$ torr).

Various candidate working fluids were examined with regard to these properties during the course of the LBR design program. The results of these experimental investigations are presented in the following sections.

6.2 Surface Tension/Wettability Tests: Introduction

6.2.1 Introduction

The formation of stable menisci on a mesh substrate is a complex physical phenomenon involving interactions between fluid material properties, mesh material properties, mesh configuration, and externally imposed forces. Work presented in previous sections, and in Appendices B and C, indicate the importance of wetting between the fluid film and the mesh geometry. These preliminary studies did not, however, take into account the full range of physical phenomena which govern the film formation process. For this reason, a series of bench top tests were undertaken to do the following:

- o Experimentally determine the wettability of selected film materials and mesh substrates of interest for lower temperature applications.
- o Determine the impact of mesh geometry on meniscus stability and, in particular, to determine if the absolute stability criteria, estimated in Appendix B, must be followed in practice.
- o Draw a prototypical LBR model from baths of candidate fluid materials in order to:
  - Verify that fluids wet the belt structure with meniscus formation occurring over some range of conditions.

- Identify issues requiring additional study in order to fully explore the potential of the LBR concept.

The bench top tests undertaken to achieve the above objectives are described in the following sections.

6.2.2 Wettability Tests

A number of wettability tests were conducted in order to screen the candidate liquid/belt material combinations. Wettability is measured by the contact angle made between a liquid drop on a solid surface. Figure 6.1 depicts the contact angle, θ, in relation to both a wetting ($<90°$) and non-wetting ($>90°$) condition. Using a microscope with a reticuled eyepiece, the contact angle between various liquids (diffusion pump oils and low melting point liquid metals) and solid substrates was determined.

The wettability bench tests were carried our using the apparatus shown in Figure 6.2. Wetting tests were made using substrate materials in the "as received" condition and after they had been cleaned. The cleaning procedure consisted of the following steps:

- o The application of jeweler's rouge on all metal surfaces to remove surface coatings.
- o Successive rinsings of the surfaces with trichloroethane, methanol, and distilled water.

This simple procedure provided a grease-free surface, but did not ensure that oxides and other surface tension influencing contaminants, were removed.

The data presented in Table 6.1 lists the contact angles associated with potential screen materials and liquid bath candidates. The experimental results lead to the following general conclusions:

- o Diffusion pump oils wet all surfaces regardless of cleaning.
- o The liquid metals tested (low melting point eutectics and gallium) generally do not wet the substrate tested. One exception noted is the alloy Woods Metal which wetted a cleaned polypropylene surface.

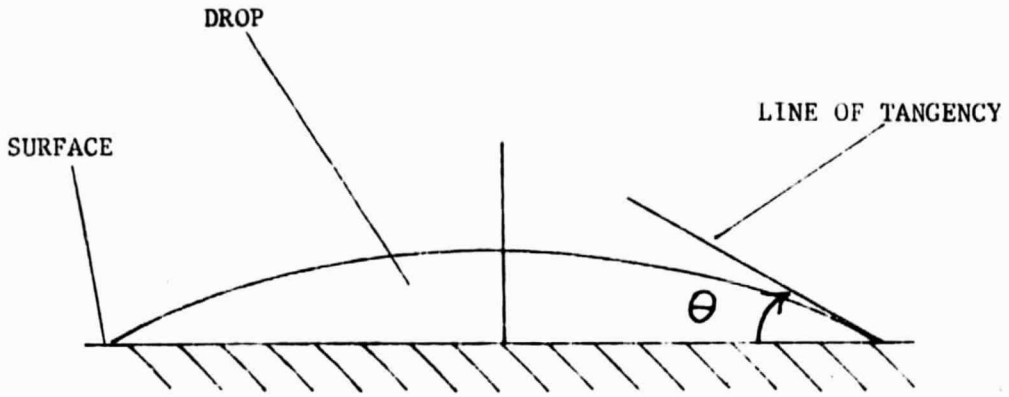

Figure 6.1a EXAMPLE OF CONTACT ANGLE θ, FOR A WETTING CONDITION

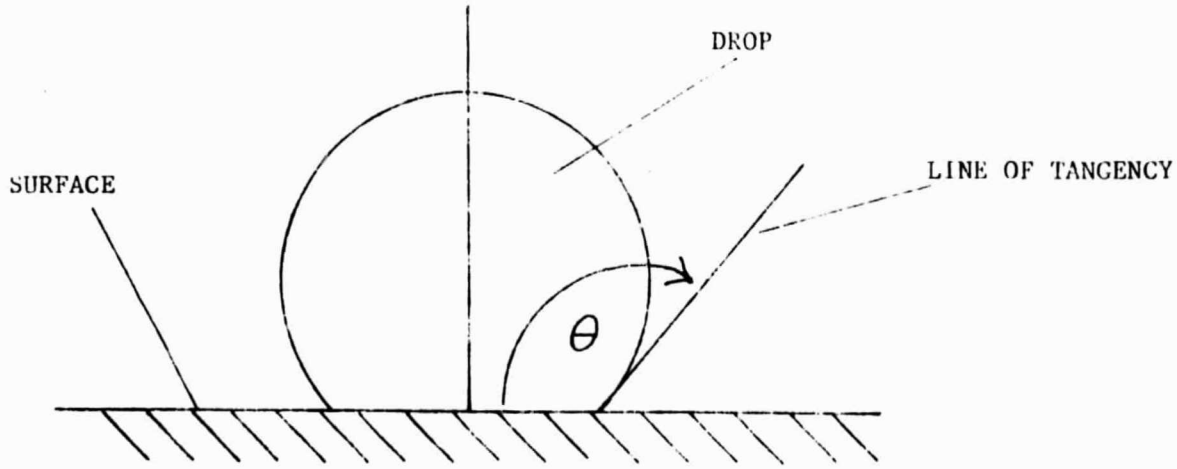

Figure 6.1b EXAMPLE OF CONTACT ANGLE θ, FOR A NON-WETTING CONDITION

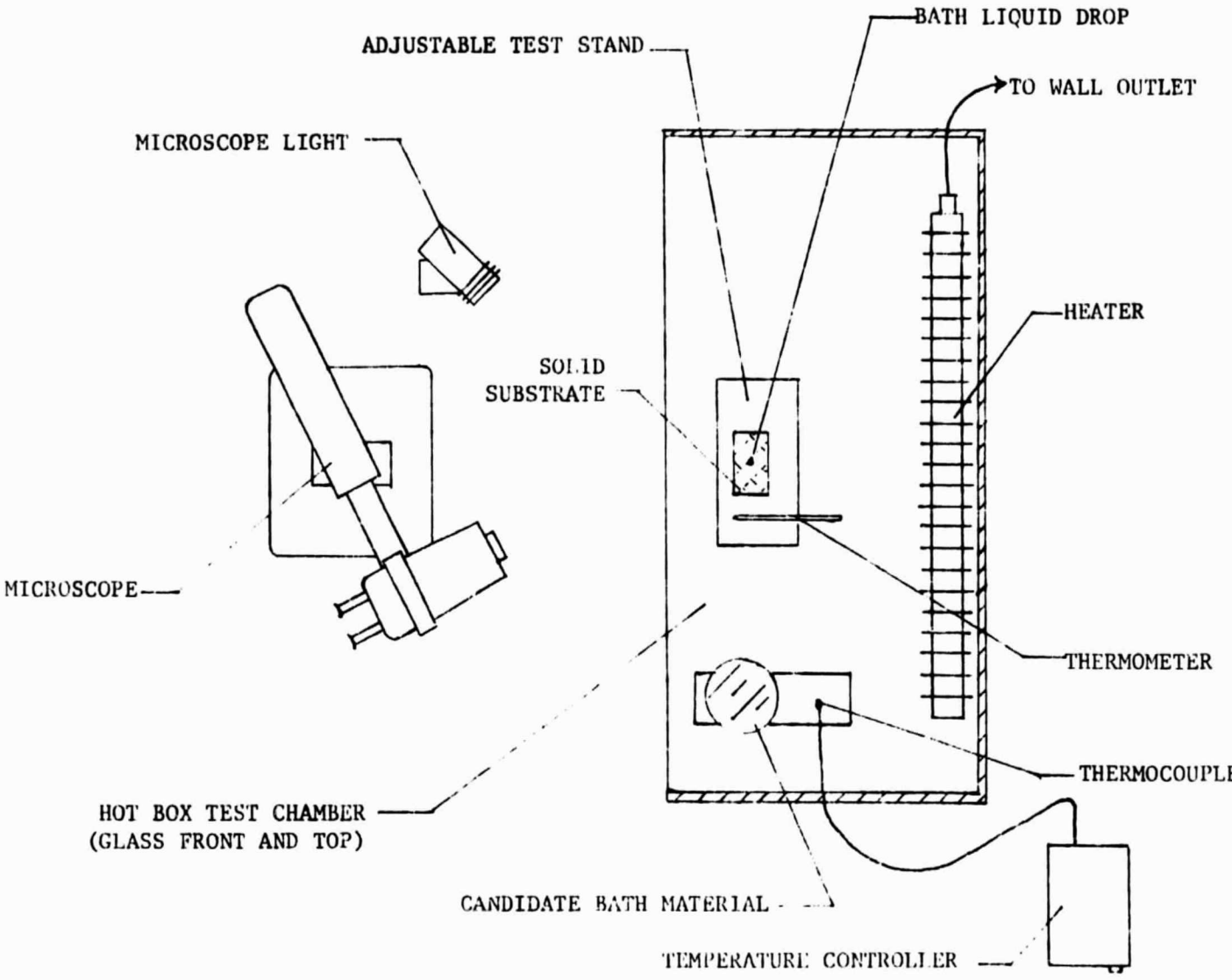

Figure 6.2 SCHEMATIC OF WETTABILITY EXPERIMENTAL TEST RIG (TOP VIEW)

Table 6.1

SUMMARY OF WETTABILITY TEST RESULTS

1) Coolant Liquid Candidate — Diffusion Pump Oil D-7040 (Varian Corp.)

Possible Belt Material	As Received		Cleaned*	
	Temperature (K)	Contact Angle Θ (Degrees)	Temperature (K)	Contact Angle Θ (Degrees)
Nylon	297.2	8 ± 1	297.2	5 ± 1
Polyethylene	297.2	17 ± 1	297.2	15 ± 1
Polypropylene	297.2	30 ± 1	297.2	17 ± 1
Vaspel	296	45 ± 1	296	5 ± 10 **
Teflon	297.2	50 ± 1	296	60 ± 1
Glass	295.2	15 ± 2	296	7 ± 2
Tantalum	--	--	--	--
Steel	297	7 ± 2	297	7 ± 2
Aluminum	297	5 ± 2	297	3 ± 1

*Cleaning Procedure, discussed in text.

**Angle Difficult to Measure

2) Coolant Liquid Candidate Convoil (CVC)

Possible Belt Material	As Received		Cleaned*	
	Temperature (K)	Contact Angle Θ (Degrees)	Temperature (K)	Contact Angle Θ (Degrees)
Nylon	297.2	3 ± 2	297.2	10 ± 2
Polyethylene	297.2	4 ± 1	297	17 ± 2
Polypropylene	297.2	13 ± 1	297.2	25 ± 2
Vespel	297.8	∿0	297.8	∿0
Teflon	296.5	50 ± 2	296.5	50 ± 2
Glass	297.2	17 ± 2	297.5	15 ± 1
Tantalum	--	--	--	--
Steel	297.5	7 ± 2	297.5	15 ± 1
Aluminum	297.2	5 ± 1	297	10 ± 2

* Cleaning Procedure, discussed in text.

3) **Coolant Liquid Candidate** Santovac 5 Oil (Monsanto)

Possible Belt Material	As Received		Cleaned*	
	Temperature (K)	Contact Angle Θ (Degrees)	Temperature (K)	Contact Angle Θ (Degrees)
Nylon	295	8 ± 2 **	295	5 ± 2
Polyethylene	295	49 ± 2	295	32 ± 2
Polypropylene	295	45 ± 2	295	46 ± 2
Vespel	296	20 ± 2	295	12 ± 2
Teflon	296	85 ± 2	296	61 ± 2
Glass	296	26 ± 2	296	13 ± 2
Tantalum	296	15 ± 2	296	32 ± 2
Steel	295	18 ± 2	295	14 ± 2
Aluminum	296	18 ± 2	296	24 ± 2

* Cleaning Procedure, discussed in text.

**Santovac Continues to Spread With Time

4) Coolant Liquid Candidate — Gallium (M.P. = 303K)

Possible Belt Material	As Received		Cleaned*	
	Temperature (K)	Contact Angle Θ (Degrees)	Temperature (K)	Contact Angle Θ (Degrees)
Nylon	321	135 ± 2	318	135 ± 2
Polyethylene	340	115 ± 2	336	135 ± 2
Polypropylene	325	108 ± 2	328	125 ± 2
Vespel	329	153 ± 2	337	157
Teflon	338	127 ± 2	--	133 ± 2
Glass	341	133 ± 2	325	115 ± 2
Tantalum	326	133 ± 2	316	123 ±2
Steel	331	120 ± 2	325	143 ± 2
Aluminum	351	148 ± 2	355	121 ± 2

*Cleaning Procedure, discussed in text.

5) Coolant Liquid Candidate — Cerrolow (M.P. = 320.2K)

Possible Belt Material	As Received		Cleaned*	
	Temperature (K)	Contact Angle θ (Degrees)	Temperature (K)	Contact Angle θ (Degrees)
Nylon	336	135 ± 2	333	145 ± 2
Polyethylene	348	130 ± 2	363	117 ± 2
Polypropylene	383	133 ± 2	380	133 ± 2
Vespel	337	137 ± 2	329	106 ± 2
Teflon	321	148 ± 2	321	148 ± 2
Glass	367	131 ± 2	363	133 ± 2
Tantalum	344	127 ± 3	339	141 ± 2
Steel	321	117 ± 3	323	122 ± 2
Aluminum	338	122 ± 2	338	122 ± 2

*Cleaning Procedure, discussed in text.

6) Coolant Liquid Candidate — Woods Metal (M.P. 343K)

Possible Belt Material	As Received		Cleaned*	
	Temperature (K)	Contact Angle Θ (Degrees)	Temperature (K)	Contact Angle Θ (Degrees)
Nylon	365	94 ± 2	373	107 ± 2
Polyethylene	381	120 ± 2	375	127 ± 2
Polypropylene	356	109 ± 3	378	70 ± 3 **
Vespel	358	125 ± 2	354	114 ± 2
Teflon	356	129 ± 3	374	129 ± 2
Glass	380	97 ± 2	383	117 ± 2
Tantalum	378	133 ± 2	376	133 ± 2
Steel	376	115 ± 2	367	129 ± 2
Aluminum	381	139 ± 2	383	136 ± 2

* Cleaning Procedure, discussed in text.

**Note: Woods Metal Wets Polypropylene When Cleaned

7) Coolant Liquid Candidate — Cerrobend (M.P. = 343K)

Possible Belt Material	As Received		Cleaned*	
	Temperature (K)	Contact Angle Θ (Degrees)	Temperature (K)	Contact Angle Θ (Degrees)
Nylon	375	152 ± 3	373	137 ± 2
Polyethylene	---	145 ± 2	361	145 ± 2
Polypropylene	364	120 ± 2	368	109 ± 2
Vespel	355	117 ± 2	358	122 ± 2
Teflon	369	142 ± 3	375	145 ± 2
Glass	347	130 ± 2	347	135 ± 2
Tantalum	373	127 ± 2	371	127 ± 2
Steel	388	137 ± 2	388	137 ± 2
Aluminum	358	135 ± 2	360	135 ± 2

* Cleaning Procedure, discussed in text.

- o Gallium wets the alloy tantalum marginally better when cleaned. This result is consistent with fact that gallium is known to wet a pure, clean tantalum surface. Further experiments involving more rigorous cleaning procedures on tantalum are warranted since gallium may be a very attractive material for use in an LBR.
- o The cleaning procedure generally improved the wettability between the solid and liquid combinations tested. However, as the experimental results show the effects were neither large nor consistent.

Future program phases should investigate the wetting properties of higher melting point materials such as lithium or tin which have potential in higher temperature heat rejection applications. In addition, more thorough cleaning procedures should be pursued in order to obtain a controlled environment for accurate measurement of surface tension phenomena.

6.2.3 Screen Pulling Tests

A bench top radiator model was designed and constructed (Figures 6.3). The structure is 33 centimeters long by 7.6 centimeters (13 inches by 3 inches) wide and driven by a variable speed motor. The bottom of the model sits in a bath of the liquid material which is maintained at a fixed temperature by electric heaters. Belts of polypropylene mesh were constructed for use with the test apparatus.

This apparatus was used with three potential liquid bath materials.

- o Diffusion Pump Oil (Santovac 5, Monsanto Corp.)
- o Cerrolow (Cerro Metal Products)
- o Gallium

The results of these experiments are discussed below.

Diffusion Pump Oil

Figure 6.4 shows the formation of the liquid film as it was drawn from a bath containing diffusion pump oil. As portrayed, a perfect film was formed

ORIGINAL PAGE IS
OF POOR QUALITY

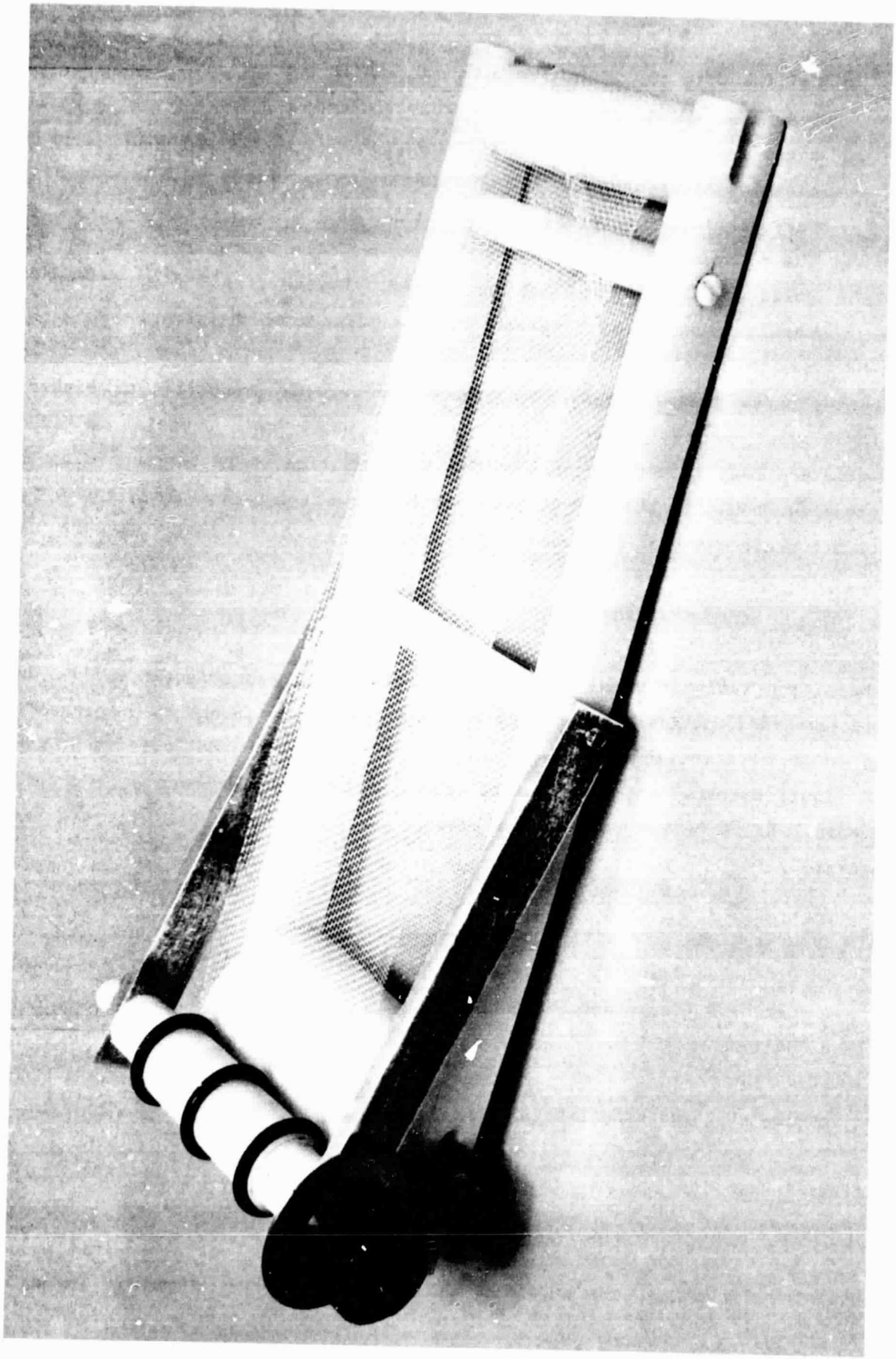

Figure 6.3 BELT RADIATOR MODEL

ORIGINAL PAGE IS
OF POOR QUALITY

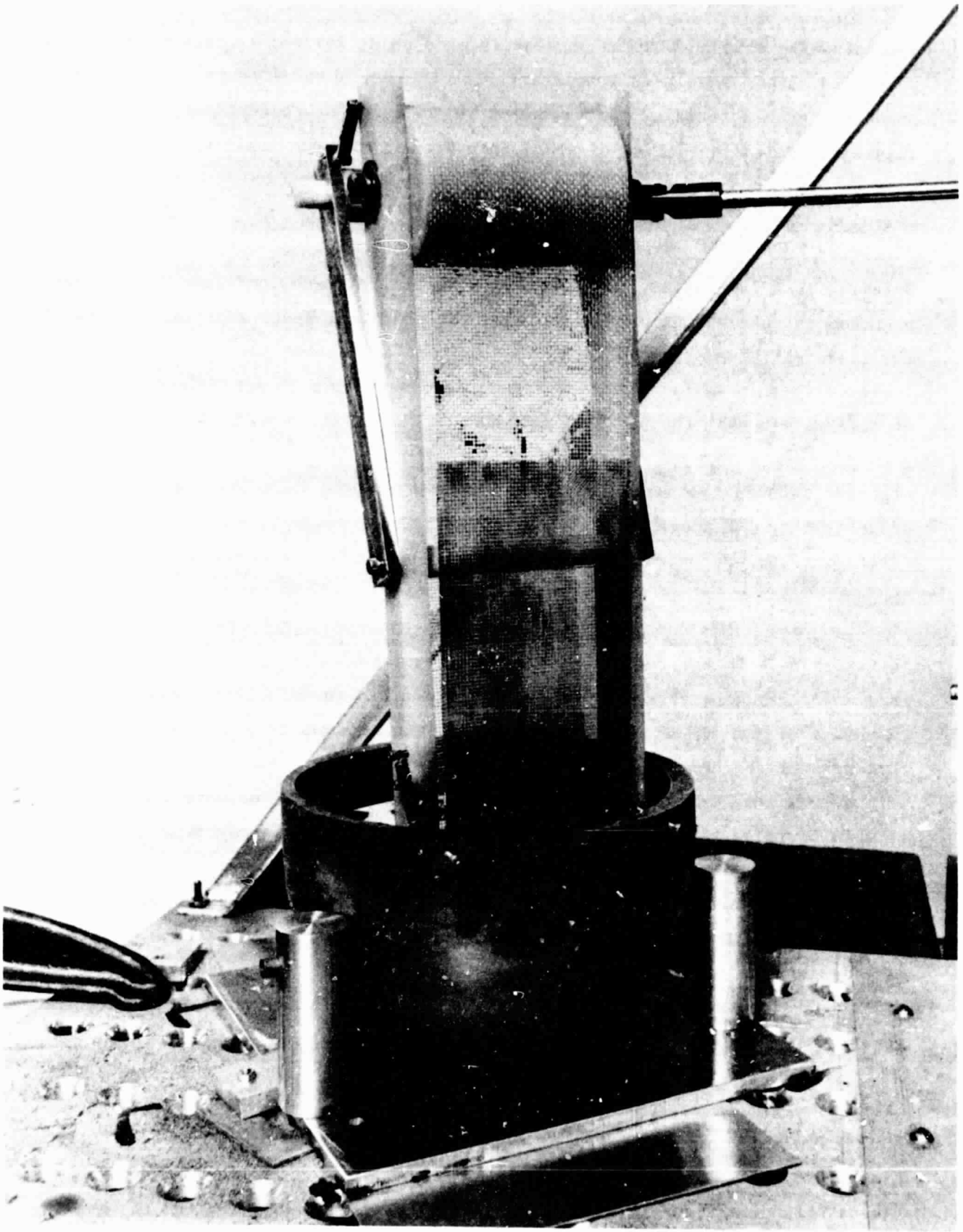

Figure 6.4 MENISCUS FORMATION ON THE LBR TEST RIG USING DIFFUSION PUMP OIL

demonstrating that an LBR can be readily made using low vapor pressure diffusion pump oils. This result is consistent with the wettability tests using various potential mesh materials. As will be discussed in future sections, these oils also have optical qualities of special interest for space applications.

Cerrolow

Cerrolow is a low melting point eutectic of tin, bismuth, and lead. Its vapor pressure is unknown but may be too high for practical space applications due to the preferential evaporation of lead (10^{-6} torr at melting point). Experimental tests using this material were designed to observe the formation and stability of a metal material for LBR applications.

Figure 6.5 shows the formation of an LBR when drawing Cerrolow from a bath of 322 K (120°F, 3°F above the melting point). Under these conditions an LBR was formed whereby approximately 85 percent of the surface was covered by a metal menisci.

In its transit to the roller system, the liquid belt changed phase demonstrating the capability of a change of phase LBR to conform to relatively small radii of curvature of the roller without failure. This is due, in part, to the small thickness of the belt (0.025 cm, ∿10 mils). The ability to form a stable fluid film despite the fact that the wettability tests did not indicate good wetting between Cerrolow and the mesh material suggests that there may be considerable flexibility in the selection of liquid film/mesh combinations. A contributing factor to the ability to form an LBR under these circumstances may be that the liquid metal starts to solidify shortly after exiting from the bath, thereby stabilizing the menisci. These phenomena merit additional investigation in order to better define the acceptable combinations of materials and operating conditions.

Gallium

Figure 6.6 shows the formation of an LBR using gallium as the film material. The bath temperature for these tests was 316 K, which is 13 K above the melting

ORIGINAL
OF POOR

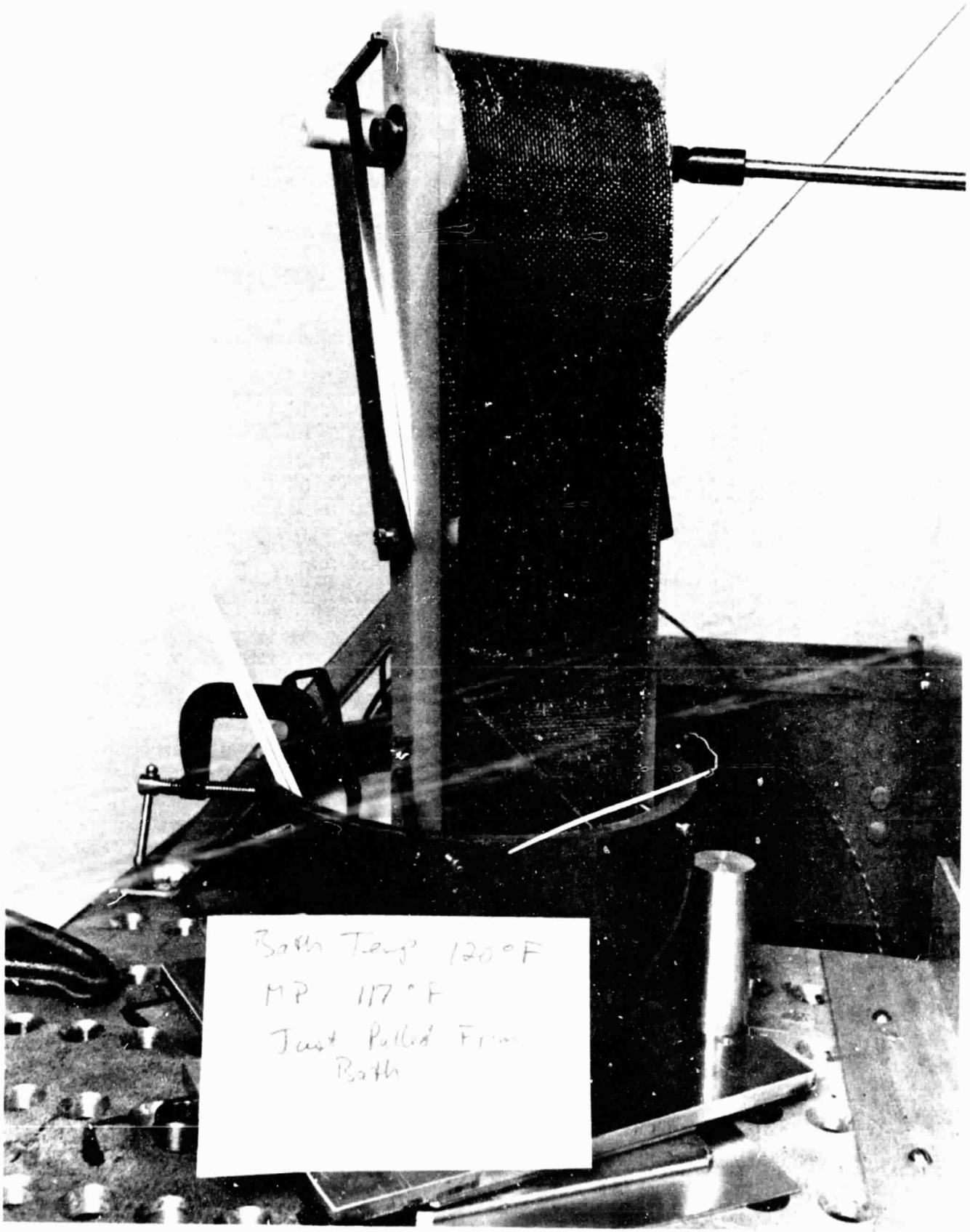

Figure 6.5 MENISCUS FORMATION IN THE LBR TEST RIG USING CERROLOW EUTECTIC

ORIGINAL PAGE IS
OF POOR QUALITY

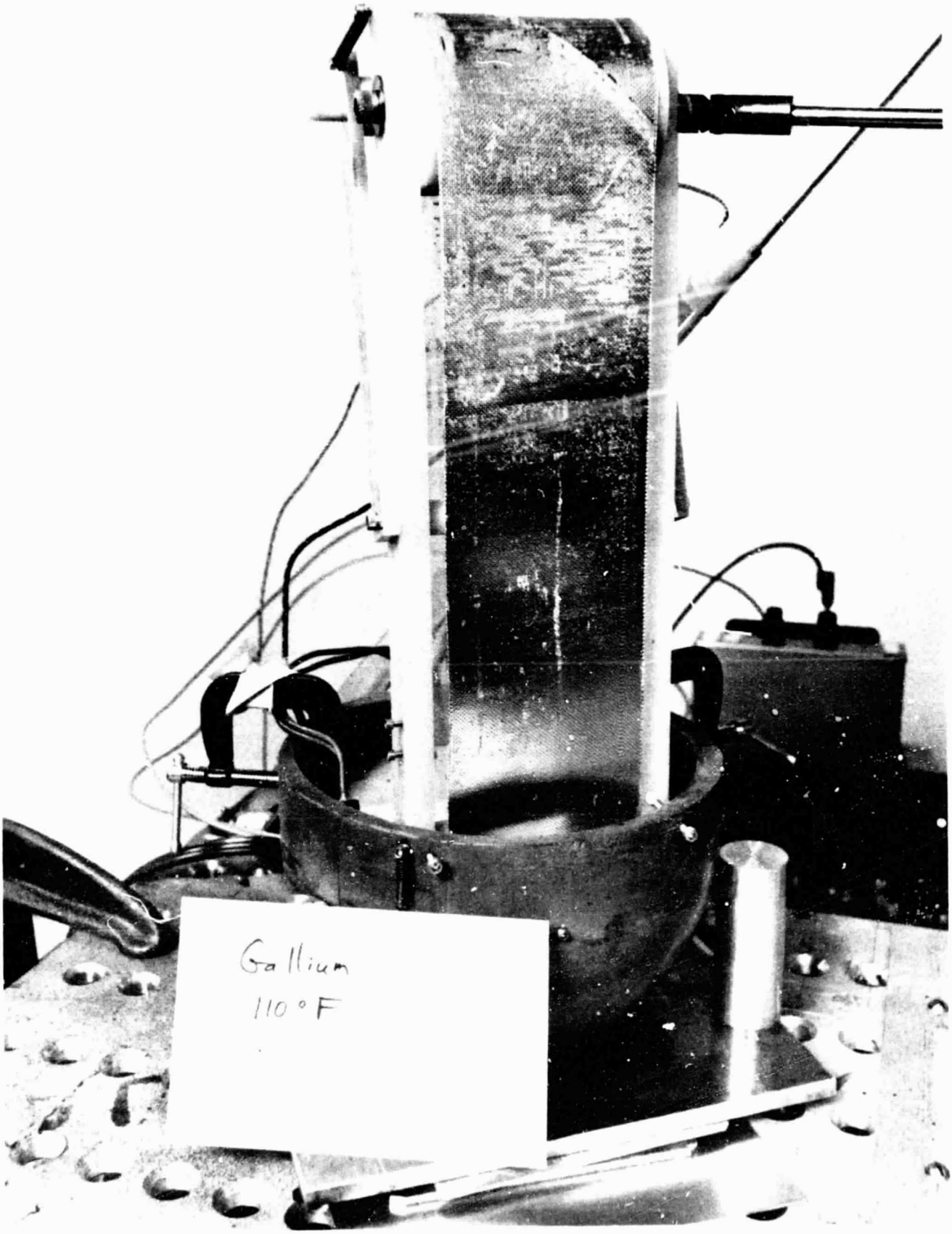

Figure 6.6 MENISCUS FORMATION ON THE LBR TEST RIG USING GALLIUM

point. As indicated, the meniscus covers about 70 percent of the surface despite the poor wetting properties of gallium on the screen material. This verifies the observations made during the Cerrolow tests that an LBR can be formed even if the materials do not wet - at least in the change of phase mode. Further investigation of the reasons behind these observations must be explored.

6.3 Optical Property Determinations

An important parameter governing the required radiating area and mass of the LBR system is the total emissivity of the working fluid. Earlier work (Section 2) documented the necessity of selecting bath materials with sufficiently large emissivities ($\varepsilon \geq 0.3$) and vapor pressures low enough to ensure minimum evaporative mass loss.

During the course of this program, experiments were conducted to measure various candidate fluids' optical properties. These materials included diffusion pump oils and the low vapor pressure metal gallium. The procedures and results of these investigations are presented in the next sections. An overview of this important experimental information acquired during these tests is given in Table 6.2.

6.3.1 Optical Property Measuring Equipment

The determination of a material's emissivity, or other optical properties may be accomplished through a variety of techniques. Initially, thermal imagers and spot radiometers were viewed as the best means to determine emissivity. The majority of these devices however, only function within the bandwidths of 3-5 μm, and/or 8-12 μm depending upon the detector used. Such narrow intervals correspond to only a small portion (<50 percent) of the black body emitted energy associated with temperatures between 310 K and 505 K. It was viewed as questionable whether the data obtained from these particular wave length bands would provide enough information to extrapolate the remainder of the emissivity spectrum. Due to these shortcomings, use of these devices was excluded.

Table 6.2

EXPERIMENTALLY DETERMINED EMISSIVITY VALUES

MATERIAL	PHASE	TEMPERATURE (K/°F)	THICKNESS (mm/mil)	WAVELENGTH RANGE (μm)	NORMAL EMISSIVITY RANGE from 2000-400 cm^{-1} (from 1600-400 cm^{-1})
Santovac 5	Liquid	318/113	~0.89/35	5-25	0.72-1.0[1] (0.82-0.95)
DC-704	Liquid	318/113	0.28/11	5-25	0.35-0.85[1] (0.40-0.85)
DC-704	Liquid	318/113	0.64/25	5-25	0.70-0.99[1] (0.81-0.99)
Gallium	Solid	295/72	5/197	5-25	0.35-0.65[2,3]
Gallium	Liquid	306/91	5/197	5-25	Results Inconclusive[2,3]

(1) Wavenumber range from 2000-1600^{-1} speculated to have wide variation due to presense of extraneous water vapor and instrument noise.
(2) Derived from specular reflectance measurements assuming $\epsilon_N = 1-r_{sp}$.
(3) Experimental results viewed as questionable.

Additional investigations suggested that an apparatus available in Arthur D. Little laboratories could be adapted to perform the required emissivity measurements. At the heart of this technique is a Fourier Transform Infrared Spectrometer manufactured by the Digilab Corporation. This Fourier transform spectrometer (FTS) has the capability to measure a variety of optical properties (i.e., reflectance, absorptance, transmittance) including normal emittance. The operation of the FTS and its software are discussed in Appendix K.

One of the many salient advantages of the FTS is that a continuous range of infrared wavelengths (2.5-22.2μm) may be simultaneously examined. This wave length band corresponds to what is defined as the mid-infrared region and represents a dominant portion (i.e., >75 percent) of the black body radiation for temperatures between 306 K and 463 K (100-370°F). Thus, the FTS eliminates the need for the extrapolation necessary in most thermal imaging systems.

The measurement of emissivity is carried out through the special optical apparatus used in conjunction with the Fourier Transform Spectrometer. This piece of equipment, shown in Figure 6.7, was designed and built at Arthur D. Little and has been used extensively in a variety of emissivity measurement programs.

The emissivity apparatus consists of an optical path defined by two mirrors and three shallow cylinder measurement areas located on a rotating lazy susan. By nature of the mirror arrangement, only the energy emitted within an azmuthal angle of 8° to the normal is recorded. From the work of Schmidt and Eckert, this experimentally determined normal emissivity value may be used to deduce the total hemispherical emissivity of a substance.

Of the three measurement areas, two are thirty degree V groove experimental blackbodies. These disks may be run at various temperatures, and act as a reference for emissivity comparisons. The third position consists of a cell in which sample materials (i.e., fluids, solids, powders) may be heated. Provisions are made for not only measuring emitting surface temperatures, but for detecting any gradients within the material as well. In order to align each measurement area with the FTS, the lazy susan is simply rotated.

ORIGINAL PAGE IS
OF POOR QUALITY

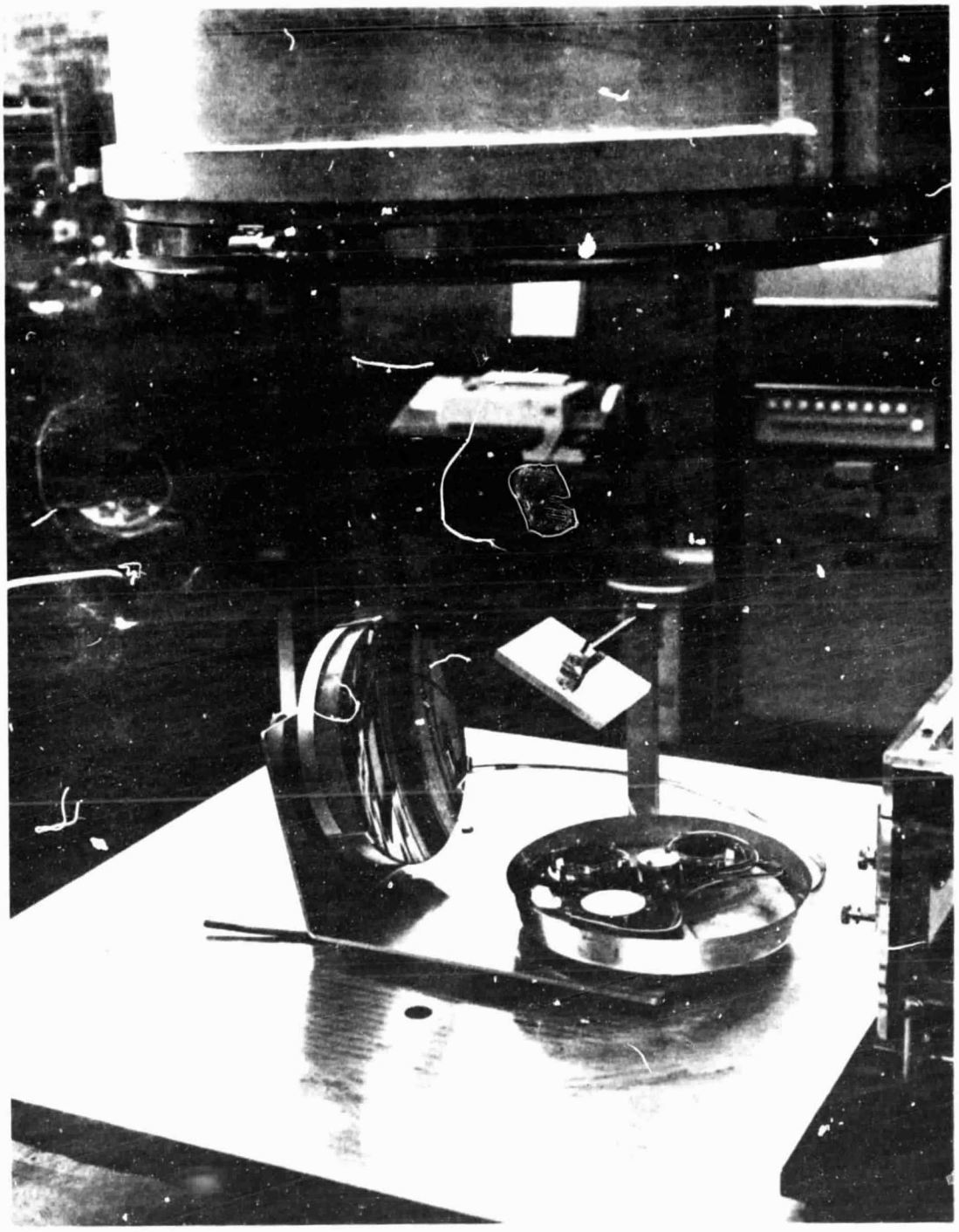

Figure 6,7 EMISSIVITY APPARATUS OPTICS

The emittance optics are surrounded by a temperature monitored black cavity, and enclosed in a bell jar so that inert gas or vacuum measurements can be made. In order to distinguish the sample from the background thermal environment, sample temperatures are approximately 20°C above ambient. The spectral characteristics of the emitted radiation are calculated from spectrometer data and measured temperatures using software developed at ADL for that purpose. When displayed, this data is plotted as a spectrum, having zero to unity emittance as the ordinate and reciprocal wavelength (wavenumber) as the abscissa.

6.3.2 Transmission Measurements

In order to evaluate the spectral characteristics of low temperature working fluids, experimental determinations of transmission spectra were completed. The goal of these experiments was to evaluate the behavior of low vapor pressure oils at a range of wavelengths corresponding to dominant energy emission at temperatures between 311 K and 331 K (100-135°F). The ideal fluid would be characterized by near unity transmission in the infrared region up to 6.25μm, and an opaque appearance (i.e., no transmission) for wavelengths greater than 6.25μm. This behavior would imply that the majority of incident short wavelength solar radiation would be transmitted through the material, with longer wavelengths either absorbed or reflected. If Kirchhoff's law is assumed to be valid in this opaque region, the energy balance at the surface may be written as:

$$\varepsilon \equiv \alpha \equiv 1-r-T$$

Where: r is the hemispherical reflectivity, α is the absorptivity, T is the transmittance and ε is the hemispherical emissivity. Since most oil-like materials characteristically have small reflectivities, near unity emittance could be expected if T is near zero at the relevant thickness.

Three candidate low temperature diffusion pump oils were tested to determine their transmission spectra. The FTS system (See Appendix K for transmission mode operations) evaluated the transmission through the oils D-7050 (McGhan Nusil Corp.), Santovac 5 (Monsanto Corp.), and Convoil (Consolidated Vacuum Corp.) over the wavenumber range 4000-450 cm^{-1} (2.5-22μm). For each of the oil samples tested, two thicknesses (0.01 cm/4.0 mils and 0.002 cm/0.8 mils) were run.

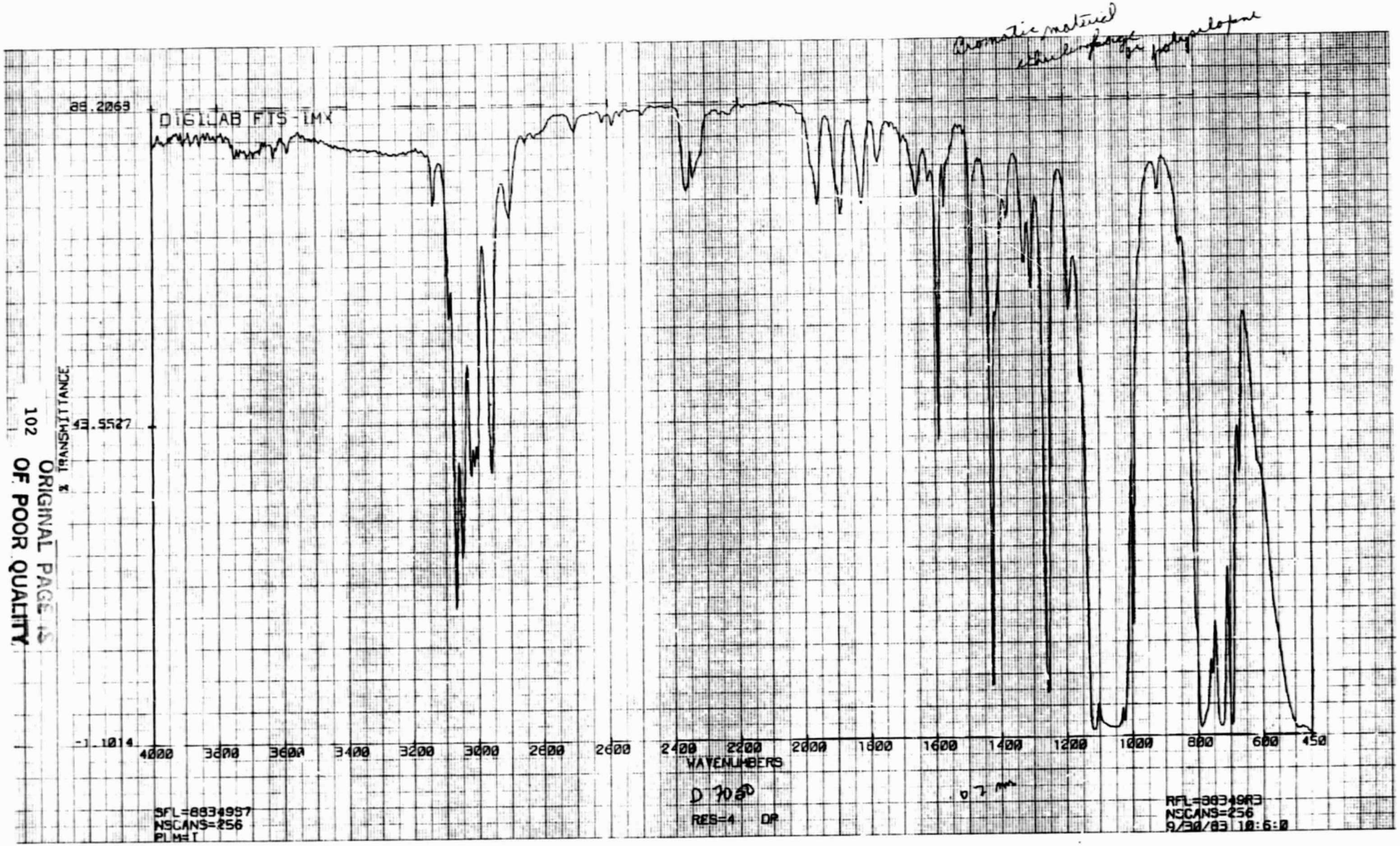

Figure 6.8a D- 7050 TRANSMISSION SPECTRUM AT 0.02 mm THICKNESS

ORIGINAL PAGE IS
OF POOR QUALITY

ORIGINAL PAGE IS
OF POOR QUALITY

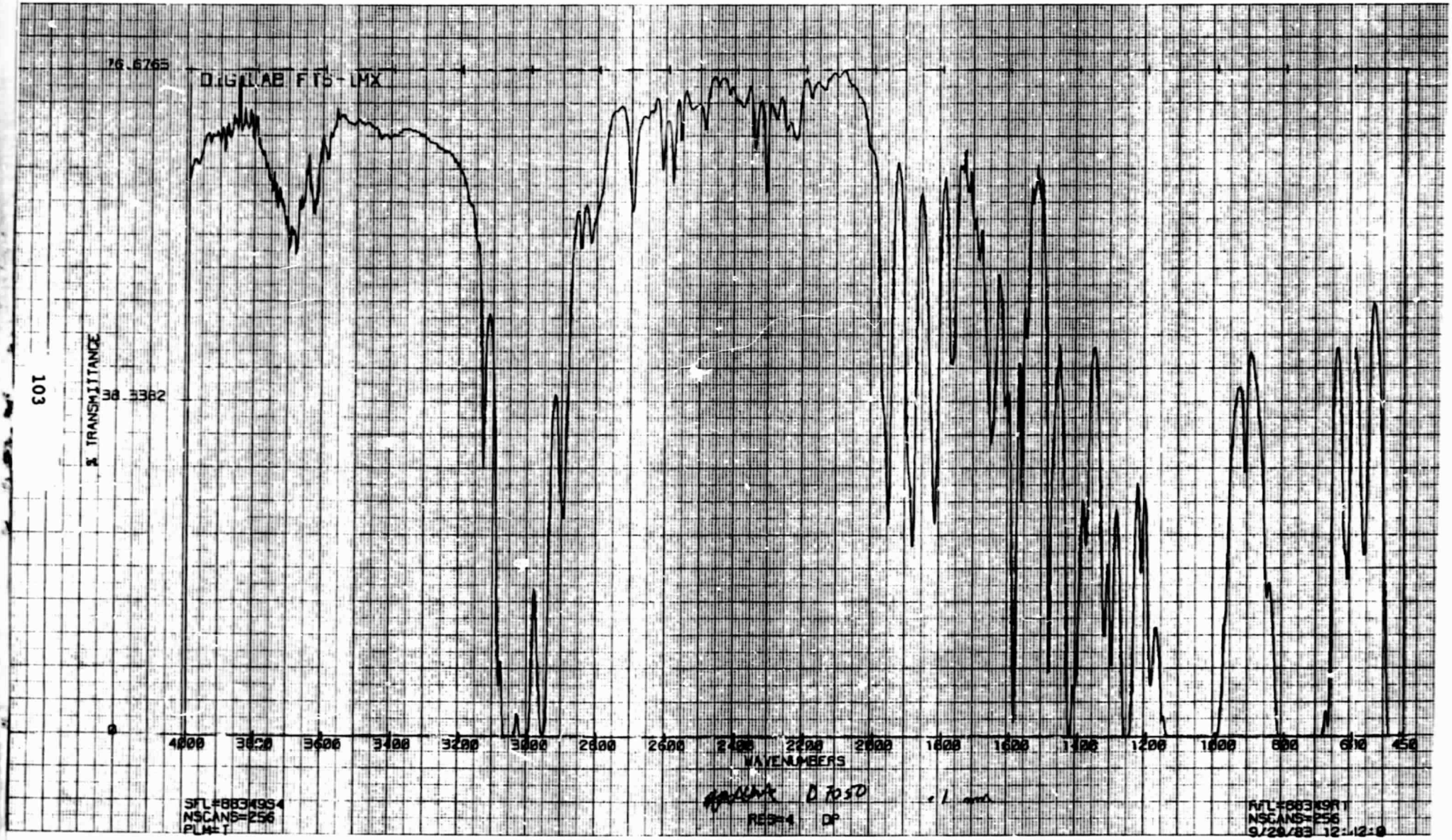

Figure 6-8b D-7050 TRANSMISSION SPECTRA AT 0.1 mm THICKNESS

ORIGINAL PAGE IS
OF POOR QUALITY

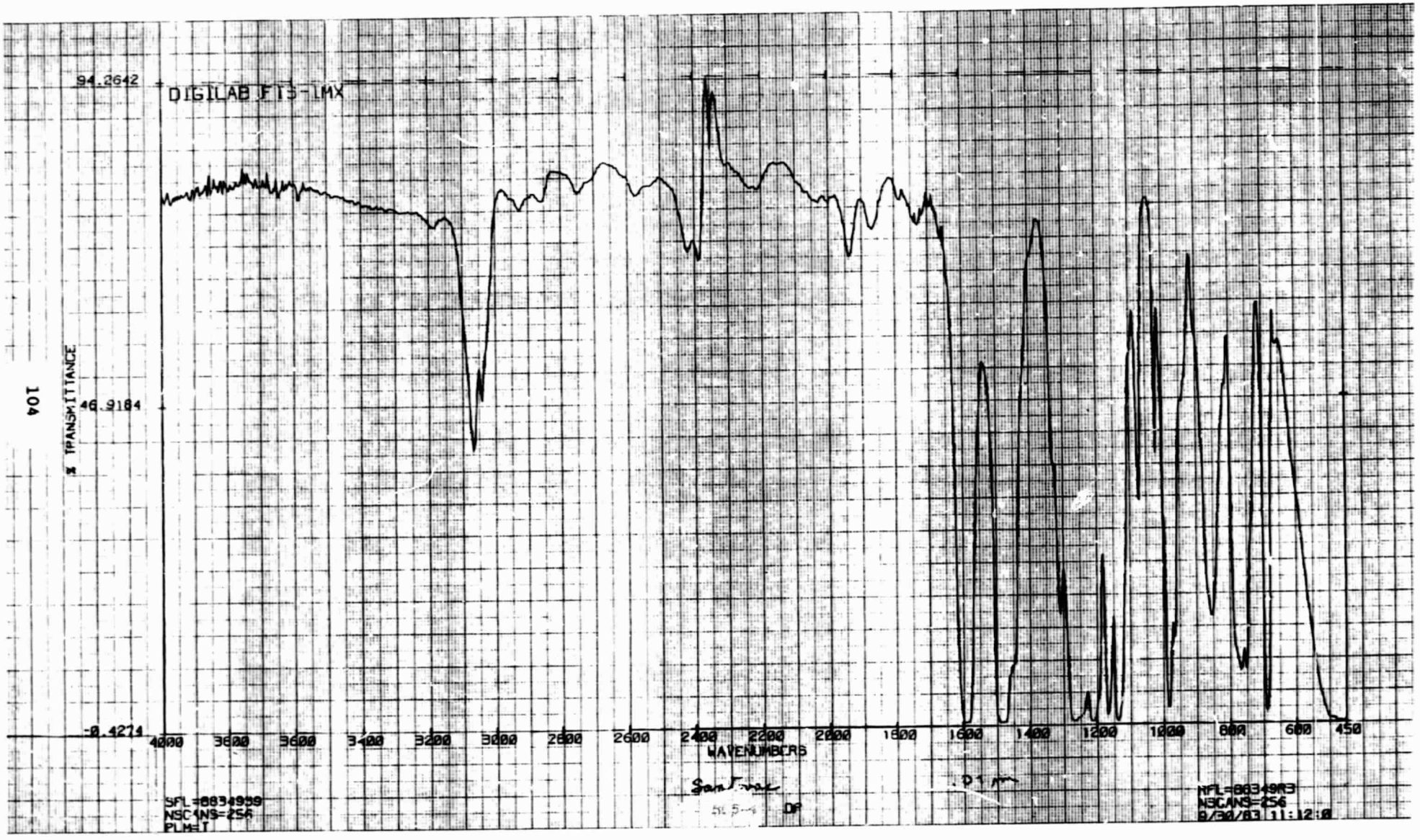

Figure 6.9a SANTOVAC 5 TRANSMISSION SPECTRA AT 0.02 mm THICKNESS

ORIGINAL PAGE IS
OF POOR QUALITY

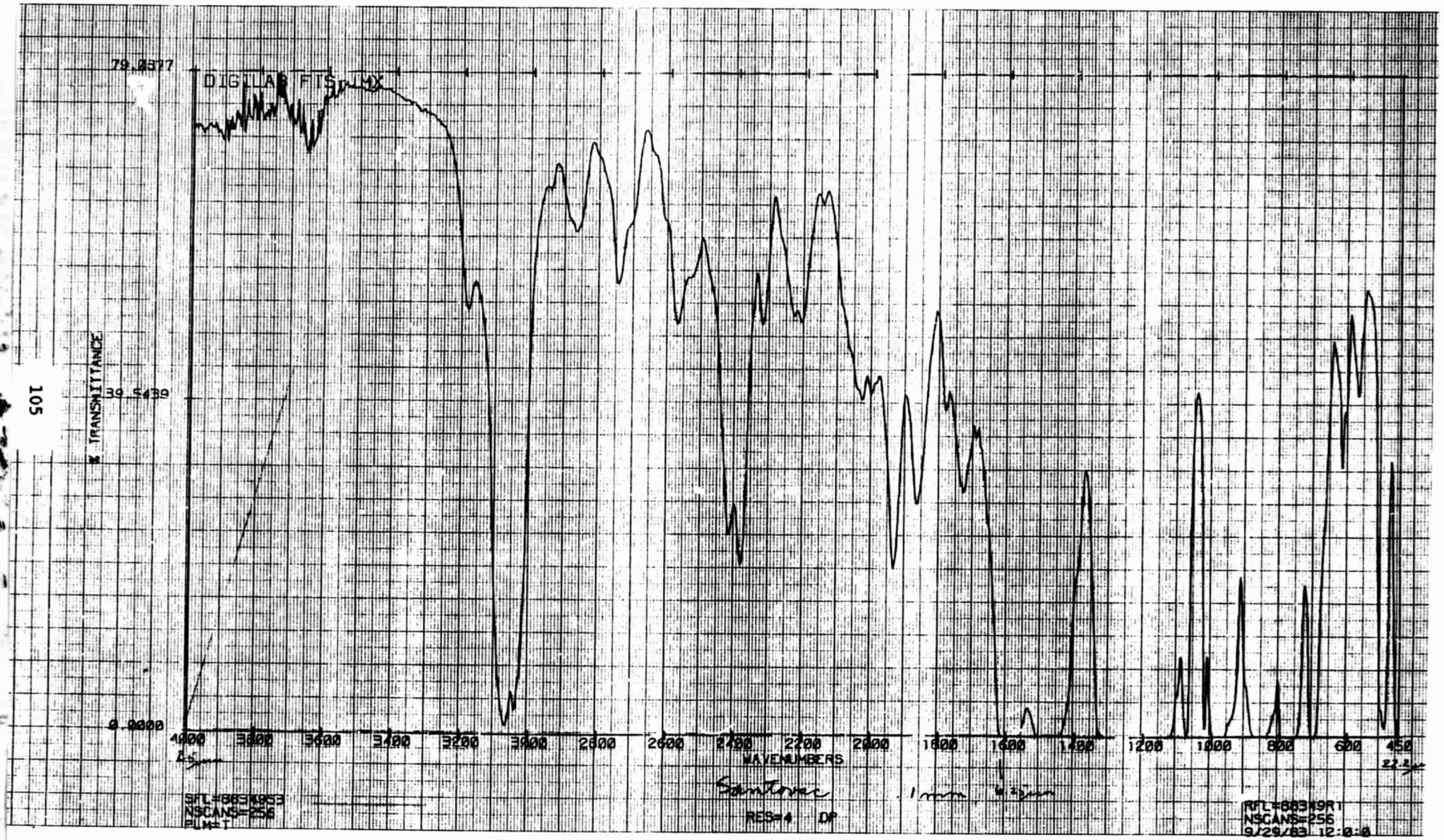

Figure 6.9b SANTOVAC 5 TRANSMISSION SPECTRUM AT 0.1 mm THICKNESS

ORIGINAL PAGE IS
OF POOR QUALITY

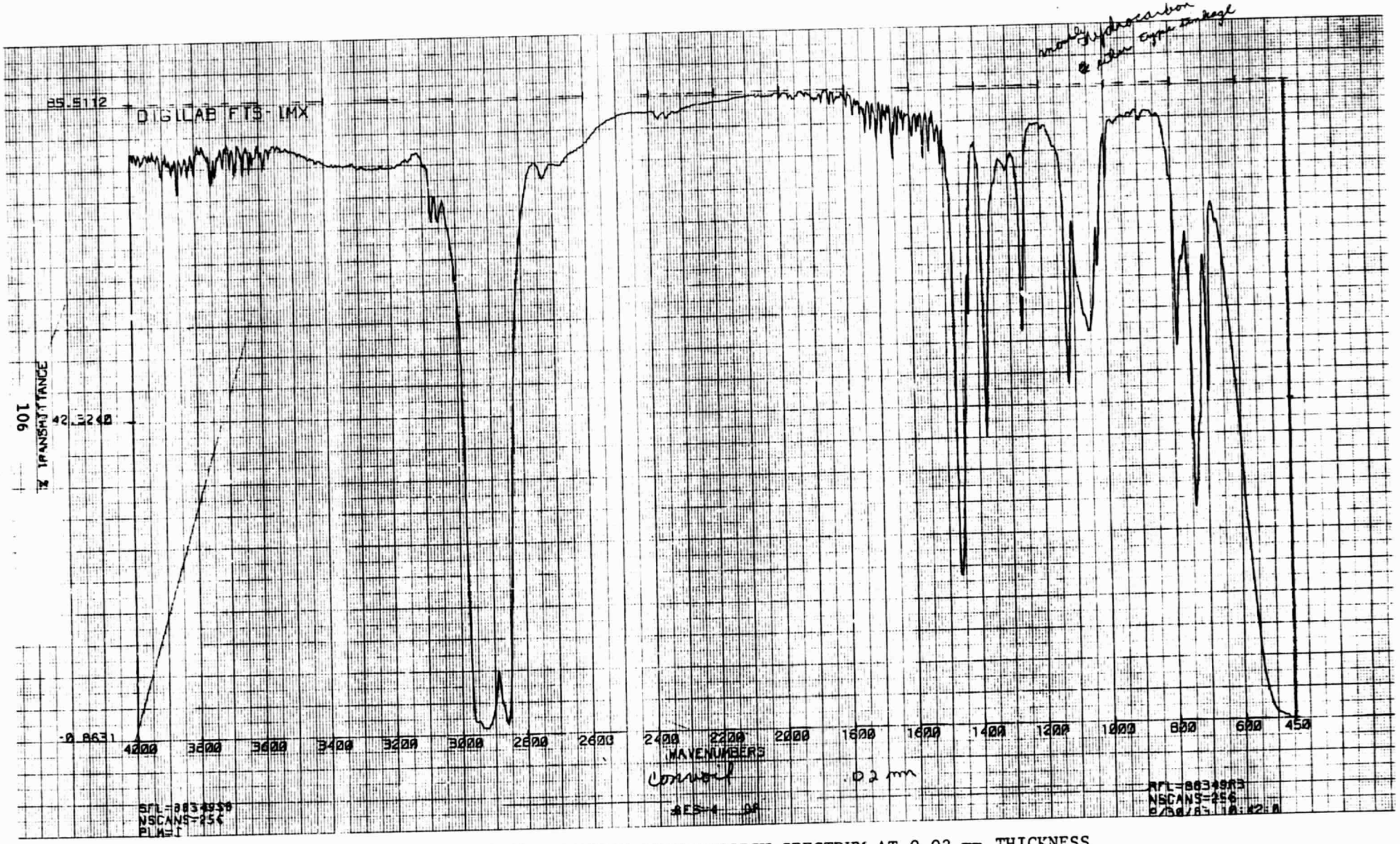

Figure 6.10a CONVOIL TRANSMISSION SPECTRUM AT 0.02 mm THICKNESS

ORIGINAL PAGE IS
OF POOR QUALITY

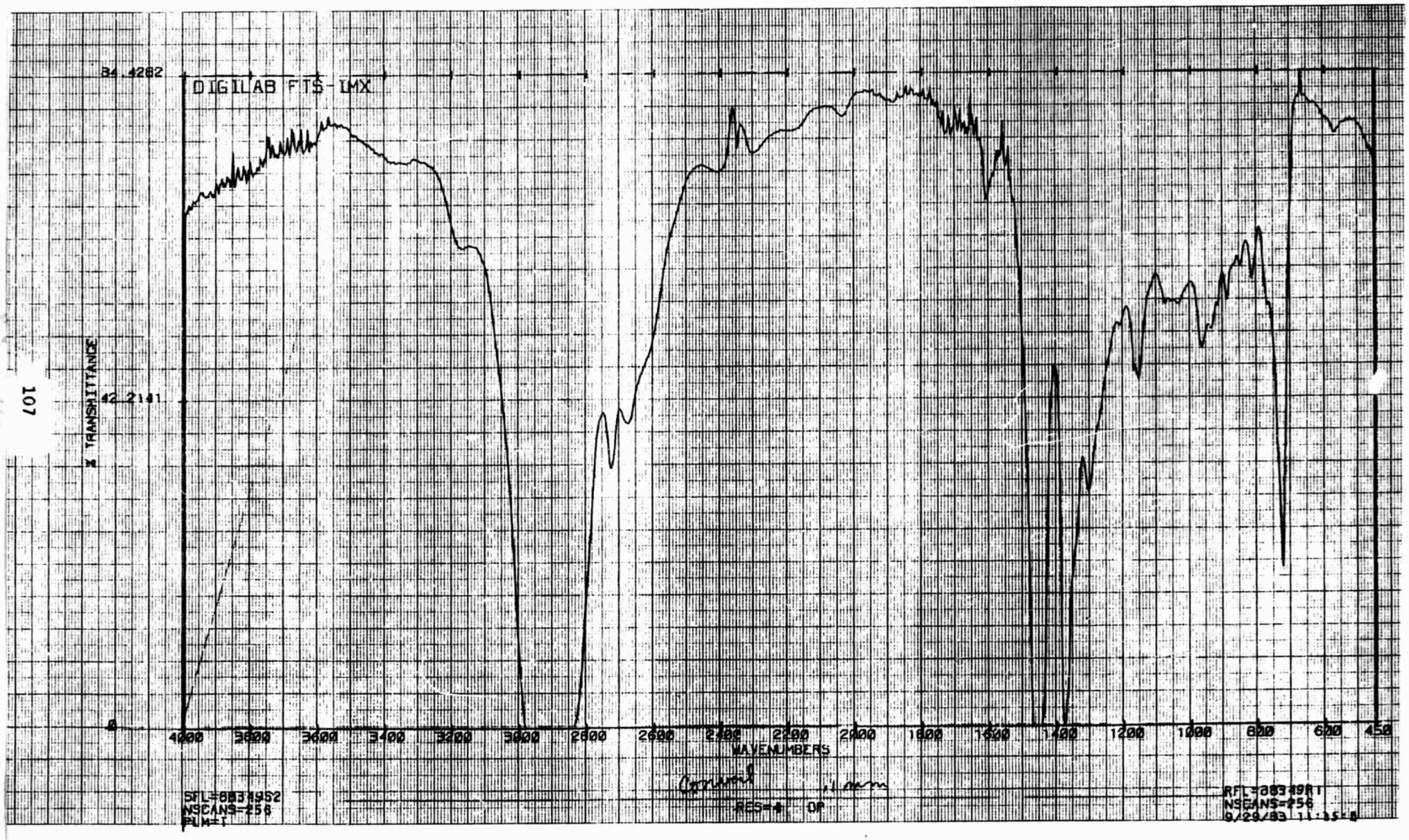

Figure 6-10b CONVOIL TRANSMISSION SPECTRUM AT 0.1 mm THICKNESS

The results of these experiments are represented by percent transmittance versus wavenumber plots and are shown in Figures 6.8-6.10. From these plots, certain observations may be made:

- o For the given thicknesses, all the oils are transparent in the near infrared (wave numbers in the range of 4000-2000 cm^{-1}). A preliminary conclusion would be that such materials are transparent to solar radiation.
- o At thicknesses of 0.01 cm and 0.002 cm, the transmission of all the oils (particularly Santovac 5 and D-7050) drops off as the wave numbers exceed 1670 cm^{-1}. The wave number range (1670-450 cm^{-1}) corresponds to the region of dominant black body radiation for a temperature of 310 K. Since oils are characteristically not reflective, an initial conclusion would be that these materials would exhibit a potentially good value for the emissivity ($\varepsilon > 0.7$), and therefore closely approximate ideal black body behavior.
- o For each oil, the thickness of the sample is inversely proportional to the percent transmitted.

6.3.3 Emissivity Measurements

In order to verify the above hypotheses, the emissivity of particular oils were measured. After reviewing the transmission plots, Santovac 5 was selected for additional study. This material, a five ring polyphenyl ether is characterized by low vapor pressure and a close approximation of opaque behavior through the wavelengths of interest ($\geq$ 6μm). In addition to Santovac, the Dow Corning Corporation oil DC-704 was tested. This material has been specified as a potential working fluid for other radiator systems, and was examined at the request of NASA LeRC.

The results of these experiments are given in terms of normal emissivity vs. wavenumber and are depicted in Figures 6.11-6.13. Both oils were tested under an atmosphere of 750 mm of nitrogen and a temperature of approximately 318 K (113°F). Extraneous results in the 2000-1600 cm^{-1} range are conjectured to be

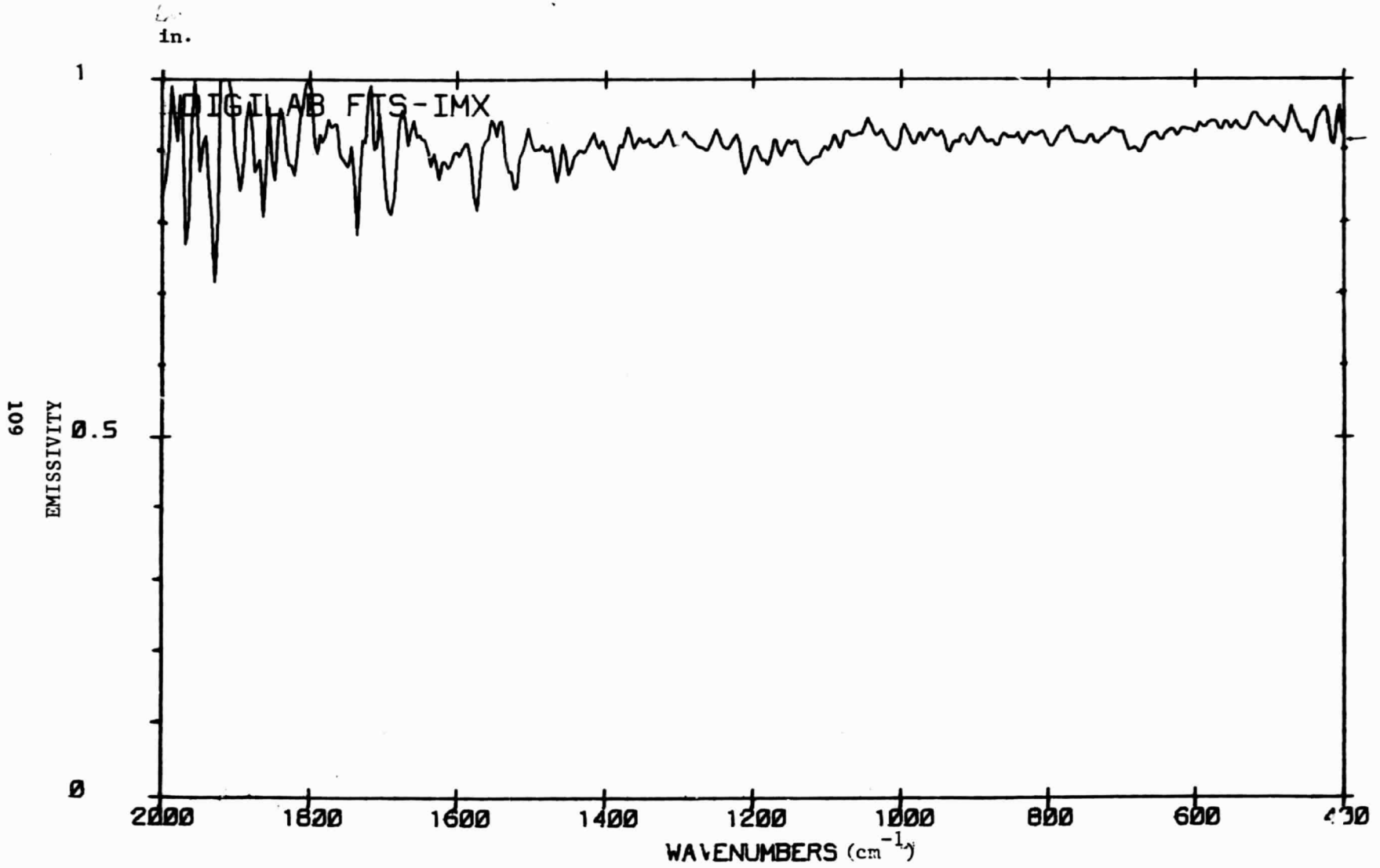

Figure 6.11 SPECTRAL EMISSIVITY OF SANTOVAC 5 DIFFUSION PUMP OIL at 0.09 cm THICKNESS

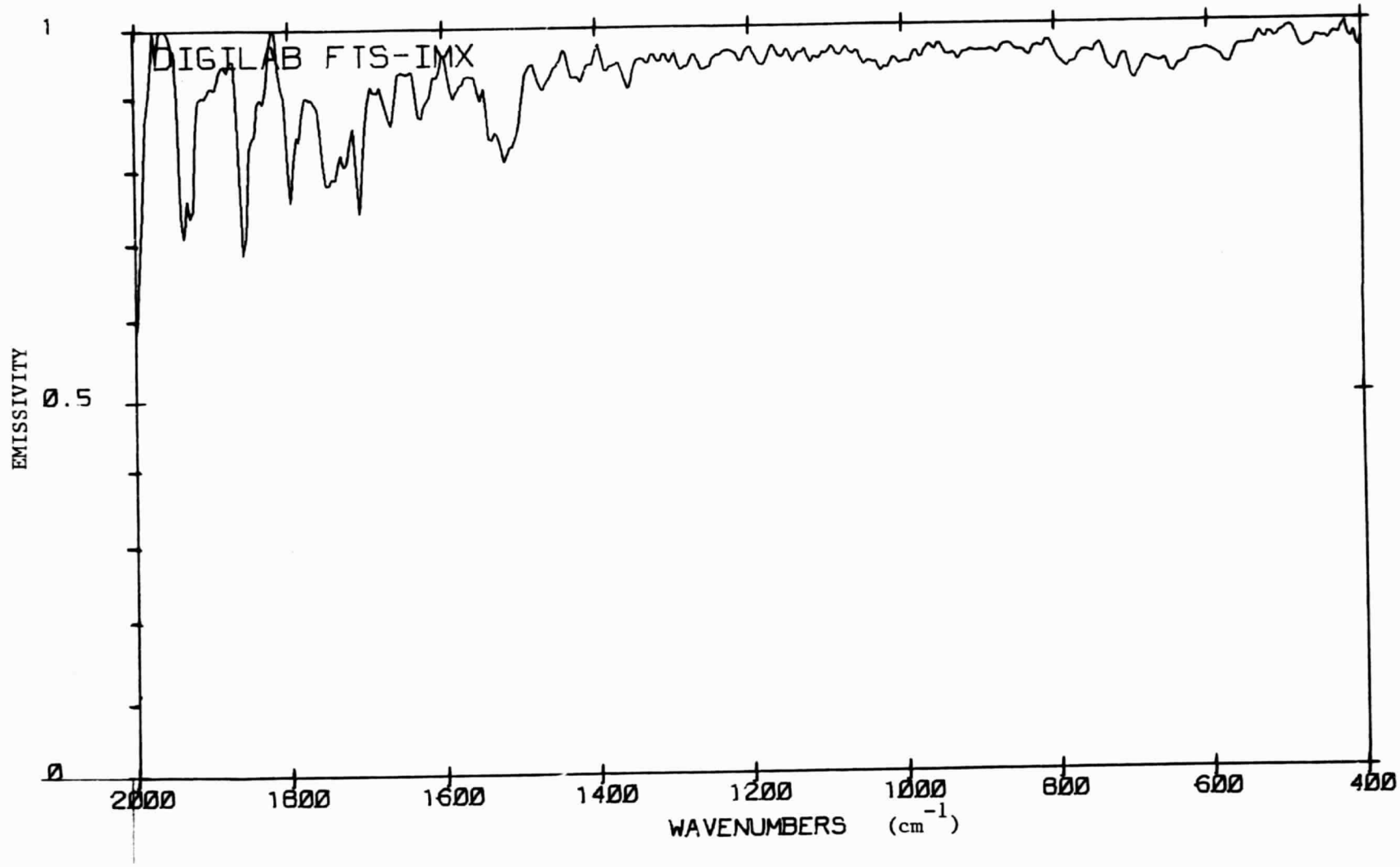

Figure 6.12 SPECTRAL EMISSIVITY OF DC-704 DIFFUSION PUMP OIL AT 0.06 cm THICKNESS

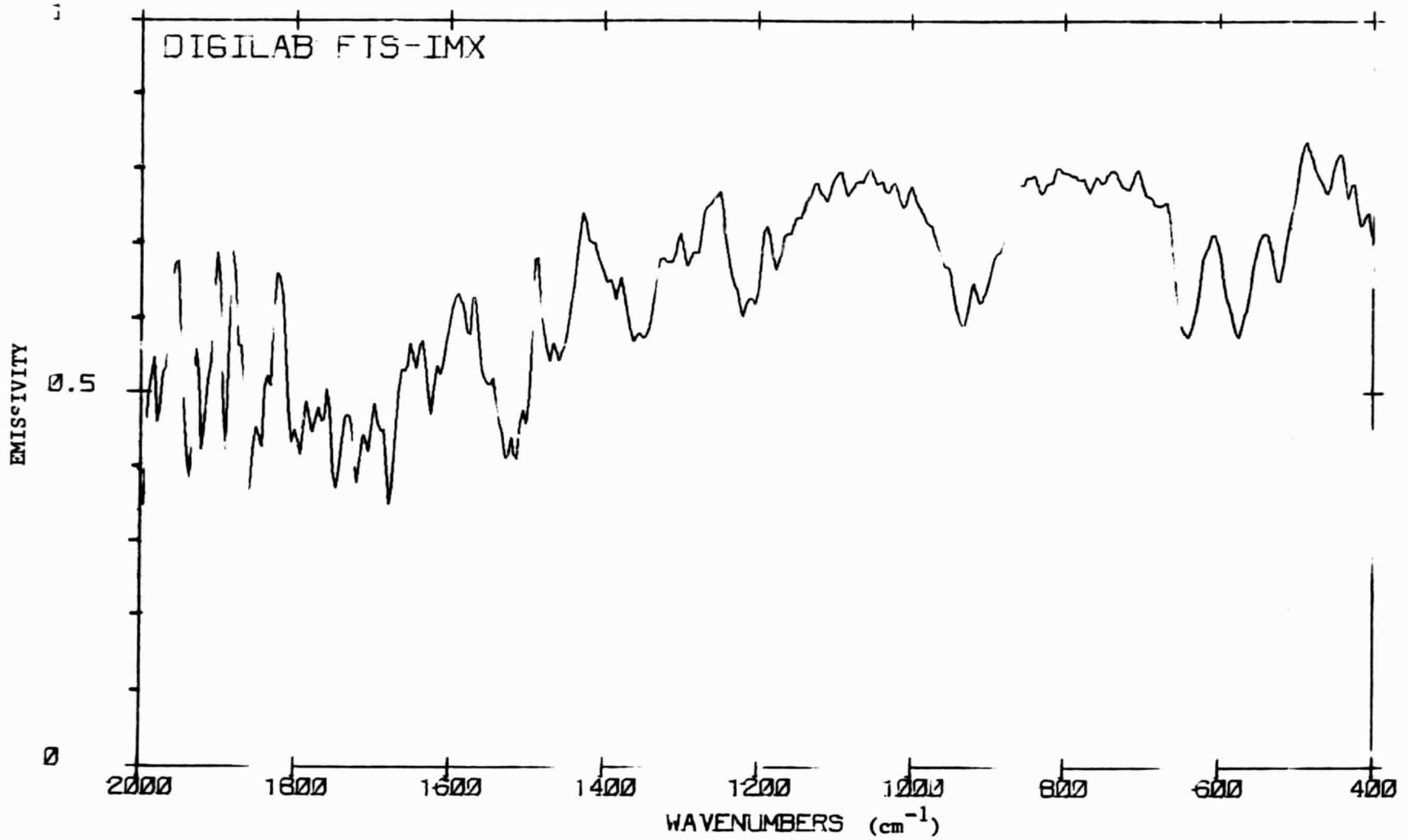

Figure 6.13 SPECTRAL EMISSIVITY OF DC-704 DIFFUSION PUMP OIL AT 0.03ccm THICKNESS

due to water vapor not completely purged from the emissivity measurement apparatus and a poor sample signal to instrument noise ratio at this temperature.

The results of these experiments indicate that the thicker samples (> 0.06 cm, 25 mils) of both materials have normal emissivities which are relatively flat in the 1600-400 cm^{-1} range with values of 0.9 or better. The 0.03 cm (11 mils) sample of DC-704 (Figure 6.13) reveals a band structure associated with the spectral emissivity. These crests and troughs indicate some form of vibrational molecular interactions. This particular sample has an average normal emissivity in the waveband of interest of approximately 0.7. This lower value indicates that thinner layers of oil are sufficiently non-absorbing in the infrared to affect the average emissivity. However, since belt thicknesses may be of the order to 0.05-0.08 cm (20-30 mils), the criteria for optical thickness (negligible transmission) and hence high emissivity can be met. It should also be noted that the large normal emissivities recorded verify the hypotheses stemming from the transmission experiments.

6.3.4 Gallium Measurements

Because of gallium's very low vapor pressure and long liquid state range (from 303 K - 2344 K) this material was considered as a possible LBR working fluid. Gallium's properties make it potentially suitable for a wide range of NASA missions including both low temperature phase change and high temperature sensible heat rejection applications.

A key factor in the utilization of gallium is its emissivity. Like all metals, pure gallium is a highly reflective substance. Because of this mirror-like behavior, very little radiation is absorbed into the material, despite its internal free electron character. In accordance with Kirchhoff's Law, this low absorptivity will necessarily imply very small emittance values.

In order to verify these predictions, an experimental investigation of the emittance of gallium was conducted. Due to gallium's mirror-like surface characteristics and low melting point, the apparatus and techniques used in the

oil emissivity measurements were considered to be ill-suited for this study. Instead the Fourier transform spectrometer was used to measure the infrared specular reflectance of liquid and solid gallium surfaces.

It may be recalled that in the absence of transmission, Kirchhoff's Law implies that:

$$\varepsilon_H = 1-r_{H,\theta} = 1-r_{\theta,H}$$

where:

ε_H is the directional emissivity
$r_{H,\theta}$ is the hemispherical/directional reflectance
$r_{\theta,H}$ is the directional/hemispherical reflectance

In a bidirectional experiment, if it is assumed that the reflectance is 100 percent specular (i.e., no diffuse component exists). This relation may be re-expressed in the following form:

$$\varepsilon_\theta = 1-r_{\theta,\theta}$$

where:

$\varepsilon\theta$ is the directional emissivity
$r_{\theta,\theta}$ is the purely bidirectional reflectance

This assumption was made in order to simplify the experimental procedure and may be justified by the mirror-like behavior (i.e., bidirectional reflectance) of polished metals. In practice, this formulation will result in directional emissivities on the high side, since all materials (including metals) exhibit some form of diffuse behavior.

The gallium sample was prepared by melting it into a standard diffuse reflectance sample holder and allowing it to resolidify. An area 8 mm in

diameter was examined. It should be noted that no special surface preparations (i.e., vacuum bake) were undertaken, resulting in "as is" gallium surface measurements. Spectral conditions were:

- Detector: Liquid nitrogen cooled mercury/cadmium/telluride device; a bandwidth 4500-457 cm^{-1}
- Scans: 1024
- Infrared Reference: Front Surface Aluminum Mirror (reflectance 99.1 percent for wavelengths of concern)
- Resolution: 4 cm^{-1}

The results of these experiments are shown in Figure 6.14. In the solid state, the gallium showed a reflectivity ranging from approximately 0.35 at 4000 cm^{-1} to about 0.65 at 450 cm^{-1}. In the liquid state, the reflectivity dropped to approximately 0.15 over the entire spectral range.

These results would indicate the spectral emissivity of liquid and solid gallium to be in the range of 0.35-0.85. Such findings are in conflict with various theoretical studies, and most likely are the consequence of the following two problems.

- As a liquid, gallium forms a meniscus which will change the curvature of the surface. In this case the angle of incidence will not equal the angle of reflection, and the directionality of the surface will change. This cannot be compensated for because any IR transparent material placed on the surface will have its own reflective and refractive properties. It is speculated that the majority of reflected energy missed the detector thus leading to the low measured spectral reflectance.
- The second problem involves the formation of a cloudy film of organic or oxide contaminant on the surface of the solid and liquid gallium. This material greatly changes the apparent optical characteristics of the gallium and in fact may result in a highly absorbing, low reflectance material.

ORIGINAL PAGE IS
OF POOR QUALITY

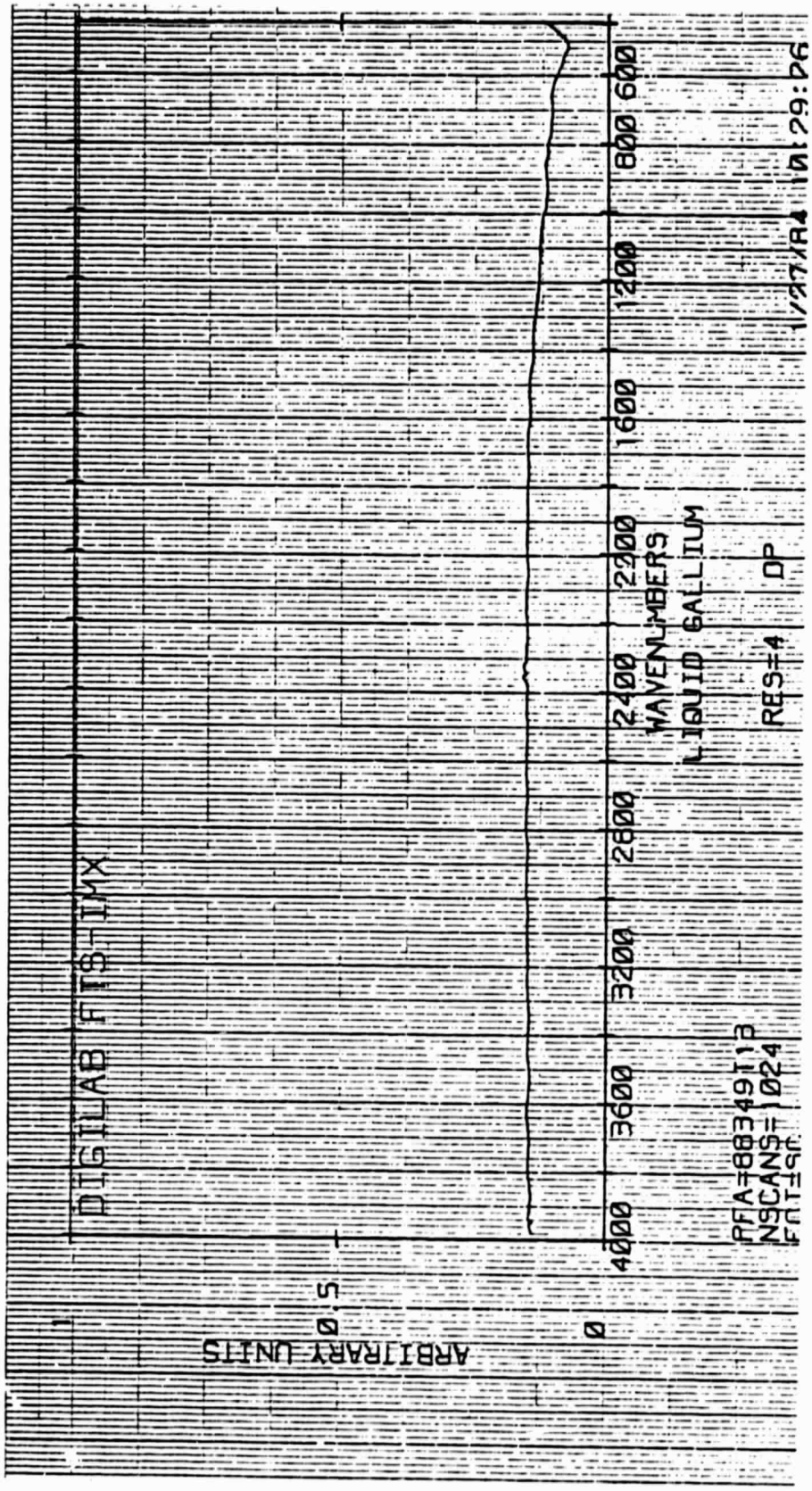

Figure 6.14a LIQUID CALLIUM REFLECTANCE SPECTRUM

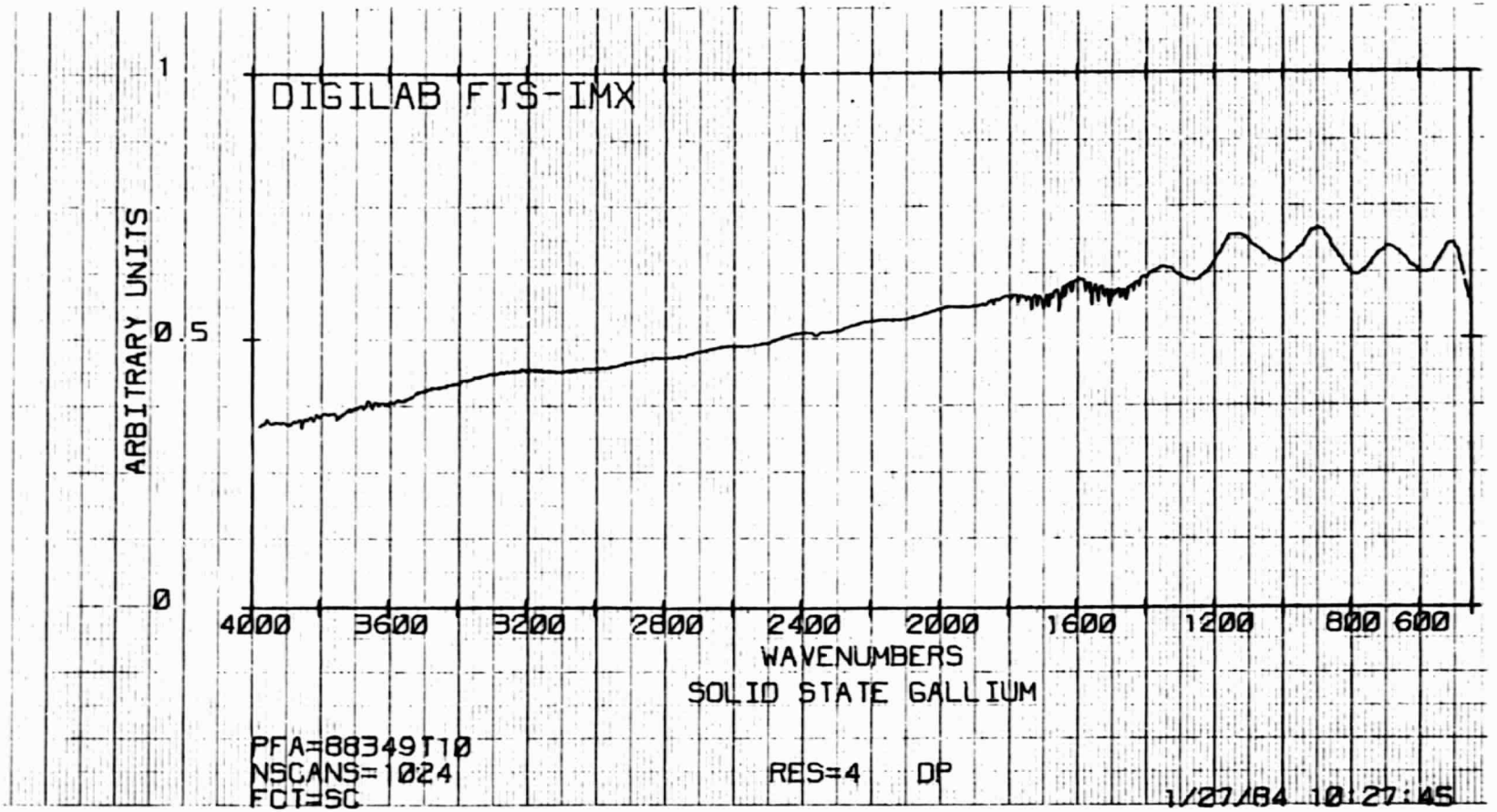

Figure 6.14b SOLID GALLIUM REFLECTANCE SPECTRUM

ORIGINAL PAGE IS
OF POOR QUALITY

Theoretical investigations using the Hagen-Rubens formula predict solid gallium reflectance values of approximately 0.94. Additional experimental work carried out with a thermal imaging system operating over an 8-12 μm bandwidth revealed that the reflectance of liquid gallium compared to the 0.95 reflectance value of a similarly heated piece of solid aluminum. While this result is not quantitatively rigorous, this fact along with the analytical results of the Hagen-Rubens formular does cast further doubt on the results obtained in the specular reflectance experiments. More experimentation, involving controlled conditions and clean gallium surfaces, is necessary to validate the results obtained from the spectral reflectance investigations.

7.0 TECHNICAL ISSUES

This study served to provide a preliminary characterization of the LBR concept and to quantify its performance potential as compared to conventional radiator technology. It also helped highlight many of the technical issues that must be addressed in more detail in order to fully assess the potential for the LBR and to commit to its development for flight ready hardware. These issues include:

o Liquid Metal Emissivities

In the lower temperature ranges (<350 K) selected diffusion pump oils can be used as LBR working fluids. As shown in this study, these oils have high emissivities which favor their use with an LBR system. However, for higher temperature operation or in missions where the evaporation loss from diffusion oils is unacceptable, it will be necessary to use metals such as gallium, indium, or tin as the heat transfer media.

As suggested by measurements in this program and elsewhere, the emissivities of these materials in the liquid state are unacceptably low (<0.1). Their emissivities in the solid state (which would prevail in a change of phase operating mode) may, however, be sufficiently high to make their use attractive (~0.3+) - particularly if small amounts of stable impurities are present. More information on the emissivities of candidate metals both pure and with stable impurities are needed in order to properly assess their potential within the LBR concept.

o Liquid Bath Containment and Parasitic Power

The design of the heat rejection bath requires that the moving belt exits without dragging an excessive amount of fluid through the exit slot. Preliminary analysis indicates that this can be done by making the gap between the belt and the slot walls sufficiently low that capillary forces contain the liquid. The required gaps are a function of liquid properties and belt speed but would typically be on the order of 0.25-0.64 cm (100-250 mils). This is an important issue in determining potential bath material losses and parasitic

power requirements which need to be addressed in more detail in subsequent program phases.

o Dynamic Stability

The cylindrical shape of the belt assumed in the point design study is only valid as long as no inertial forces act on the belt during spacecraft maneuvers. Preliminary analysis indicates relatively low maneuvering rates (5 degrees per second) could be implemented with the attendant inertial forces being lower than those due to the belt motion itself. The dynamic response of the belt to sustained higher maneuvering rates could be important in determining under what conditions a belt retracting or stabilizing system would be necessary. Additional analysis of belt dynamic response will, therefore, be needed to further refine design parameters and operational limits.

o Deployment Approaches

The point design assumes that the belt is spring loaded in its stowed position. During deployment the belt material is forced into space and subsequent rotational motion slowly forces it into its equilibrium cylindrical shape. This rather simplistic model was sufficient for estimating weights and stowed volumes in this preliminary study. However, much more attention needs to be given to the design of the deployment approach and how this can be done with minimum weight and mechanical complexity impacts.

o System Optimization and Design Refinement

The point design of this study is based on judgements resulting from the parametric analysis. Within this program, resources were not available to undertake optimization studies which would tend to minimize system weights, parasitic power draws, or design complexity.

Defining the full potential of the LBR concept will require more detailed system optimization studies and additional levels of detail in defining resultant system designs.

8.0 CONCLUSIONS AND RECOMMENDATIONS

A preliminary assessment of the LBR concept indicates its potential for resulting in a radiator system having the following characteristics:

- Overall radiator system weights which are about 50 percent those of more conventional radiators using heat pipe/fin configuration or pumped liquid loops. This observation applies for those belt materials having emissivities above 0.3.

- Arrangement which can be readily stowed in compact geometries during launch and then deployed in space without the need for complex assembly procedures.

- Arrangement which can readily accommodate to changing heat rejection requirements.

- Potential for reliable operation over extended periods due to a minimum of moving parts or sensitive components.

- Applicability over all the temperature ranges of interest to NASA by proper selection of heat transfer materials (300-800 K).

These favorable characteristics warrant further development of the LBR as one of the options for large low weight radiator systems which will become increasingly important as mission power requirements increase over the coming decades. As indicated in Section 7.0, the analysis and design studies done in this preliminary study show the potential performance capabilities of the concept and to identify technical issues which must be addressed before committing to hardware development. All the technical issues identified to date appear to be resolvable given sufficient analytical and experimental resources. It is, therefore, recommended that the LBR concept be further refined by undertaking additional efforts in the following areas:

- Liquid Bath Design for Liquid Containment and Heat Exchange
- Belt Storage and Deployment System Design and Analysis
- Belt Dynamics During Maneuvering/Design to Insure Dynamic Stability
- Material Options and Further Characterization
- System Optimization and Design Refinements

The output of this program would:

- Allow for decisions to be made as to the merits of the LBR as compared to other advanced radiator concepts under development.
- Define which combination of design and proof of concept experiments would be required to bring the LBR system to the point where it could be tested in a space environment (e.g., a shuttle experiment).

BIBLIOGRAPHY

Aronson, J.R., et al "The Prospects for Mineral Analysis by Remote Infra-Red Spectroscopy" The Moon: An International Journal of Lunar Studies," D. Reidel Publishing Co., Dordecht - Holland, 1972.

De la Bretheque, Pierre, "Gallium and Gallium Compounds," Encyclopedia of Chemical Technology.

Griffiths, Peter R., Chemical Infra-Red Fourier Transform Spectroscopy, J. Wiley Science, New York, 1975.

Handbook of Geophysics, Revised Edition, Air Force Research Division, Geophysics Research Directorate, 1960.

Hottel, H.C. "Radiant Heat Transmission," Heat Transmission, Chapter 4, McGraw Hill Book Company, Inc., New York, Toronto, London, Third Edition, 1954.

Howell, J. and R. Siegel, Thermal Radiation Heat Transfer: Volume II, Office of Technology Utilization, Science and Technical Information Division, Washington, DC, 1969.

Jacob, M., Heat Transfer Volume II, John Wiley and Sons, New York, 1959.

Jaffe, L. and J.B. Rittenhouse, "Behavior of Materials in Space Environments," ARS Journal, March 1962, pp. 320-346.

Kays, W. and A. London, Compact Heat Exchangers, McGraw Hill Book Company, U.S.A., Second Edition, 1964.

Kennard, E., Kinetic Theory of Gases, Chapter 8, McGraw Hill Book Company, New York and London, 1938.

Knapp, K., "Final Report: Lighweight Moving Radiators for Heat Rejection in Space," Astro Research Corporation, Report No. ARC-TN-1107, November 10, 1981.

Knapp, K., "Study of Moving Belt Radiators for Heat Rejection in Space," Air Force Rocket Propulsion Laboratory, Report No. AFRPL TR-84-001, January, 1983.

Rohsenow, W.M. and H.Y. Choi, Heat, Mass, and Momentum Transfer, Prentice Hall, Englewood Cliffs, N.J., 1961.

Santeler, D.J., et al, "Vacuum Technology and Space Simulation, NASA SP-105, 1966.

Sparrow and Cess, Radiation Heat Transfer, Brooks/Cole Publishing Company, a Division of Wadsworth Publishing Company, Belmont, CA, 1966.

Sparrow, E.M. and V.R. Janssen, "Absorption and Emission Characteristics of Diffuse Specified Enclosures," Journal of Heat Transfers ASME, May 1960.

Appendix A

LIST OF NOMENCLATURE

Symbol	Parameter	Units
A	Frontal area of LBR cylindrical surface = W x D	m^2
A_B	Surface area of belt exposed to space	m^2
A_S	Single sided area (See Appendix I)	
a	Fluid gap between belt and heat exchanger plates	m
b	Radiation heat transfer linearization parameter	
	$1 + \left(\frac{T_s}{T_{RMAX}}\right) + \left(\frac{T_s}{T_{RMAX}}\right)^2 + \left(\frac{T_s}{T_{RMAX}}\right)^3$	none
C_D	Belt drag coefficient = 2.5	none
c_p	Specific heat of belt fluid	W/kg . K
D	Belt diameter	m
E	Heat exchanger effectiveness	none
F_{RS}	Radiative view factor from belt radiator to space	none
G	Newton's Gravitational constant	Nom/kg^2
$\dot{m}$	Mass flow rate	kg/s
m_e	Mass of earth	kg
M	Molecular weight of fluid	gm/gmole
P	Pressure	N/m^2
P_v	Vapor pressure of fluid	N/m^2
ℓ	Exposed belt length = $2\pi R$	m
Q''_{load}	Radiator heat transfer rate	W/Hr
Q_{load}	Radiator heat transfer rate per unit area	$W/Hr \cdot m^2$
r	Reflectivity of surface to thermal radiation	none

r_o	Orbital radius from center of earth	m
R	Belt radius	m
R'	Radius of roller over which belt passes	m
$\bar{R}$	Universal gas constant - 8.314	J/gmole . K
T_R	Radiator temperature	K
T_{RMAX}	Maximum radiator temperature at bath outlet	K
T_{RMIN}	Minimum radiator temperature at bath inlet	K
T_s	Background or equivalent space temperature = 250 K	K
t	Thickness of fluid layer on belt or total belt thickness	m
V	Belt velocity	m/s
V_v	Vehicle or station velocity	m/s
W	Belt width	m
X	Mass scaling factor for LBR	
x	Arbitrary distance of belt travel since leaving bath	m
α	Absorptivity of surface to thermal radiation	none
ρ	Density of belt fluid	kg/m^3
ρ_{air}	Air density at altitude of LBR	kg/m^3
ε	Emissivity of belt surface looking at space	none
ν	Fluid kinematic viscosity	m^2 . s
μ	Fluid dynamic viscosity	N . s/m^2
ϕ	Mass ratio LBR/Heat Pipe	
ϕ_ψ	Belt radiative heat transfer transient response variable	
	$\frac{2F_{RS}\ \sigma\ \varepsilon\ b\ T_{RMAX}^3}{\rho\ \delta\ V\ C_p}$	m^{-1}

θ	Liquid to solid surface meniscus contact angle	Rad
σ	Stefan-Boltzman Constant	$W/m^2 \cdot K^4$

Appendix B

MENISCUS FORMATION AND STABILITY

In order to form a meniscus on the mesh, the following must be true:

- The liquid must wet the mesh material.
- The maximum spacing between the wires in the mesh must not exceed a certain dimension or the meniscus will be unstable under normal dynamic motions of the belt.

Through suitable lab tests, it has been found that diffusion pump oils wet a variety of materials that are suitable candidates for a belt design. Although liquid metals have large values of surface tension, other experiments have shown that liquid metal menisci form on various belt materials (see Section 6.0).

After examining various models for the maintenance of a stable meniscus, it was concluded that absolute equilibrium occurs if the following relationship for a rectangular mesh holds true:

$$\frac{D}{W} < 7.58 \qquad \text{(B-1)}$$

where: D = wire spacing distance, and
W = wire thickness

This derivation is based on the assumption that surface energy is dominant and directly proportional to surface area. If the minimum energy principle is used, the absolute stability criterion implies that a meniscus will be in stable equilibrium if its exposed surface before a potential rupture is equal to or less than that after the rupture.

If modest dynamic disturbances of small perturbations occur, it is expected that the menisci will remain intact due to their inherently metastable character.

More detailed analyses are required to identify any specific dynamic conditions and accelerations under which instability would be expected.

Appendix C

STRENGTH CHARACTERISTICS OF SCREEN MESH BELTS

In order to complete a first order analysis of the strength of a screen mesh structure, the rectangular screen mesh model shown in Figure C.1 was used.

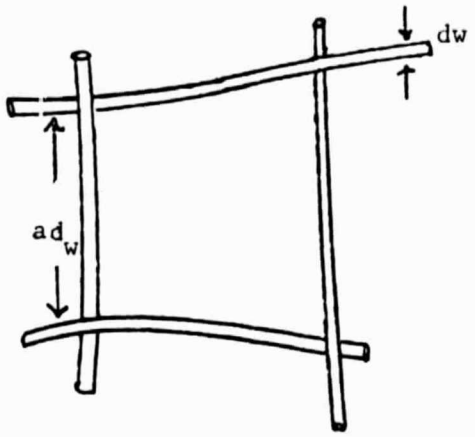

Figure C-1 RECTANGULAR SCREEN MESH MODEL

The important geometrical dimensions of this model are:

d_w = wire diameter

ad_w = wire spacing

The strength per unit length of this structure Fs may be thought of as:

Strength per unit length = (# wires per unit length) X (circular cross sectional area per wire) X (allowable or material ultimate stress)

This may be represented as:

$$Fs = \left(\frac{1}{ad_w}\right) \quad \left(\frac{\pi (d_w)^2}{4}\right) (\sigma)$$

or finally

$$Fs = \left(\frac{\pi d_w}{4a}\right) \sigma$$

Thus this first order analysis gives the strength per length of the mesh as a function of the allowable or ultimate stress of the screen material and the mesh geometry.

Appendix D

THE DEVELOPMENT OF THE PARAMETRIC RADIATIVE AREA EQUATION

The net energy transfer from the parametric belt radiator to space is presented from the figure below. The total output energy may be written as:

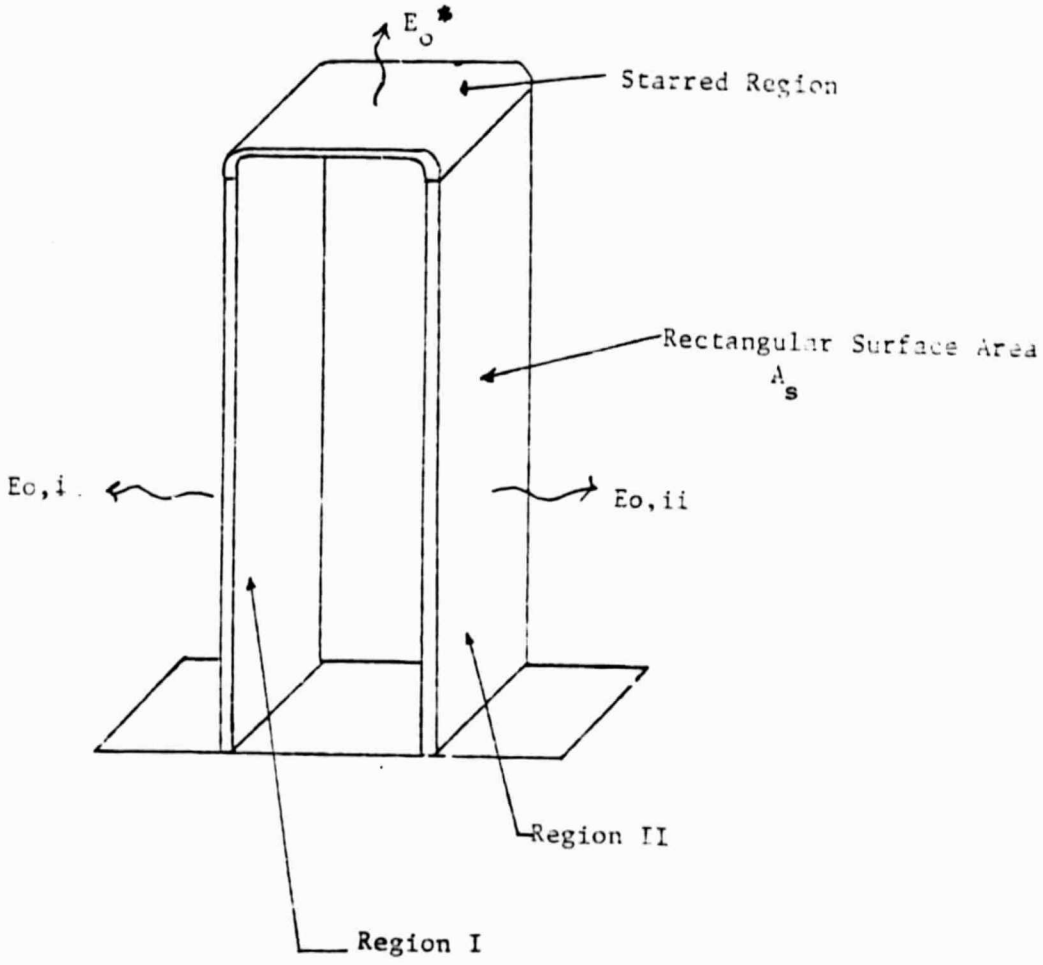

$$E_{oTOT} = E_o, i + E_o, ii + E_o^* \quad , \quad (D-1)$$

where: E_o, i is the output energy from Region I.

E_o, ii is the output energy from Region II.

E_o, * is the output energy from the starred region.

If the energy emitted from the starred region is neglected this figure reduces to:

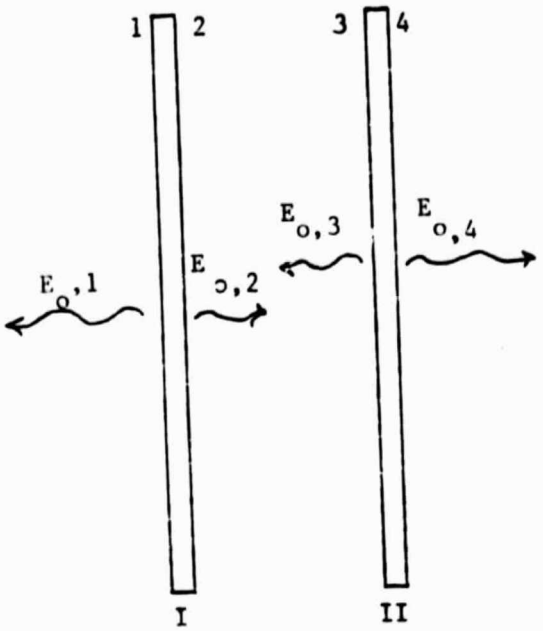

where 1, 2, 3, and 4, refer to the individual surfaces of Region I and II, respectively.

The energy emissions to space from Regions I and II may be expressed in more detail as:

$$E_o, I = e_{o,1} A_1 F_{1s} + e_{o,2} A_2 F_{2s}$$

$$E_o, II = e_{o,3} A_3 F_{3s} + e_{o,4} A_4 F_{4s}$$

where:

F_{is} refers to the view factor of surface i with respect to space.

$e_{o,i}$ refers to the output energy flux from surface i.

A_i refers to the radiative area of surface i.

If all the areas A_i are assumed to be the same, i.e.,

$$A_1 = A_2 = A_3 = A_4 = A_s$$

then from Equation 1, the total output of energy of the two parallel Regions I and II may be expressed as:

$$E_{o,TOT} = A_s (e_{o,1} F_{1s} + e_{o,2} F_{2s} + e_{o,3} F_{3s} + e_{o,4} F_{4s}) \qquad (D-2)$$

where:

A_s is defined as the common projected rectangular surface area common to surface 1-4 of Regions I and II.

The surfaces 1 and 4 are exposed only to space which is assumed to be at zero degrees Kelvin. Their view factors with respect to space are further assumed to be unity. The surfaces 2 and 3 however face each other at non-zero temperatures and therefore will radiate between themselves. The extent to which this internal radiation occurs, affects the net amount of energy these inside belt surfaces can radiate to space.

From basic view factor algebra, the total energy output of surfaces 2 and 3 may be written as:

$$F_{2s} + F_{23} = 1$$

$$F_{3s} + F_{32} = 1$$

where:

F_{23} is the view factor of 2 with respect to 3.

F_{32} is the view factor of 3 with respect to 2.

Further, from the reciprocity relation:

$$A_2 F_{23} = A_3 F_{32}$$

however:

$$A_2 = A_3 = A_s$$

so therefore:

$$F_{23} = F_{32}$$

Using these results, the view factors of the surfaces with respect to space may be written as:

$$F_{23} = F_{32} = 1 - F_{2s} = 1 - F_{3s}$$

Thus the relation for total emitted energy from the LBR becomes:

$$E_{o,TOT} = A_s \left[e_{o,1} + (1-F_{23}) \left(e_{o,2} + e_{o,3}\right) + e_{o4}\right] \qquad \text{(D-3)}$$

In order to make the first order thermal analysis possible, we assume that:

- Optical properties are the same for all surfaces; i.e.,

$$\varepsilon_1 = \varepsilon_2 = \varepsilon_3 = \varepsilon_4$$

- A constant radiating temperature $\overline{T}_{rad}$ exists for all the surfaces, i.e.,

$$\overline{T}_1 = \overline{T}_2 = \overline{T}_3 = \overline{T}_4 = \overline{T}_{rad}$$

In this case, the problem becomes symmetrical with all reflection effects between inside surfaces cancelling. Hence, the individual surface output energy fluxes may be written as:

$$e_{i,o} = \sigma \, \overline{T}_i^{\,4} \, \varepsilon_i$$

where:

$e_{i,o}$ is the energy flux from surface i
e_i is the emissivity of the i^{th} surface
$\overline{T}_i$ is the average radiating temperature of surface i
σ is the Stefan-Boltzman Constant

The total energy emitted from the LBR to space (including the inside belt surfaces) thus (i.e., Equation 3) reduces to the form:

$$E_{o,TOT} = 2\sigma \left(\overline{T}_{rad}^{\,+4}\right) \varepsilon \, A_s \, (2 - F_{23}) \qquad \text{(D-4)}$$

where the total area available for radiative heat transfer is given as:

$$A_{TOT} = 2\ (2-F_{23})\ A_s$$

In further analysis the total output energy emitted to space by the LBR is defined as:

$$E_{o,TOT} = Q_{load}$$

In this case Q_{load} refers to the thermal energy rejection requirements specified by NASA.

Thus, the area defined in terms of the convenient projected rectangular surface area A_s, may be written as:

$$A_s = \frac{Q_{load}}{2\ (2-F_{23}\ \varepsilon\sigma\ T\ (\bar{T}_{rad}{}^4)} \qquad \text{(D-5)}$$

Appendix E

CONTAINMENT OF MENISCUS IN CENTRIFUGAL ACCELERATION FIELD

The fluid meniscus formed between the screen wire elements is positioned by surface tension forces. As the screen belt passes over a roller, centrifugal forces are present which tend to dislodge the fluid web. To calculate the limitations on roller radius which prevent liquid disengagement from the belt, the following analysis was conducted.

Applying a very simple model, we obtained a reasonable estimate of the relationship between roller diameter, belt speed, and fluid parameters. We assumed the fluid (of original film thickness, t_o, before deformation) to be in a hemispherical shape at the point of disengagement from the belt (as shown in Figure E-1). The belt wire spacing, D, angular speed, ω, surface tension, σ, and fluid density, ρ are represented in the following equation which balances centrifugal forces with surface tension forces as the belt moves over a roller of radius, R':

$$\rho \frac{(\pi D^2)}{4} t_o R' \omega^2 = 2\pi D\sigma \qquad \text{(E-1)}$$

In equation (E-1), two film surfaces are assumed to exist. Thus the factor 2 is used on the right side of the equation. This equation leads to the criterion:

$$R'_{min} = \frac{\rho D t_o u_{belt}^2}{8\sigma} \qquad \text{(E-2)}$$

for the medium radius over which the belt must travel while in space. In

equation (E-2) $u_{belt} = R\omega$ is the belt linear velocity.

Substitution values from the point design (Santovac 6 diffusion pump oil of thickness 0.051 cm, moving at approximately 1 m/s, belt wire spacing D = 0.1 cm) results in a value of $R'_{min} = 0.3$ cm (.12 in).

Therefore, we can conclude that for diffusion pump oil in a thickness of .051 cm (.02 in.), there should be no fluid disengagement from the mesh as a result of either motion over the rollers or the circular transit on the cylindrical LBR. Similar calculations also indicate that no problems can be expected for liquid metals.

Appendix F

DEVELOPMENT OF THE PARAMETRIC MASS RATIO, ϕ

In order to compare the mass of the LBR design with that of existing radiator system, the ratio ϕ has been defined. Thus:

$$\phi = \frac{\text{Mass of the Belt Radiator System}}{\text{Mass of the Heat Pump System}}$$

The mass of the belt radiator system may be divided into two main categories:

1) Mass of the fluid material.
2) Mass of the support structure.

a) Mass of the Fluid Material

The fluid is the coolant or bath material which will form menisci on the moving screen belt mesh. For simplicity, it has been assumed that the entire volume of the belt contains only bath fluid. Thus, any effects of the mass of the screen mesh have been ignored. This assumption may be thought to represent a lower bound for the belt mass.

Although the entire volume of the belt has been assumed to be composed of bath material, the effect of the screen mesh mass on the overall mass of the belt, and why it has been ignored, is worthy of mention. The absolute stability criteria, developed in Appendix B may be applied in the determining of individual screen mesh sizes. From this, a ratio of the volume of the screen mesh structure to the volume available for meniscus formation may be derived. The effects of the presence of the screen vary in accordance with the density of the fluid material, the density of the screen itself, and individual mesh sizes. In general, as the size of the mesh increases, the effects of the screen mass diminish.

Experimental results with oils have demonstrated the formation of menisci on large area meshes, the dimensions of which exceed those stipulated by the stability criterion. These findings must be verified for liquid metals. On a

preliminary level, however, these results indicate that larger screen meshes are possible and hence, screen mass effects are small. For this reason the screen mass has been ignored, and a belt comprised totally of fluid is analyzed.

From Appendix D, it may be seen that the mass of the fluid contained by the parametric belt model is:

$$M_{fl} = (2)\ \rho_{fl}\ [A_s\ (\epsilon)]\ t$$

where ρ_{fl} is the density of the bath material; t is the thickness of the belt, A_s (ϵ) the rectangular surface area of the belt (a function of emissivity) and the (2) referring to the two parallel sections of the belt.

In order to provide adequate energy exchange within the bath, additional fluid (exclusive of any make up mass for evaporation) amounting to the arbitrary value of 10 percent of that contained by the belt, was deemed necessary. Thus we define:

$$M_{mat'l} = 1.1 M_{fl}$$

where $M_{mat'l}$ refers to the total amount of fluid carried into orbit by the spacecraft.

b) Mass of the Support Structure

For purposes of analysis, however, the mass of the miscellaneous support structure components was defined to be some multiple X of the mass of the material. Thus:

$$M_{structure} = X\ M_{mat'l}$$

where X is the arbitrary structural mass factor.

Using the above formulations, the entire LBR mass may be written as:

$$M_{LBR\ system} = M_{mat'l} + M_{structure}$$

or

$$M_{LBR} = M_{mat'l} \ (1 + X)$$

and finally;

$$M_{LBR} = 2 \ (1.1\rho_{fl} \ t \ A_s \ (\varepsilon)) \ (1 + X)$$

It is apparent that the primary influences on the belt radiator system mass are the mass multiple factor X and the emissivity ε. A design goal will be to reduce the factor X (ideally making X = 0, and thus reducing the entire system mass to that of the fluid contained by the belt) while enhancing the emissivity of the bath material.

c) Mass of the Heat Pipe Radiator

In order to evaluate the ratio ϕ, some determination of the mass of the heat pipe radiator must be made. The specific mass (i.e., mass per unit prime area) of such systems ranges from 3-5 kg/m^2, where the associated area is the active thermal radiating area. Thus we define:

$$M_{HP} = 4 \ A_{HP}$$

where we have selected the specific mass to be 4 kg/m^2.

Using standard radiative heat transfer equations, the heat pipe radiating area may be written as:

$$A_{HP} = A_{prime} = \frac{Q_{load}}{\sigma \varepsilon_{HP} (T_{HP})^4}$$

where we have assumed as view factor of unity and a space temperature of 0°K.

Thus we may finally write:

$$M_{HP} = \frac{4}{\sigma \varepsilon_{HP} (T_{HP})^4} Q_{load}$$

d) ϕ Evaluation

Recalling the definition of ϕ:

$$\phi = \frac{M_{LBR}}{M_{HP}}$$

The above results may be applied so that ϕ may be expressed as:

$$\phi = \frac{1.1 \rho_{f\ell} t}{4} \frac{(1 + X)\ T_{HP}^4\ \varepsilon_{HP}}{(2-F_{23})\ T_{BR}^4 \varepsilon_{BR}}$$

where we have employed the formulation for the rectangular surface area A_s (ε) derived in Appendix D.

If we stipulate that both the average radiating temperatures and the thermal energy rejection loads are the same for both radiator systems, the absolute mass ratio ϕ may be reduced to:

$$\phi \equiv \frac{1.1\ \rho_{f\ell} t}{4} \frac{(1 + X)\ \varepsilon_{HP}}{(2-F_{23})\ \varepsilon_{BR}}$$

where ρ is the density of the liquid bath material, t the thickness of the belt; X the mass multiple factor associated with the structural components of the belt radiator system; the total hemispherical emissivity (for the heat pipe and the belt radiator); and F_{23} the view factor associated with the inside surfaces of the belt radiator.

Intuitively, the dependence of the ratio ϕ on the emissivity is apparent. Since heat pipe radiators have large emissivities (of the order of unity) the emissivity of the LBR is of prime importance.

Appendix G

EFFECT OF TEXTURING ON BELT SURFACE EMITTANCE

MODEL

The LBR concept fundamentally involves the formation of liquid menisci between wire strands in a mesh or screen. In practical light-weight belt constructions, the average spacing between strands is large with respect to the wavelengths comprising the band of emitted radiation. The 'textures' of interest in the belt (i.e., approximate spherical cavity formed by the menisci) are also on the scale of the wire spacing. A simple model of this texture for analytical purposes is shown in Figure G-1.

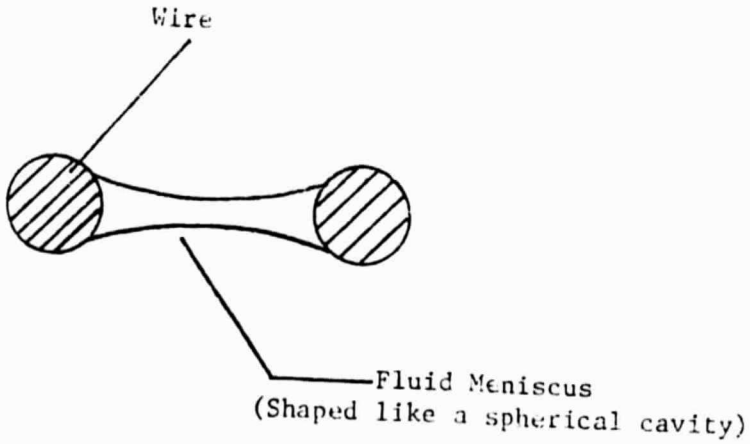

Figure G-1. Model of LBR Textured Surface

ANALYSIS

The determination of the emittance, ε_a of the cavity can be obtained by calculation using Sparrows expression for the total hemispherical emittance of a spherical cavity with a large aperture (Sparrow, 1960):

$$\varepsilon_a = \frac{\varepsilon}{1 - 0.5(1 - \varepsilon)(1 + \cos\phi)} \qquad \text{(G-1)}$$

Where: ε_a = The total hemispherical emittance of the cavity as seen at the aperture,

ε = the total hemispherical emissivity of the material of the cavity wall, and

ϕ = The half angle subtended by the aperture at the center of the sperical cavity.

In simple screen structures, a reentry cavity is impossible. The cavity shape most realizable and conducive to emittance augmentation is a hemisphere. Yet even this shape cannot result in practice for wire spacing-to-diameter ratios characteristic of practical meshes. In addition to these geometrical constraints, the formulation of Equation (G-1) assumes diffuse emittance and reflectance at the cavity wall. Metal-walled materials however would approximate diffuse emittance and specular reflectance. Therefore, the actual value of $\varepsilon/\varepsilon_a$ is expected to be higher than that calculated from equation (G-1).

Nevertheless for the purpose of analysis a configuration of matching hemispheres is assumed. Equation (G-1) will then represent an upper bound of the possible improvement in surface emittance as a result of texturing (assuming $\phi = 90°$, $\cos\phi = 0$). This may be expressed as:

$$\frac{\varepsilon_a}{\varepsilon} = \frac{2}{1 + \varepsilon} \qquad \text{(G-2)}$$

RESULTS

Figure G-2 illustrates the upper bound of emittance improvement by considering the texture of a LBR surface through the application of equation (G-2). For diffusion pump oils, with an expected emittance of approximately 0.8, belt

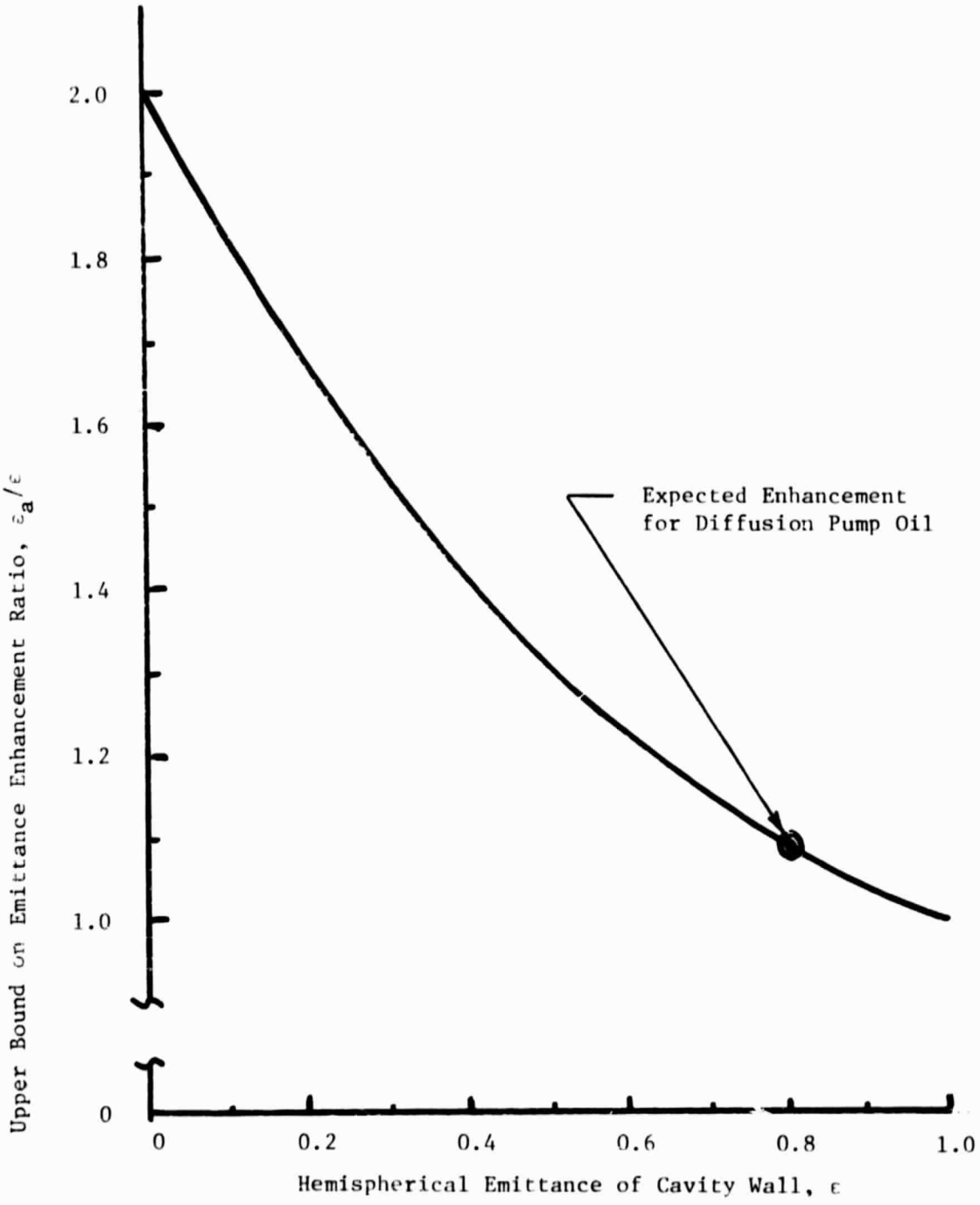

Figure G-2 Emittance Enhancement as a Result of Belt Texturing

texturing might improve overall emittance by only 11 percent. Improvements of up to 80 or 90 percent might be expected for liquid metals with typical flat-walled emittance in the range of 0.1.

REFERENCE TO APPENDIX G

Sparrow, E.M., and V.K. Jansson, "Absorption and Emission Characteristics of Diffuse Spherical Enclosures," Journal of Heat Trans. ASME, May 1960.

Appendix H

VIEW FACTOR RELATIONSHIP FOR CYLINDRICAL LBR

The LBR point design discussed in Sections 4 and 5 of this report is based on the assumption that the radiator is in a cylindrical configuration of radius, R, and axial dimension (or width), W. For purposes of this analysis, the outside surface of the radiator will be called surface 1 and the inside surface 2. It will be assumed that the portion of the LBR surface area that passes through the bath can be neglected as small compared to the full LBR surface. Therefore, an analysis for a full open cylinder will be assumed.

The key parameter required in the analysis is the total view factor of the entire radiator to space, F_{RS}. It is composed of: (1) the view factor of the outer surface to space, F_{1S}, which is always unity; and (2) the view factor of the inner surface to space F_{2S}. The three view factors are related according to the relation:

$$A_B F_{RS} = 0.5 A_B F_{1S} + 0.5 A_B F_{2S} \qquad \text{(H-1)}$$

where: $A_B = 2A_s$ = inner and outer belt surface area.

Equation (H-1) reduces to:

$$F_{RS} = 0.5(1 + F_{2S}) \qquad \text{(H-2)}$$

F_{2S} is calculated by referring to equations previously derived in Jakob (1957) for the view factor, F_{34}, of two cylindrical disks (discs 3 and 4) of radius R spaced a distance w apart. This relationship is given as follows and is illustrated in Figure H-1.

$$F_{34} = \frac{1 + 2\left(\frac{R}{W}\right)^2 - \sqrt{1 + 4\left(\frac{R}{W}\right)^2}}{2\left(\frac{R}{W}\right)^2} \qquad \text{(H-3)}$$

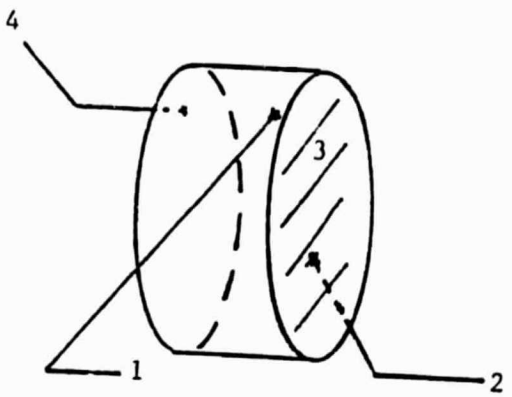

Figure H-1. Geometry for View Factor Calculations

Equation (H-3) is related to the view factor of the inner surface of a cylinder, surface 2, to space (in this case the ends of the cylinder) via the following relationships:

Since it may be proved that:

$$F_{23} = F_{24}$$

the expression:

$$F_{22} = 1 - F_{23} - F_{24}$$

may be rewritten as:

$$F_{22} = 1 - 2F_{23} \qquad \text{(H-4)}$$

Furthermore, since

$$A_3F_{32} = A_2F_{23}$$

and:

$$F_{32} = 1 - F_{34}$$

or we may write:

$$F_{23} = \frac{A_3}{A_2} (1 - F_{34}) \qquad \text{(H-5)}$$

By substituting equation (H-5) into (H-4), the useful expression:

$$F_{22} = 1 - 2 \left[\frac{A_3}{A_2} (1 - F_{34}) \right] \qquad \text{(H-6)}$$

can be derived. F_{34} is calculated from equation (H-3).

Finally, the view factor to space of the inner surface of the cylindrical belt array is given by:

$$F_{2S} = 1 - F_{22}$$

$$F_{2S} = 2\left[\frac{A_3}{A_2} (1 - F_{34}) \right] \qquad \text{(H-7)}$$

The calculation of the full LBR view factor to space is completed derived by substituting equation (H-7) into (H-2) to give:

$$F_{RS} = 0.5 + \frac{A_3}{A_2} (1 - F_{34}) \qquad \text{(H-8)}$$

The results of a parametric evaluation of equations (H-6), (H-7), and (H-8) are plotted in Figure H-2.

REFERENCE TO APPENDIX H

(1) Jacob, M., Heat Transfer, Vol. II, John Wiley & Sons, New York, 1957.

ORIGINAL PAGE IS
OF POOR QUALITY

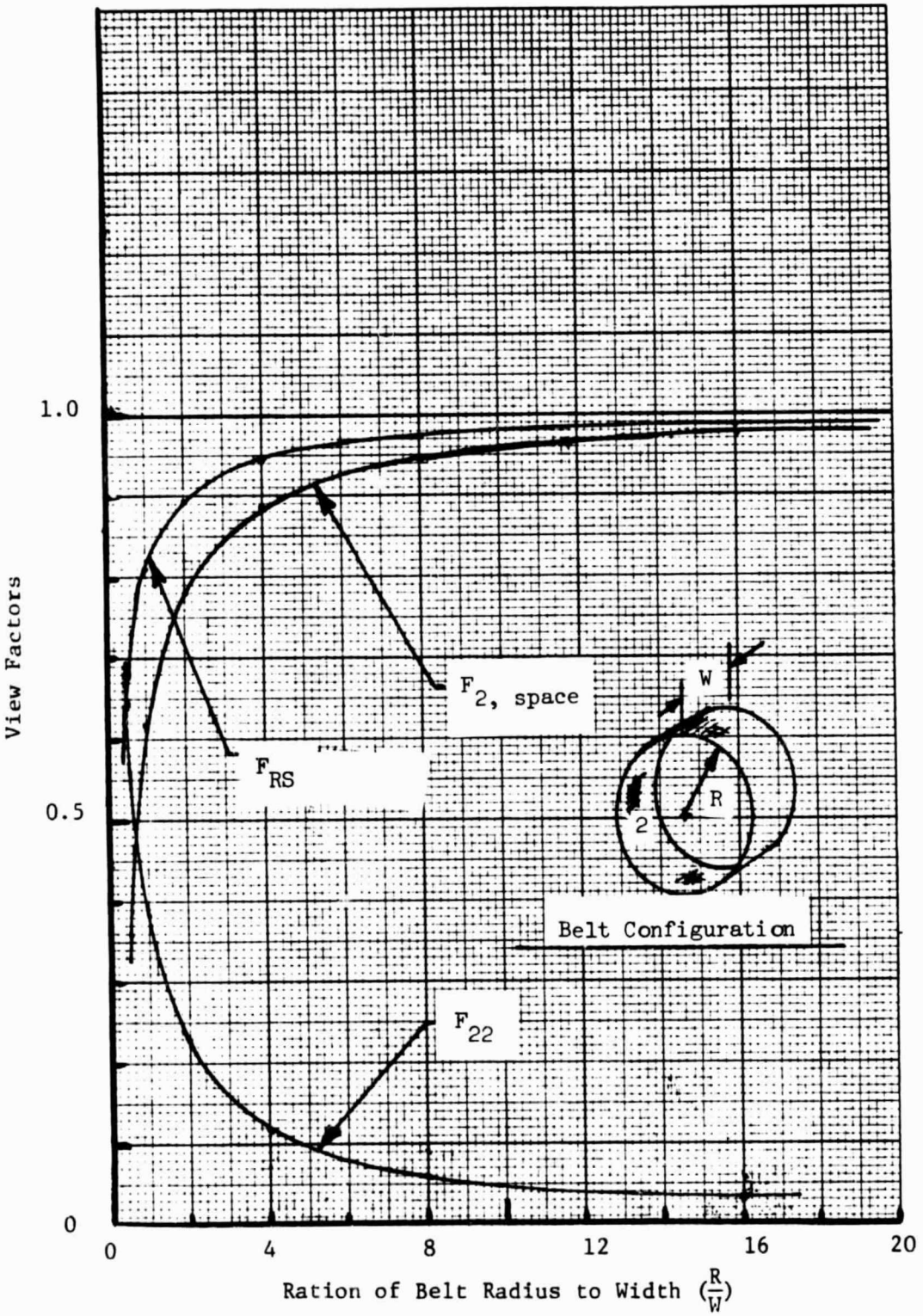

Figure H.2 VIEW FACTORS FOR CYLINDRICAL LBR CONFIGURATION

Appendix I

POINT DESIGN EQUATION DEVELOPMENT AND ANALYSIS METHODOLOGY

The development of the point design Equations is presented in this appendix. Although applied to the particular mission defined in this report, the formulations given here are sufficiently general to be of use in any Liquid Belt Radiator design.

I.1 Radiative Heat Transfer Equations

For this analysis, the initial assumptions that 1) the radiator is shaped like a cylindrical hoop, 2) the radiator surfaces are edge on to the sun, and 3) no net exchange between radiator elements that view each other are made. The radiative exchange between a radiative element having a projected area dA_s and its equivalent black-body surroundings is given by the relation:

$$dQ_{net} = 2\sigma F_{RS} \varepsilon_R \left[T_R^4 - \frac{\alpha_{RS}}{\varepsilon_R} T_s^4\right] \, dAs \qquad (I\text{-}1)$$

where:

ε_R is the total hemispherical emissivity of the radiator surfaces

α_{RS} is the absorptance of the radiator surface to the radiation from its surroundings

F_{RS} is the combined view factor of the radiator surface element $2dA_R$ to its surroundings (same for all elements)

T_R is the temperature of the radiator element

T_S is the equivalent black-body temperature of the surroundings

σ is the Stefan-Boltzmann constant

Making the further assumption that the spectral character and the radiant flux emitted by the surroundings is that of a black-body having a temperature near that of the radiator and evoking Kirchoff's Law, $\frac{\alpha RS}{\epsilon_R}$ is approximately unity. Therefore Equation (I-1) reduces to:

$$d^{Q}_{net} \equiv 2\sigma F_{RS} \epsilon_R \left[T_R^4 - T_S^4\right] dAs \qquad \text{(I-2)}$$

The radiation actually coming from the surroundings may include that in the visible range (reflected sunlight from the earth and spacecraft) as well as that in the infrared range (emitted from the earth and spacecraft). A refined analysis would consider the spectral character of the radiation from the surroundings incident on the radiator and its absorptance to it. For example, assume that the surroundings have an incident flux equal to that of a black-body at 250K but has 30 percent of the energy due to reflected sunlight (Earth's albedo) and the remainder resulting from radiation from bodies near 300K. In this example a radiator using vacuum oil would have an absorptivity to the long wavelength radiation near unity and an absorptivity/emissivity ratio in the visible band near 0.1, resulting in an effective $\frac{\alpha RS}{\epsilon_R}$ = 0.73 and an effective black-body temperature = 231K. This lower effective temperature of the surroundings reduces the radiator area required to reject a specified amount of heat by 8 percent from that calculated on the basis of Equation (I-1) with T_S = 250K. Similarly, a LBR using gallium operating in the sensible heat mode has an estimated absorptivity/emissivity ratio in the visible band of 3, an effective $\frac{\alpha RS}{\epsilon_R}$ = 1.6, and an effective black-body temperature of 281K. In this case, Equation (I-2) underestimates the required radiator area by 11 percent.

I.2 LBR Geometrical Relationships

To further simplify, Equation (I-2) was linearized about the maximum operating temperature. This linearization was assumed valid for the temperature ranges and variations considered in this analysis. The quartic temperature difference:

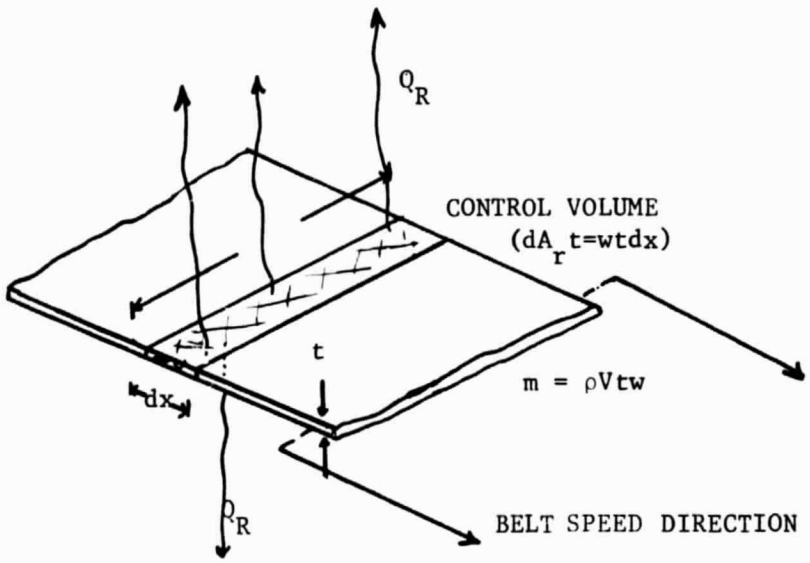

Figure I-1 LBR DIFFERENTIAL CONTROL VOLUME

$$T_R^4 - T_S^4$$

may be expressed as:

$$T_R^4 - T_S^4 = (T_R^2 + T_S^2)(T_R - T_S)(T_R + T_S)$$

or in the final form:

$$T_R^4 - T_S^4 = T_R^3(b)(T_R - T_S)$$

In this case:

$$b = 1 + \frac{T_S}{T_R} + \left(\frac{T_S}{T_R}\right)^2 + \left(\frac{T_S}{T_R}\right)^3$$

where T_R^3 is the linearized constant term fixed at the maximum belt radiating temperature occurring at the exit of the bath heat exchanger. Thus, the net differential radiative exchange equation may be rewritten in linear form as:

$$dQ_{net} = 2\sigma F_{RS}\, \epsilon_R b\, (T_{Rmax})^3\, (T_R - T_S)dA_S \qquad (I\text{-}3)$$

Where T_R is the radiating temperature of the differential area dA_S.

Figure I.1 portrays this differential area. This segment may be used to determine the energy transfer for the entire LBR system. Using a differential form at the first law, we may write:

$$\dot{m}c_p dT_R = -Q_R''\,(wdx) \qquad (I\text{-}4)$$

where:

w = width of the radiator belt (Figure I-1)

dx = differential length in the direction of belt travel

dT_R = temperature variation across the differential control volume

$\dot{m}$ = mass flow of the belt material

Q_R'' = dQ_{NET}/dA_S, or the net energy flux rate from the differential element

Since the material flow rate can be written as:

$$\dot{m} = \rho V t w$$

where:

ρ is the density of the working fluid

V is the tangential belt speed

t is the belt thickness

w is the belt width

Equation (I-3) can be reformulated to:

$$\frac{dT_R}{dx} = \frac{2F_{RS}\ \sigma\varepsilon_R b\ (T_{RMAX})^3\ [T_R - T_S]}{t\rho V c_p} \qquad \text{(I-5)}$$

The variation of the radiator temperature over the length of the belt expressed in the above equation may now be easily solved by the separation of variables technique.* If the initial condition is given as:

$$T_R\ (x = 0) = T_{RMAX}$$

The solution of the differential equation, expressing belt temperature as a functive position may be written as:

$$T_R(x) - T_S = [T_{RMAX} - T_S]e^{-\psi x} \qquad \text{(I-6)}$$

where:

$$\psi = \frac{2\ F_{RS}\sigma\epsilon_R b\ (T_{RMAX})^3}{\rho V c_p t}$$

ψ however may be written in such a way as to greatly simplify Equation (I-5). Since an overall first law balance on the radiator implies:

$$Q_R = \rho V c_p t\ \Delta T_{RAD}$$

then

$$\rho V c_p t = \frac{Q_R}{w\ (\Delta T_{RAD})}$$

where: ΔT_{RAD} is the temperature difference over the entire length of the belt.

Q_R is the total net radiative heat transfer.

This allows ψ to be re-expressed as:

$$\psi = \frac{2\ F_{RS}\sigma\epsilon b(T_{RMAX})^3(\Delta T_{RAD})}{Q_R}\ w$$

---

*Assuming the properties ϵ, c_p, ρ, t and F_{RS} do not to vary with position x.

or

$$\psi = kW$$

This causes Equation (I-6) to become:

$$T_R(x) - T_S = [T_{RMAX} - T_S]e^{-kWx}$$

or over the entire length of the belt:

$$T_R(\ell) - T_S = (T_{RMAX} - T_S)e^{-kW\ell} \qquad \text{(I-7)}$$

Since: $w \cdot \ell = A_s$

where A_s is the single sided radiator area, Equation (I-6) may be used to generate this area directly. Thus:

$$A_s = \frac{1}{k} \ell n \left(\frac{T_{RMAX} - T_s}{T_{RMIN} - T_s}\right) \qquad \text{(I-8)}$$

where:

$$k = \frac{2F_{RS}\sigma\epsilon_R b(T_{RMAX})^3(T_{RMAX}-T_{RMIN})}{Q_R}$$

and:

$$T_{Rmin} = T_R(\ell)$$

It must be noted that all of the above terms are either given or derived properties based on such specific criteria as minimum evaporation mass loss, etc. This is true except for the view factor of the radiator with respect to space, F_{RS} which must be selected. For the cylindrical hoop LBR design, the selection of a view factor defined a particular geometrical relationship between

the diameter and width of the cylindrical structure. For example, a view factor of 0.9 resulted in a ratio of the diameter to width of four. From the single sided area, A_s derived in Equation (I-8), the diameter, width, and circumference of the cylindrical LBR may be determined. Specifically:

$$A_s = \ell \cdot w = \pi \cdot D \cdot w \qquad \text{(I-9)}$$

where now D and w (the diameter and width of the LBR) are interrelated by the view factor.

The mass of the LBR follows quite readily from this formulation, since:

$$M_{LBR} = \rho \cdot A_s \cdot t \qquad \text{(I-10)}$$

The density of the LBR only includes that of the working fluid, with any screen mass effects ignored. Analysis has shown this approximation to be reasonable in the case when an oil is used in conjunction with a plastic mesh structure. Different material combinations, metals and plastics for example, must be carefully examined to determine their individual effects on the mass of cylindrical ribbon structure.

In the point design developed in Chapter 5 of this report, Santovac 6 was used as the working fluid operating over a 30K temperature range (330K inlet). The thickness of the mesh was 0.051 cm (to insure optical thickness) and a view factor of 0.9 was selected. The resulting point design specifications were calculated from Equations (I-7-I-10) and were determined to be:

A_S (Single Sided Area) = 145 m^2 (1555 ft^2)

w (width) = 3.4 m (11 ft)

D (diameter) = 13.7 m (45 ft)

M_{LBR} (Mass of Ribbon Structure) = 92 kg (202 lbm)

1.3 Belt Speed Determination

The speed of the belt may be determined from the first law relation applied over the length of the belt. In this case:

$$Q_R = \rho V t w c_p (T_{RMAX} - T_{RMIN})$$

or

$$V = \frac{Q_R}{\rho t c_p w (T_{RMAX} - T_{RMIN})} \qquad (I\text{-}11)$$

For the point design (Q_{RAD} = 75 kw_t), the belt speed was determined to be 0.8 m/s (2.5 fps).

1.4 Interface Heat Exchanger Sizing

An important component of the LBR system design was the interface heat exchanger. This heat exchanger was to provide the means for the transfer of Brayton power cycle reject heat to the LBR working fluid for eventual dissipation in space. It is predicted that both heat and mass transfer will act as energy transfer modes in this system. For purposes of analysis, however, the former phenomenon only was used as a basis for design thus resulting in more conservative exchanger size estimates.

This design of heat exchanger was based on a compact heat exchanger theory[1]. The device was a counter flow model with the Brayton power cycle fluid being pumped through tubes in a direction opposite to the direction of belt travel. Figure I-2 schematically portrays this structure device. From this figure it may be seen that there are two sides available for heat exchange. Figure 5-4 in the report shows the heat exchanger design in greater detail, including the Brayton tubes heat exchanger plates, etc.

Using the general form for convective heat transfer, we may write:

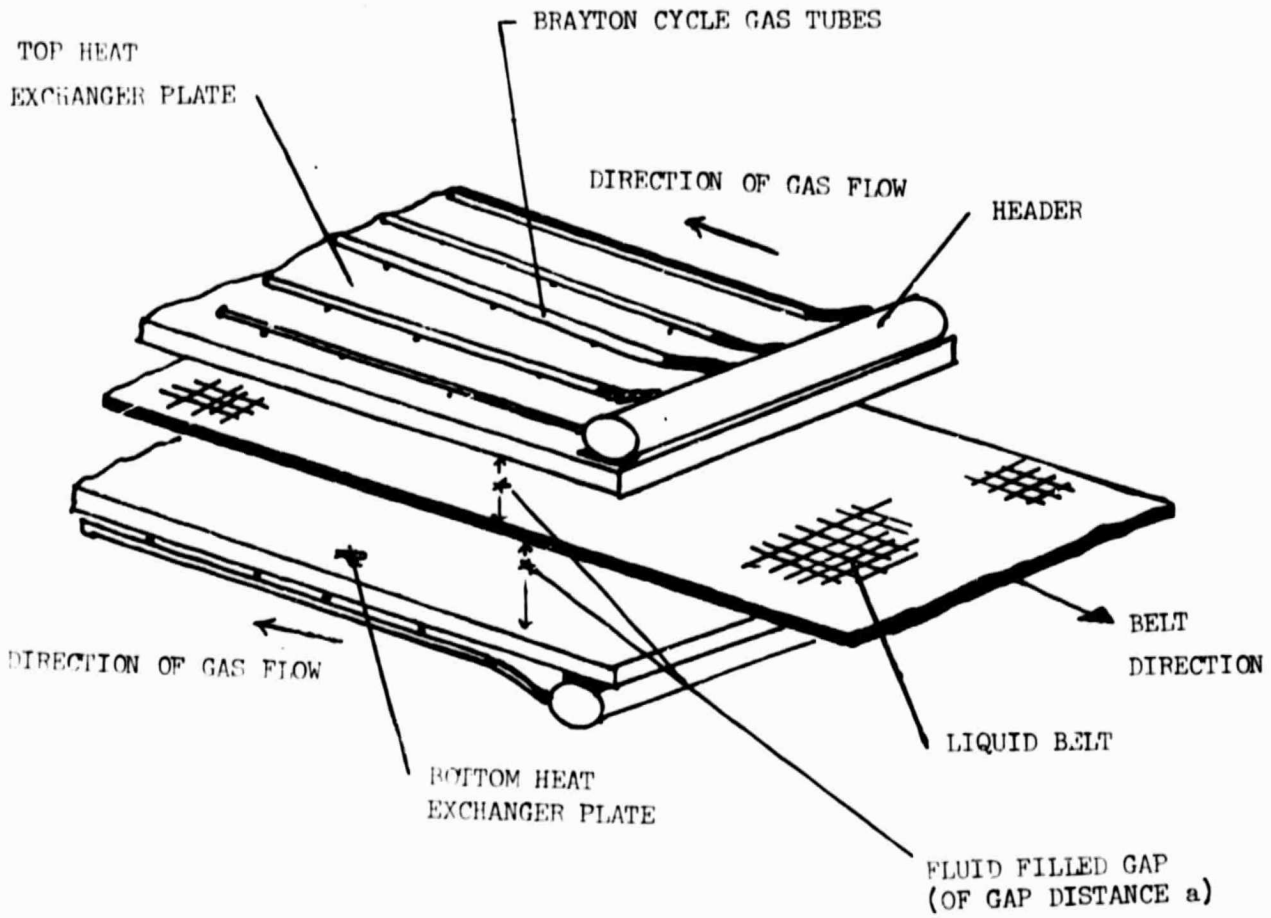

Figure I-2 SCHEMATIC OF INTERFACE HEAT EXCHANGER

$$Q = UA\Delta T \qquad \text{(I-12)}$$

where:

Q is the amount of heat to be transferred

ΔT is a temperature difference which accounts for the temperature variation of each stream as it moves through the exchanger

U is the overall heat transfer coefficient

A is the area available for heat transfer.

In order to account for the change of temperature of a stream as it moves through the exchanger, the log mean temperature difference concept was used[2]. This is defined as:

$$LMTD = \frac{\Delta T_a - \Delta T_b}{\ell n \Delta T_a / \Delta T_b} \qquad \text{(I-13)}$$

For the point design conditions specified, Figure I-3 depicts the temperature differences ΔT_a, and ΔT_b occurring at the interface heat exchanger.

Evaluation with respect to these values gives:

$$LMTD = 52.7K$$

The overall heat transfer coefficient U was assumed to be 567.6 W/m^2K ($\sim$100 Btu/hr $ft^2°F$). This value was believed readily attainable and in fact somewhat conservative for the interface heat exchanger.

Employing these results and assumptions allows a heat exchanger area to be calculated. This area however may be re-expressed as:

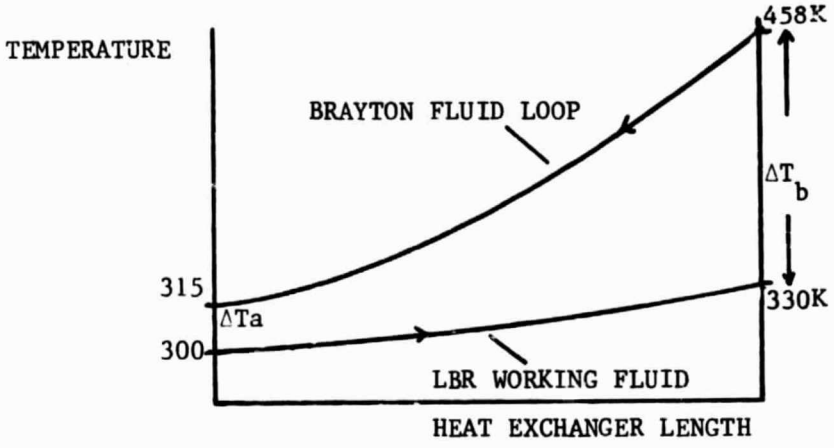

Figure I-3 POINT DESIGN INTERFACE HEAT EXCHANGER TEMPERATURE DIFFERNTIALS FOR USE IN LMTD CALCULATIONS (Rohsenow and Choi, pg. 310)

$$A_{HX} = 2wL_{HX}$$

where:

w is the width of the heat exchanger (assumed to be the same as the width of the belt determined in section I.2)

L_{HX} is the length of the heat exchanger in the direction of belt travel.

The "2" in the above formulation, it may be recalled, accounts for the two sides available for energy transfer. Employing these many results leads to the relationship:

$$L_{HX} + \frac{Q}{2Uw(LMTD)} \qquad \text{(I-14)}$$

or more specifically:

$$L_{HX}(m) = \frac{Q[kw] \cdot 10^3}{59825\ w[m]}$$

For the point design, this equation was used to calculate a heat exchanger length of 0.37 m (1.21 ft) corresponding to a total area of 2.51 m^2 (27.0 ft^2).

I.5 Parasitic Power Losses

The parasitic power refers to the rate of energy required to overcome the drag forces encountered as the belt moves through the bath. This analysis assumes the existence of Couette flow with a linear velocity distribution across the gap of the interface heat exchanger. The power required to overcome viscous drag was written as:

$$P = \frac{\mu V^2}{a} 2wL_{HX} \qquad \text{(I-15)}$$

where:

μ is the viscosity of the working fluid

V is the speed of the belt

w is the width of the belt

L_{HX} is the length of the heat exchanger as calculated in section I.4.

a is the single sided gap distance from the top heat exchanger plate to the surface of the belt structure

To account for other drag forces including bath containment seals (i.e., wipers), bearing drag, etc., the viscous drag defined in Equation (I-15) was doubled. Thus the total system power required to overcome all sources of drag may be written as:

$$P = \frac{4\mu V^2}{a} L_{HX} \cdot w \qquad \text{(I-16)}$$

For the purposes of this analysis, the viscosity μ was assumed to be a logrithmic function of temperature (Figure I-4). The value used in calculations was determined from the arithmetic mean temperature of the bath for particular inlet and outlet conditions.

For the point design, temperatures of 330K at the outlet and 300K at the inlet resulted in an average viscosity for the working fluid of 1.75 Ns/m (0.0365 lbf-s/ft^2). Employing this result along with the other relations determined in this appendix, a gap width of 0.56 cm (0.22 inch) resulted in a total parasitic loss of less than 1 kw. The actual power required to overcome this 1 kw would be at most 33% higher depending on the efficiency of the motor(s) used to drive the belt. It should be noted that alternative interface heat exchanger designs are possible which not only provide the required heat transfer but minimize drag losses.

ORIGINAL PAGE IS
OF POOR QUALITY

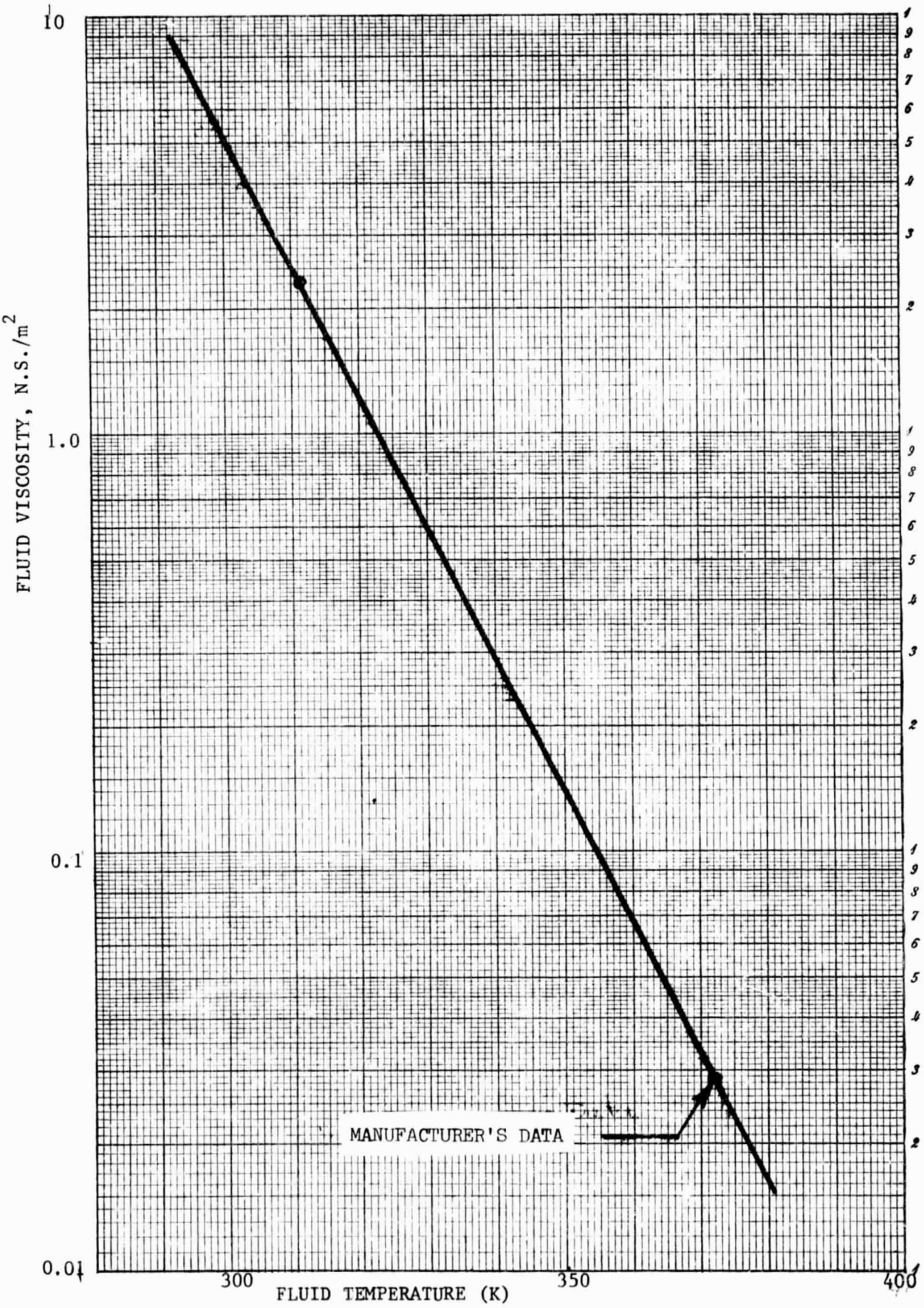

Figure I-4 VISCOSITY OF SANTOVAC 6 AS A FUNCTION OF TEMPERATURE

I.6 Orbital Aerodynamic Drag

An estimate of the aerodynamic drag force on the LBR can be gained by considering a model consisting of a normal plane area travelling through a rarefied atmosphere at orbital velocity. Attention is focused on aerodynamic conditions at an orbital altitude of 270 nautical miles, where[3]:

orbital velocity, V_o	=	7.9 km/S
mean molecular weight of atmosphere, M	=	18.3 (principally atomic and molecular oxygen and nitrogen)
average particle mass, M	=	3.04×10^{-23} g
mean free path of particle	=	10^4 m
average particle velocity	=	1.4 km/s
particle concentration, n	=	$10^8/cm^3$

As the mean free path is very much greater than any radiator dimension, the radiator operates in the free-molecular flow regime. The drag force can be computed by considering the momentum exchange of particles colliding with the radiator surface. As the orbital velocity is much (approximately 8 times) larger than the particle velocity, the pressure at the radiator surface is determined by the orbital speed. Assuming that the collisions of particles with the surface are elastic and reflected diffusely, the pressure on the front face of the normal area is:

$$P = nmV_o\left(V_o + \frac{V_o}{3}\right) = \frac{4}{3} nmV_o^2 \qquad \text{(I-17)}$$

and the pressure on the back surface is insignificant. Accordingly, an estimate of the drag force on the LBR is given by:

$$F_D = PA_p = \frac{4}{3} A_p nmV_o^2 \qquad \text{(I-18)}$$

where:

F_D is the aerodynamic drag force

A_p is the area projected normal to the orbital velocity

other quantities as previously defined

Substituting the appropriate numerical values, we get

$$\frac{F_D}{A_p} = 2.53 \times 10^{-5} \text{ N/m}^2$$

It may be of interest to note that the drag in free-molecular flow (calculated from Equation (I-18)) is 2.67 times that appropriate to a bluff body (drag coefficient equal to unity) in a continuim flow having the same density and approach velocity.

REFERENCES TO APPENDIX I

1) Kays and London, Compact Heat Exchangers, Figure 2-12.

2) Rohsenow, W and H. Choi, Heat Mass and Momentum Transfer, 1961, page 310.

3) Santeler, D.J. et al. "Vacuum Technology and Space Simulation," NASA SP-105, 1966.

Appendix J

EVAPORATIVE LOSS IN SPACE

The loss of material in a space environment is a crucial factor affecting the performance of any radiator concept. This is especially true for designs involving the direct exposure of a material to space (i.e., the liquid belt radiator, and the liquid droplet radiator). It is quite important to accurately access the material loss due evaporative phenomena since the contamination of sensitive instruments or equipment is becoming increasingly important in all facets of space vehicle design.

The basis of explanation for the evaporative mass loss phenomenon is found in kinetic theory. As discussed in Appendix I, the rarified atmosphere existing 270 nautical miles above the earth results in the change from continuum hydrodynamics to free molecular flow. This is apparent since the mean free path of particles at this altitude is of the order of ten thousand meters, well in excess of the most salient dimensions of the LBR point design.

Free molecular flow implies that the net effusion of material from a surface may be expressed in terms of the average molecular velocity V, derivable from Maxwell Boltzman statics. This may be written as a mass flux rate defined as:

$$\Gamma_m = 1/4 \, \rho_v . (\overline{V}) \qquad \text{(J-1)}$$

where:

Γ_m is the evaporative loss in terms of mass per unit time per unit area

ρ_v is the vapor density of the material

$\overline{V}$ is the average Boltzman molecular speed.

Using this relationship, and assuming the evaporated material to behave as an ideal gas, Equation (J-1) may be rewritten as

$$\Gamma_m = \sqrt{\frac{M}{2\pi\bar{R}}} \frac{P_V}{(T)^{1/2}} \qquad \text{(J-2)}$$

where:

M is the molecular weight of the material

T is the absolute temperature of the material

P_v is the vapor pressure of the material

$\bar{R}$ is the universal gas constant

If the material's vapor pressure variation with temperature is known, the evaporative loss relation may be expressed solely as a function of temperature. Since vapor pressure variations are logrithmic, the evaporative mass loss Equation would take the form:

$$\Gamma m \simeq \frac{Ke^{-c/T}}{(T)^{1/2}} \qquad \text{(J-3)}$$

In the case of Santovac 6, a linear regression fit of manufacturer's data gave rise to the form:

$$\ell nP_v(\text{torr}) = 23.79 - \frac{14040.24}{(T)^{1/2}[K^{1/2}]} \qquad \text{(J-4)}$$

which in turn resulted in the following evaporative mass loss function:

$$\Gamma_m = \frac{8.99 \times 10^{18}}{(T[K])^{1/2}} \exp(-14040.24/T[K]) \left[\frac{kg}{yr\text{-}m^2}\right] \qquad \text{(J-5)}$$

To determine the annual losses over the entire belt radiator, Equation (J-5) must be integrated. This is a very complex formulation, ammenable only to approximate numerical solution. For purposes of this analysis, an interval loss summation program was written. This program evaluated the mass loss for a set of ten intervals each operating at different temperatures (Figure J-1). The individual losses corresponding to these intervals were summed to determine the total loss for the point design LBR configuration.

For Santovac 6, this interval mass summation takes the following form:

$$A_{TOT}\Gamma_m = 2\sum_{i}^{10}\Gamma_{mi}\Delta A_{si} = 2\sum_{i}^{10}\left(\frac{K}{(\bar{T}_i)^{1/2}}\exp\left(-14040.24/\bar{T}_i\right)\cdot\Delta A_{si}\right) \quad \text{(J-6)}$$

where:

$\bar{T}_i$ is either the log or arithmetic mean temperature for some interval

ΔA_S is the single sided belt area corresponding to the same interval

K is a conversion constant for dimensional similarity

In this point design case, for operating temperatures between 300-330K and a double sided area at 290m^2, the total mass loss corresponded to 15 kg per year.

REFERENCES TO APPENDIX J

1) Jaffe, A. "Behavior of Materials in a Space Environment" ARS Journal 1961.

2) Handbook of Geophysics; Revised Edition, Air Force Research Division, Geophysics Research Directorate, 1960.

3) Kennard, E., Kinetic Theory of Gases Chapter 8, 1938.

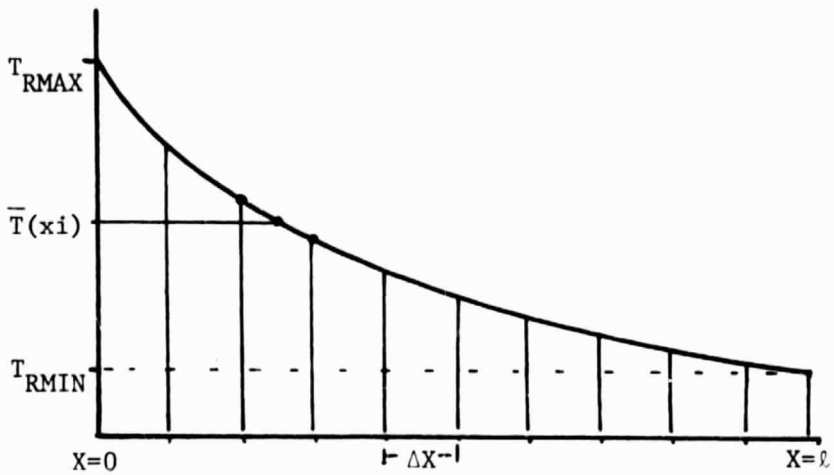

BELT TEMPERATURE DISTRIBUTION

$$\text{ANNUAL MASS LOSS } 2\sum_{i=1}^{10}\left(\frac{K}{\bar{T}_i}\right)^{1/2}\exp\left(-14040.24/\bar{T}i\right)\cdot w\Delta Xi\left[\frac{Kg}{yr}\right]$$

Figure J-1 INTERVAL SUMMATION EVAPORATIVE MASS LOSS FORMULATION

APPENDIX K

OPERATIONAL DESCRIPTION OF THE DIGILAB CORPORATION FOURIER TRANSFORM SPECTROMETER

The Fourier Transform Spectrometer (FTS), manufactured by Digilab Corp., is comprised of a Michelson Interferometer tied to a dedicated digital computer. The optical schematic of this device is shown in Figure K-1. The test sample is placed in a sealed cell to evaluate its transmission or absorption properties. The cell consists of an enclosure which contains two potassium bromide windows (bandwidths = 10000-350 cm^{-1}) that are transparent to incident infrared radiation. The sample is placed in a support structure within the cell. When a reflection measurement is made, the sample remains open to the test chamber environment, in order to minimize refraction effects.

This operation of interference based spectrometers is described below:

- Incident infrared radiation from a globar (silicone carbide) source radiating at 1200°C is collimated and directed at a flat beam splitter. The beam splitter is oriented at 45°C with respect to the incident wave front and maintained at a temperature of 40°C to avoid optical distortion and water condensation. During emission experiments at the globar source is replaced by a heated material specimen. By use of the apparatus described in Chapter 5, the emitted radiation is directed by mirrors to the spectrometer.
- The beam splitter, a potassium bromide substrate coated with germanium, divides the beam into two perpendicular paths. One beam is incident upon a fixed mirror while the other upon is incident a mirror oscillating at a frequency of 20 kHz over a known distance.
- The optics reflect the two beams from the mirror surfaces and recombine them at the beam splitter. This recombination of the original source frequencies causes constructive and destructive interference to occur, corresponding to the position of the moving mirrors.
- The resulting interferogram (i.e., interference pattern) is passed through or is incident upon a particular sample. In the process, certain

frequencies are absorbed or reflected as a result of the molecular characteristics of the test material. This interaction changes the interferogram.

- The altered interferogram is then collected by the system detector. These data are deciphered and processed via the Cooley-Tukey Fast Fourier Transform (FFT) to yield an intensity vs. wavenumber result. Additional computer software packages may be used to determine other spectral characteristics of the material

Interferometry (Interference based spectroscopy) has two main advantages over dispersive techniques. The first is that a simultaneous viewing of all desired frequencies (i.e., multiplexing) is possible. The second is that the energy throughput of interferometer-based methods is higher than dispersive means. The multiplexing effect has the added advantage of allowing a superposition or co-adding of individual interferograms. This feature results in highly reproducible, low noise spectra which are obtained much faster than by conventional means.

REFERENCE TO APPENDIX K

(1) Griffiths, Peter R. Chemical Infra-Red Fourier Transform Spectroscopy, J. Wiley Sciences, New York, 1975.

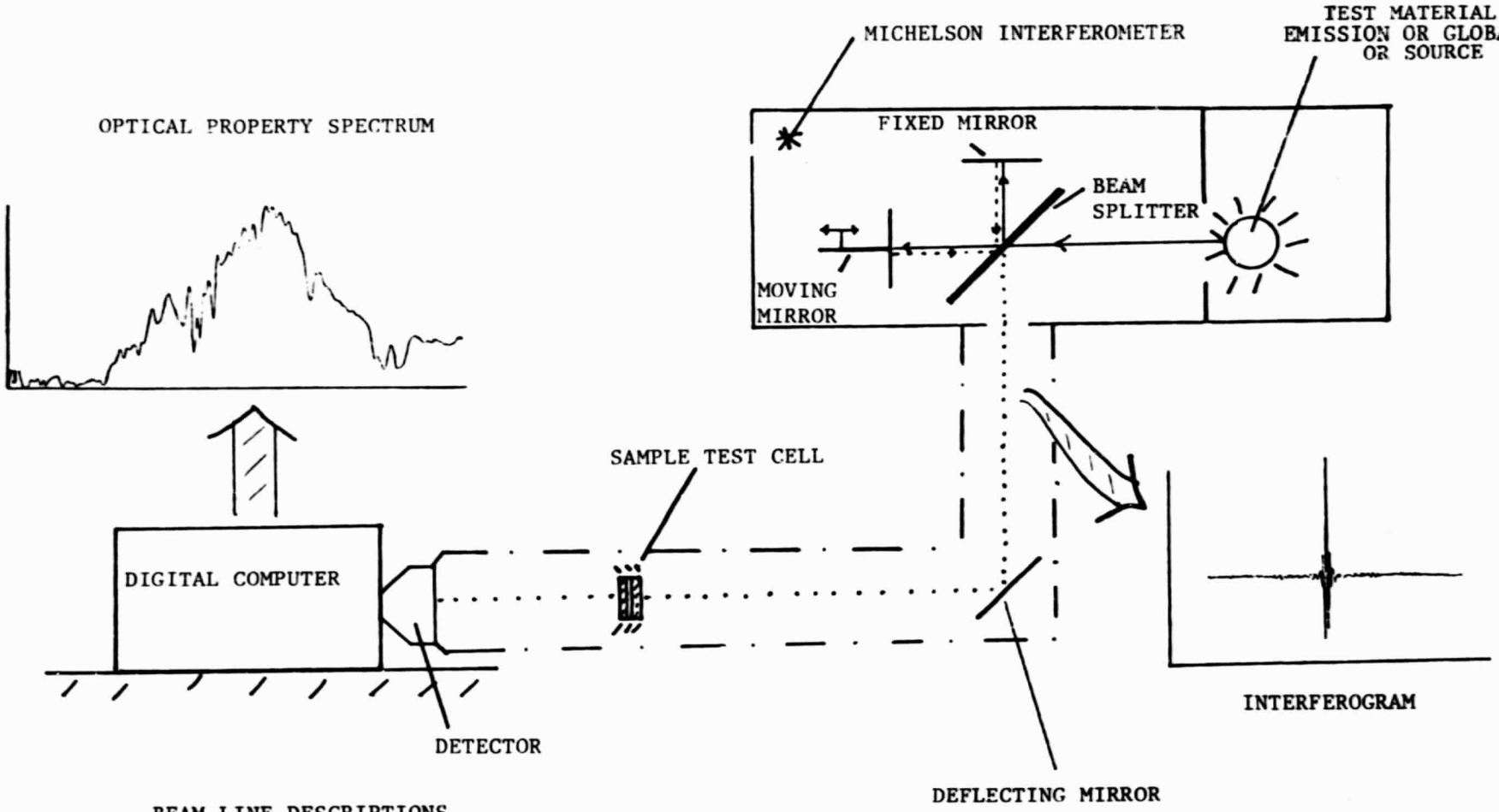

Figure F-I OPTICAL SCHEMATIC OF THE FOURIER TRANSFORM SPECTROMETER
(Griffiths, P., 1975)